MASTER'S THESIS

submitted in partial fulfillment of the requirements
for the degree of "Master of Science in Engineering"
Degree Program Mechatronics/Robotics (Master)

Lizard locomotion: Implementing body bending in a Robot

By: Viktor Gudenus, BSc
Student Number: 1010331022

Supervisor 1: Dr. Robert J. Full
Supervisor 2: Dipl.-Ing. Jakob Karner

Berkeley, 16.04.2012

FACHHOCHSCHULE TECHNIKUM WIEN

Declaration

„I confirm that this thesis is entirely my own work. All sources and quotations have been fully acknowledged in the appropriate places with adequate footnotes and citations. Quotations have been properly acknowledged and marked with appropriate punctuation. The works consulted are listed in the bibliography. This paper has not been submitted to another examination panel in the same or a similar form, and has not been published. I declare that the present paper is identical to the version uploaded."

Vienna, 10/15/2012	
Place, Date	Signature

Kurzfassung

Echsen verwenden für ihre Umorientierung in Luftmanövern, Torsos- und Schwanzkrümmungen. Obwohl solche Bewegungsabläufe auch in terrestrischen Manövern, wie dem Fluchverhalten gesehen werden kann, ist es möglich, dass der dabei entstehende Impulsmoment durch externe Impulse, wie Boden-Reaktionskräfte beeinflusst wird. Quantifizierungsmöglichkeiten des entstehenden Impulsmomenten-Austausches und externen Impulsen wurden bis jetzt nicht dokumentiert. Um das Verhalten von Echsen bei Drehung zu ergründen, wurden ein numerisches und ein analytisches Model entwickelt. Außerdem wurde ein Konzept eines dynamischen, terrestrischen, zwei-gliedriger Roboter mit aktivem Schwanz vorgeschlagen um das Gebiet der Lokomotionsbionik in der Robotik voranzutreiben.

Um das Impulsmoment der Bewegung von Echsen zu berechnen wurden kinematische Daten und Approximationen für Körpereigenschaften, wie Masse, Massenmittelpunkt und Massenträgheitsmoment gebraucht. Die kinematischen Daten der Echsenmanöver wurden mittels Hochgeschwindigkeitsaufnahmen von durchgeführten Tierstudien, unter Verwendung von sieben Siedleragamen (*Agama agama*), extrahiert. Vor den Studien wurden morphologische Daten der Tiere aufgezeichnet und Markierungspunkte aufgetragen um eine Gliederung in sechs Körpersegmente zu erhalten. Der Studien Aufbau bestand aus einem Positionierungsunterschlupf und einem Fluchtunterschlupf mit zueinander schauenden Ausgängen. Nachdem eine Fluch der Echse in den Positionierungsunterschlupf initiiert wurde um das Tier auszurichten, (gestreckter Torso und Schwanz, mit Frontalseite in gegenüberliegender Richtung zu dem Fluchtunterschlupf) wurde der Unterschlupf angehoben und ein frontaler Stimulus mit hoher Geschwindigkeit ausgeführt. Ähnlich wie im C-Start von Fischen zeigen typische Fluchtreaktionen von Echsen im ersten Schritt eine Körper- und Schwanzbiegung, mit gleichzeitiger Drehung um ihre Hinterbeine. Der zweite Schritt zeigt eine Beschleunigung in entgegengesetzter Richtung vom Stimulus. Der Fluchtunterschlupf hilft eine 180°-Drehung der Tiere im Fluchtverhalten zu initiieren.

Nach der Objektverfolgung der Punktmarkierungen und der Extraktion der Daten, konnten die Approximationen für Masse, Massenmittelpunkt und Massenträgheitsmoment der Echsensegmente durchgeführt werden. Dabei wurden zwei verschiedene Systematiken zur Approximation für Körper- und Schwanzsegmente angewendet. Für die Körperapproximation wurde mittels Vermessungen von Echsen Kadavern, Skalierungsfaktoren ausfindig gemacht. Diese wurden über die morphologischen Daten, auf die lebenden Echsen übertragen. Die Approximationen des Schwanzes wurden mittels elliptischen Kegelstumpfes berechnet.

Die beiden sechs-gliedrigen Modelle wurden verwendet um den Einfluss von Formänderungen und externen Impulsen auf die Drehung der Echse zu bestimmen. Dies wurde durch einen Vergleich der tatsächlichen Körperrotation der Echse mit einem starren stab Model mit konstantem Trägheitsmoment, einem starren stab Model mit variierendem Trägheitsmoment der Echse und einem Null-Impulsmomenten Model durchgeführt. Die beiden starren stab Modelle zeigen Einfluss der externen Impulse an, das Null-Impulsmomenten Model dagegen die Effekte der Formänderung. Im ersten Schritt des Bewegungsablaufes können 57.4% der Formänderung zugesprochen werden, wobei 70% davon auf die Bewegung des Schwanzes zurückzuführen ist. Der restliche Anteil wird durch die Körperkrümmung initiiert. Der zweite Schritt der Echse zeigt externe Impulse auf, welche der rückläufigen Bewegung des Echsenschwanzes entgegenwirkt, sodass die Echse nicht zu seiner ursprünglichen Position zurückdreht.

Nach der Einschätzung der Bewegungsabläufe wurde ein zwei-gliedriger Rumpf eines dynamischen Roboters mit beweglichem Schwanz und minimaler Aktuatorenanzahl konstruiert. Dabei wurde eine neue Fabrikationsmethode namens Smart Composite Microstructures (SCM) verwendet. Zusätzlich wurde ein Konzept erstellt die Bewegungsphasen der Echse, durch passive Ansteuerung der Roboterbeine und Körperkrümmung, umzusetzen. Es wird erwartet, dass die Synchronisierung von Körper- und Schwanzkrümmung mit der Beinbewegung sowohl die Winkelgeschwindigkeit der Drehung erhöhen wird als auch die Regelbarkeit für terrestrische Manöver von mehrbeinigen Robotern stark verbessert wird.

Schlagwörter: Trägheitsfortsatz, Echse, Fluchtverhalten, Roboter, Impulsmomenten-Austausch

Abstract

Lizards reorient in aerial maneuvers by torso bending and swinging of the tail. Although similar behavior in terrestrial maneuvers such as escape responses is seen, external impulses such as ground reaction forces may change the angular momentum. Methods of quantifying angular momentum exchange and external impulses have not yet been attempted. To investigate turning behavior in lizard locomotion a numeric and an analytic six-link model were developed and a dynamic terrestrial two-link robot with attached active tail proposed to advance the field of locomotion bionics for mobile robotics.

To calculate the angular momentum of lizard motion, kinematic data and approximations for body properties such as mass, center of mass (COM) and moment of inertia (MOI) were needed. The kinematic data of the lizard behavior was extracted using high-speed video footing of conducted animal trials with seven Red-headed Agamas (*Agama Agama*). Before the lizards were run, morphometric data measurements were recorded and tracking markers applied, subdividing the lizard in 6 segments. The trial setup consisted of a positioning and an escape shelter with exits pointing toward each other. After the lizards were chased into the positioning shelter to align them in the desired orientation (stretched body and tail, lizard pointed in the opposite direction of the escape shelter) the shelter was lifted and stimulus presented in rapid and frontal fashion. Typical escape responses in lizards show a curling of tail and body, pivoting about their hind legs in the first stride and acceleration away from the stimulus in the second stride, comparable to C-starts in fish. The escape shelter helped to initiate an escape response of 180° towards its opening.

Following the tracking and extraction of 43 animal trials, approximations for mass, COM and MOI of the lizard segments, defined by the marker position could be conducted. the approximations could be divided into two different methods according to body parts and tail parts. The body approximation was accomplished by measuring lizard carcasses and extracting scaling factors to apply on morphometric data of the living lizards. The tail approximations were conducted using truncated elliptical cones (TEC).

The two six-link models were used to extract two components of the lizard turn, revealing the extent to which shape change and impulsive force each contribute towards turning the lizard.
To this end the extracted body turn angle of the lizard was compared with a “rigid stick” model with constant MOI, a “varying inertia stick” model with changing MOI according to the lizard trials and a zero angular momentum model. The rigid stick models revealed the influence of external impulses and the zero angular momentum model the effects of the shape change of the lizard. The first stride revealed 57.4% influence on the lizard turn by shape change of the lizard. Of which 70% was due to the tail of the lizard and the remaining fraction due to the body bending. The second stride of the lizard showed external impulses to

counteract the uncurling of the tail and body, preventing the lizards to rotate back to their initial position.

After the assessment we began construction of a two-segmented torso for an minimally-actuated dynamical legged robot with attached tail. By combining a novel manufacturing process named Smart Composite Microstructures (SCM) and by a proposed passive leg motion and body bending, the phases of the lizard motion sequence could be implemented. We contend that the synchronization of body bending, tail curling and leg impulse forces will enhance the rate of rotation of turning in the horizontal plane and increase the controllability of terrestrial maneuvers in legged robots.

Keywords: Inertia appendage, lizard, escape response, robot, angular momentum exchange

Acknowledgements

First and foremost I would like to thank Professor Robert J. Full for the opportunity of conducting research in the Poly-PEDAL Lab and for introducing me to the exciting research field of bio-inspired mobile robotics. His love and engagement for what he does effects all people around him.

I would like to thank Dipl.-Ing. Jakob Karner for all his help and feedback on my research and for furthering my understanding of scientific work.

Furthermore I would like to thank all the members of the Poly-PEDAL Lab and CiBER, especially Tom Libby for long discussions about Dynamics, vital input for the work but foremost for being a good friend.

I would also like to thank the Marshall Plan Foundation for providing financial support but more importantly for making this opportunity possible in the first place.

Finally I would like to thank my family, my friends and people that shared this experience with me from my whole heart. You built the foundation I stand on.

Table of Contents

1 Introduction

This master thesis was conducted in partial fulfillment of the requirements for the degree of Master of Science in Engineering from the University of Applied Science Technikum-Wien. The research was conducted at the University of California at Berkeley, United States of America, at the Poly-PEDAL (Performance, Energetics, and Dynamics of Animal Locomotion) Laboratory and CiBER (Center for Integrative Biomechanics in Education and Research) of the Department of Integrative Biology.

In the last 20 years the field of mobile robotics has experienced rapid development. Research in this field has moved importantly and significantly towards studying dynamic behavior in robots. Earlier in robotic development, it was sufficient to be able to control robots accurately. Now mobile robotic research projects stress maneuverability and stability, while upholding velocity. One way of advancing knowledge for locomotion behavior in robots is through looking at nature for inspiration. The defining aspect of nature is the evolution process through which a natural optimization can be achieved. This optimization leads to highly evolved and complex systems that can be used as models for technical applications by the field of mobile robotics. A representative example for such a system is the escape response of lizards. Lizards are hematocryal and as such dependent on long basking which exposes them to predators. To avoid falling prey to these predators, lizards are dependent on well-developed escape responses. The motion of lizards when escaping is influenced by external impulses such as ground reaction forces and muscular contractions and also by body and tail bending, which changes characteristics such as inertia and angular moment. Due to the extreme conditions in which these maneuvers have evolved, it is likely to have optimized mechanisms for the turn towards agility and quickness.

The field of robotics is grappling with important research issues of mobility, balance and body bending, which are taken for granted in the natural world. Can robot maneuverability be improved by learning from a lizard’s agility, quickness and speed? In the conducted research it is found that learning from lizard motion can further maneuverability in robot dynamic motion in combination with inertial appendage and body bending by integrating certain motion sequences.

1.1 Motivation

The motivation for this master thesis is to map the motion sequence of lizards and understand why lizards move in particular ways in certain circumstances. Lizards move and turn in a very specific way and are able to maintain stability while upholding agility and velocity. Furthermore the fact is known that lizards use their tails to exchange angular momentum in aerial maneuvers (Libby et al., 2012; Jusufi, Kawano, Libby and Full, 2010). The motivation for this master thesis is to find out if lizards apply the same principle for terrestrial maneuvering, if tail and body bending is thereby the crucial factor and if there is a relation between body resp. tail movement and body angle. Furthermore the research outcome and findings can have far reaching implications if applied to the field of mobile robotics. If an advantageous effect can be found, the stability, agility and maneuverability of robots or other vehicles can be drastically increased. Especially in extreme environments, environments with limited space or environments where obstacle avoidance is of essence these principles would be of advantage.

1.2 Aims and Contribution

Although research of aerial maneuverability concerning the tail movement has been conducted (Jusufi et al., 2010), the question of body and tail influence for terrestrial motion in particular escape responses is a novel one. The lateral swinging behavior of lizards is a known principle of lizard locomotion but until now it was not attempted to quantify its effectiveness for lateral motion. Furthermore a method of separating forces due to ground reaction and forces due to the executed shape change of the lizard while turning has not yet been developed. Also the correlation between these forces and the turning motion of the lizard will be assessed for the first time.

These new results will not only give further insight to the general locomotion of lizards but will greatly influence how we perceive the acting forces of a lizard turn. Further, the question of the tail influence for tuning in the transversal plane will affect the way of thinking about inertial appendages for technical applications. Combined with the findings of the influence of tails in the sagittal plane technical applications could be attempted which could control perturbation in any plane using angular momentum exchange. The results of the research may be used for search-and-rescue robots but use for any aerial or terrestrial vehicles cannot be imposed.

1.3 Synopsis

The master thesis first outlines the background necessary to understand the thesis. These include a description of biomimetics, motion analysis the plum line and pendulum method and the methods used for approximation.

The main part of the thesis can be divided into two categories: the biological studies and the technical implementation. The biological studies will describe basic knowledge about the animals and their habitat. Then the data acquisition will be described which was divided into the used equipment and arrangement of the trail setup as well as the trial procedure and the behavior of the animal during the trial. At the end of this section the acquisition of the morphological data will be described. The chapter of technical implementations will start with a description of the data tracking using ProAnalyst® (Xcitex, Inc.). Then the data approximation and the validation of the resulting values will be discussed, followed by a numeric and an analytic model which were used to calculate characteristics of the lizard turn. After the description of the models the robot design and construction process is presented.

The section is followed by the results and the conclusion of the thesis for both, biological and technical aspects.

1.4 Hypothesis

The hypotheses for this master thesis are shown below and describe the central questions to this project. The null hypothesis (H0) describes the opposing statement and is designed to be contradicted during the project. The following hypotheses (H1-H3) are related questions to be answered and will be discussed in the conclusion of the thesis

H0: The shape change of the lizard during the turning motion doesn’t influence the turn.

H1: The shape change of the lizard during the turning motion increases the final body angle.

H2: The first stride and the aerial phase are influenced mainly by shape changes.

H3: The second stride and areal phase are dominated by external impulses

2 State of the Art

Due to its importance to surviving, predatory responses in animals are extremely refined and are vital for the understanding of locomotion behavior. Another reason escape responses are of importance in research is the fact that escape responses show clearly the limitations of a system due to the extreme conditions under which these systems evolved.

Not only are fast-starts in fish considered to be model system for escape responses but may indicate also that escape responses were developed early in evolution due to similar motion sequences found in escape responses in lizards. As shown in Domenici and Blake (1997) fish fast-start responses consist of three different phases: the preparatory stroke (ipsilateral electromyographic activity), the propulsive stroke (contralateral electromyographic activity) and continuous swimming resp. coasting. In both fish and lizards the escape response is optimized for high predator-prey distance (Domenici and Blake, 1997; Cooper, Pérez-Mellado and Hawlena, 2007). Although the turning angles of fish vary between 0° and 180° to each side, in most fast-start cases a bimodal pattern of 180° and 130° for the escape angle can be distinguished (Domenici and Blake, 1997) which can also be seen in escape responses of lizards (Cooper, Pérez-Mellado and Hawlena, 2007). As described in Hall, Wardle and MacLennan (1986) these maxima in flight angles are due a compromise between maximal predator-prey distance and keeping the predator in view. The performance of escape responses is furthermore influenced by the motivation of the animal, referring to choosing an escape trajectory and the angle of prey in comparison to the angle of the predator which often lead to sub-maximal turning performance (Domenici and Blake, 1997; Domenici, 2002). The escape trajectory is influenced by the direction of refuge (Cooper, 1998) as well as the number and direction of the stimuli (Cooper, Pérez-Mellado and Hawlena, 2007).

Another influencing factor for escape responses and general locomotion of lizards is the use of the tail. Tail loss will decrease in-air stability (Gillis, Bonvini and Irschick, 2009) and will reduce escape speeds and distance (Martin and Avery, 1998). However Brown, Taylor and Gist (1995) show that lizards previously subjected to caudal autotomy can learn how to compensate for the absence of a tail. Tails are also used for aerial righting maneuvers of geckos (Jusufi, Zeng, Full and Dudley, 2011) as well as active pitch control in lizards (Libby et al., 2012).
According to Jusufi, Goldman, Revzen and Full (2008) an absence of ground forces in air righting behaviors lead to a total angular momentum of zero and follows the equation:

$$I_B\left(\frac{\Delta\theta_{\boldsymbol{B}}}{\Delta t}\right)+I_T\left(\frac{\Delta\theta_{\boldsymbol{T}}}{\Delta t}\right)=0 \qquad (1)$$

Where I_B and I_T are the moment of inertias of lizard body and tail and $\Delta\theta_{\boldsymbol{B}}$ and $\Delta\theta_{\boldsymbol{T}}$ the angle change of body and tail of the lizard at a given time frame Δt. It enables the Lizard to rotate its body from a supine (upside down) position to a prone (right-side up) position seen in Figure 1b by rotating its tail in a circular motion perpendicular to the longitudinal axis of the lizard body. The lizard reaches the prone position approximately 106 ± 6 ms after dislodging in less than two of its body lengths (Jusufi et al., 2008). Furthermore Jusufi shows that an increase in tail length- body length ration increases the degrees of body yaw (Jusufi et al., 2010) which leads to the possibility of decreasing the tail inclination relative to the body or a decrease of the tail side sweep angle (see Figure 1a). The exchange of angular momentum of tail and body was later successfully implemented in RiSE, Robot in Scansorial Environment (Autumn et al. 2005) and Stickybot (Kim et al., 2007).

Jusufi et al. (2010) also claim that, contradictory to Mather and Yim (2009), tail-type inertia for righting of mobile robotics is advantageous due to its easy implementation of control algorithms, the reduced weight as well as the relative unimportance of the final position of the tail for the whole system

As described in Libby et al. (2012) lizards use exchange of angular momentum not only when dislodged from a foothold but also when transitioning between surfaces. This is especially important when lizards miss footholds, slip or face unanticipated aerial phases and therefore have no chance of generating planned ground reaction forces to control their body rotation. In these cases the tail is used through exchange of angular momentum (zero net angular momentum control) to reduce the body angular velocity enabling a stable landing behavior (Libby et al., 2012). The author describes a trial setup of a box-like vault with a vertical wall in lizard jumping distance. By reducing the friction of the surface of the vault a perturbation in the lizard's movement is induced. The perturbation is defined as angular momentum (H) and is normalized by body moment of inertia (I_B) about its center of mass (COM) and by the duration of the leap (t) to compare the perturbation magnitude between individuals. The tail effectiveness, as seen in Figure 1c, gives the amount of tailless body rotation a tail could stabilize per degree of tail rotation over the normalized perturbation $(H/I_B)t$. The diagram shows the reciprocal of effectiveness, meaning sallower slopes stand for a more efficient tail. Libby et al. (2012) show that the bio-inspired robot (Chang-siu et al., 2011) was twice as effective as the lizards due to the mass distribution to the end of the tail. Chang-siu et al. (2011) demonstrate that a dynamic robot with inertial appendage could enable rapid reorientation, improve fall survivability, and increase mobility and stability over difficult terrain. The author states that a reorientation of 90° is possible in one body length of vertical fall.

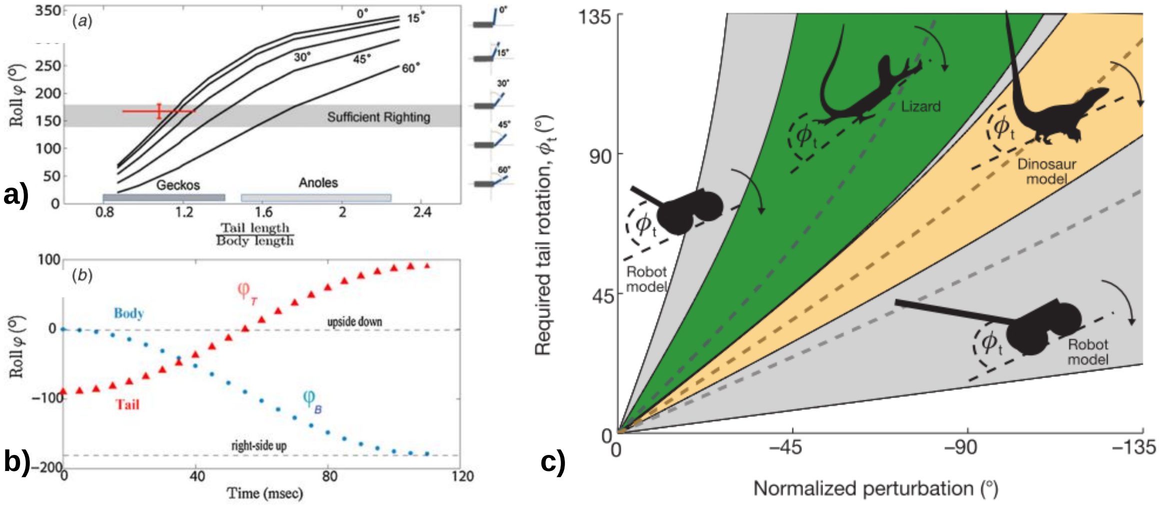

Figure 1: Zero net angular momentum control a)Tail length to body length ratio and inclination on induced body roll(φ) at tail inclination angle of 0°,15°, 30°, 45° and 60°. The shaded area depicts the area in which a complete turn from supine to prone position is possible. The red cross depicts studies of the house gecko where the vertical line indicates the final position and the horizontal line the tail length to body length ratio of the measured house geckos.(Jusufi et al., 2010) b) Righting performance of average house gecko of analytical model from supine to prone position where the body angle (blue points) and the tail angle (red triangles) are depicted over time (Jusufi et al., 2010) c) Tail effectiveness of Lizards, *Velociraptor* model and robot where the required tail rotation (Φ) is see over normalized perturbation. Averages are depicted as dashed lines. (Libby et al., 2012)

Recent research (Pullin, Kohut, Zarrouk and Fearing, 2010; Kohut, Haldane, Zarrouk and Fearing, 2012) show OctoRoACH and TAYLRoACH (Tail Actuated Yaw Locomotion RoACH) with integrated inertial appendage. Both robots are further developed versions of the Robotic, Autonomous, Crawling Hexapod, RoACH (Hoover, Steltz and Fearing, 2008). TAYLRAoCH is a 45 gram robot, with six flexible legs where each side of the robot is separately actuated. The separately actuated tail consists of a carbon fiber rod and a weight attached to its end. The total weight of the tail is 4 grams and represents a moment of inertia of $5.3\text{x}10^{-5}$ kgm^2 about its base (Kohut et al., 2012).

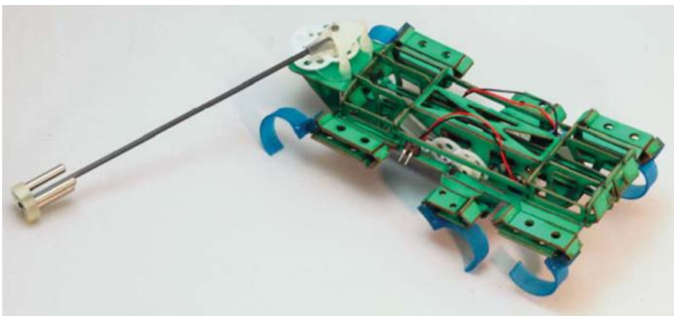

Figure 2: TAYLRoACH with integrated tail excluding electronics and battery for better overview (Kohut et al., 2012)

TAYLRoACH consists of two body components that stabilize the structure of the robot. These features are glued together, one from the bottom and one from the top. All other components are built onto this structure, enabling movement relative to this body part. The robot consists furthermore of two parts that are placed onto the front and the back of the robot to synchronize the pitch of the leg movement relative to the longitudinal axis of the robot. These parts are defined as synchronizers-front and -back. The front and back synchronizers are connected at their outer edge with the movable foot mounting and a stabilizing shaft at the center of the left and right section of the synchronizers. To achieve an asynchronous movement, meaning that at the time one set of feet are on the ground when the other set of feet are up, the leg mountings consist of three parts. The two leg mounting at the top and the bottom of the construction are non-movable mountings connected to the body structure. The middle part of the mounting, connected to the front and back stabilizer induces the movement of the legs. Every second leg at each side is connected to the top mounting on its top side and to the movable mounting on its bottom side. Every other leg is connected to the moving mounting on its top side and to the solid bottom mounting with their bottom sides.

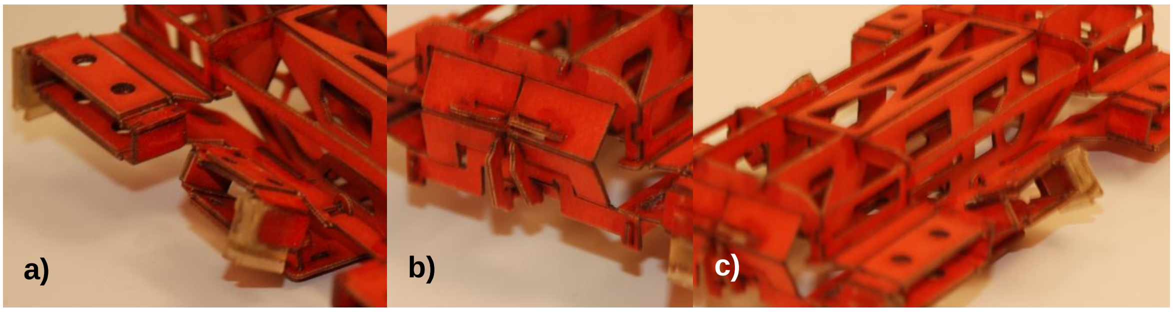

Figure 3: Design features TAYLRoACH a) Feet mounting, b) synchronizers and c) body parts

By rotating the middle section in the vertical pane, parallel to the longitudinal axis of the robot the middle mounting connected to either the top or the bottom of the legs induces movement in the legs. The leg that is about to touch the surface will make a straight movement back, parallel to the longitudinal axis, then roll to the side at an angle of approx. 45 degree and move forward without surface contact. In the TAYLRoACH, with six legs, the front and back leg of one side and the middle leg of the opposing side are doing the same movement. The phase of the remaining three legs is shifted by 90° resulting in the asynchronous motion with saddle-like feet trajectory (Figure 4b). Although the actuation of the middle foot mounting is 2-dimensional, achieved trajectory is 3-dimensional due to constraints and flexures on the feet mountings.

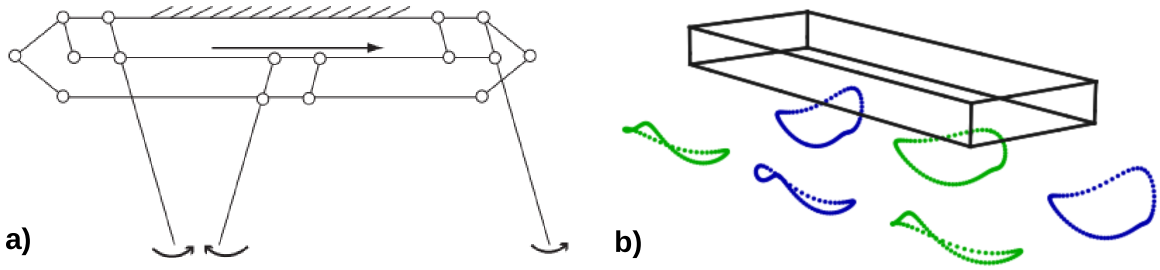

Figure 4: Feet trajectory a) Side view of feet trajectory showing upper, middle and lower feet mounting (Hoover and Fearing, 2008) b) 3D foot trajectories of robot where green and blue trajectories move in phase (Hoover et al., 2010)

N. J. Kohut et al. (2012) demonstrate that TAYLRoACH is capable of producing net turns of 90° at 300°sec^{-1}. The author furthermore points out that, due to missing sensory feedback and controlling abilities, limited to three separate actuators without phase looking, a high variation of performance was seen. Figure 5 shows an induced turn at a defined time of zero after a steady walk. Although it can be seen that the angular velocity is constant the final yaw position of the robot varies from approx. 150° to -50°. Kohut et al. (2012) state that varying factors for the turn might be friction and constraint forces as well as dynamics and mechanical constrains of the tail as well as impact forces at the end of the swing.

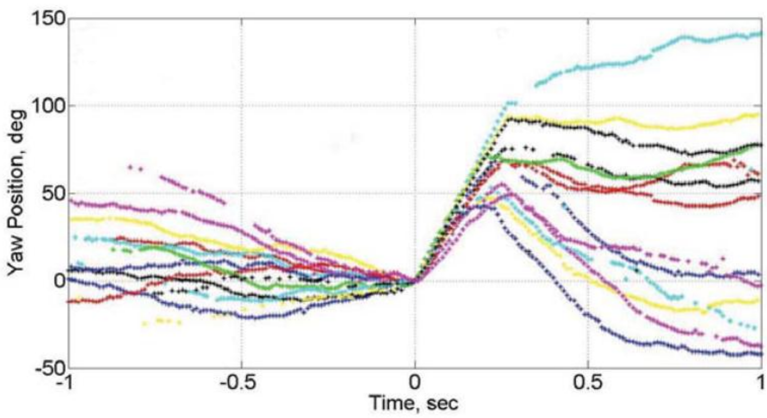

Figure 5: Body jaw versus time. Trails (n=14) normalized so that actuation of tail occurs at time and yaw rate of zero. (Kohut et al., 2012)

TAYLRoACH shows advantages in comparison to similar robots (Birkmeyer, Peterson and Fearing, 2009; Pullin et al., 2010; Kohut et al., 2011) due to both, a rigid structure and independently actuated feet rows. The rigid structure is important to withstand forces, generated when inertial appendages are actuated. The independently actuated feet rows give the advantage that it is possible to choose the foot constellation when the turn is induced.

Recent research (Chang-siu et al., 2011; Kohut et al., 2012; Lewis, Bunting, Salemi and Hoffmann, 2011) state that dynamic behavior in robots is feasible and although highly complex mechanisms have to be taken into account it increases maneuverability, stability and velocity. Further work showing dynamic ultra-high speed locomotion (Boston Dynamics Inc., 2012) implies that dynamic body bending for mobile robots in sagittal plane is implementable and successful for high speed control of velocities up to 45 km/h.

The state of the art shows the recent research necessary for the thesis and suggests that an implementation of dynamic tail and body bending behavior inspired by animals may increase maneuverability of mobile robots.

3 Background

After describing current research, this chapter demonstrates fundamental knowledge and basic principles important for the thesis. These include specifically biomimetics, motion analysis, vital information about calculation methods of the thesis and Smart Composite Microstructure (SCM), a novel fabrication process for robotic solutions.

3.1 Biomimetics

As a combination of engineering and biology this master thesis is part of the currently fast growing research area of biomimetics. Although the terms biomimetics, bionics, biomimicry and biomimesis have difference in historical origin, they are all derived from the Greek word *bios*, meaning life and *mimesis* meaning to imitate. Bionics, the first term to be added in the Merriam-Webster Dictionary (1960) is defined as:

"a science concerned with the application of data about the functioning of biological systems to the solution of engineering problems"

Even though biomimetics experienced a rapid development in the last 40-50 years, it has been used for centuries.

3.1.1 History

Due to extensive documentation Leonardo da Vinci (1452-1519) is seen as the first person who used bionics while studying the possibility of human flight (da Vinci, 1505). In the history of aviation many (Lilienthal, 1889; Tobin, 2004; Lüneberg, 2003) looked for inspiration in nature. Furthermore bionics was used in naval architecture (Baker, 1590 cited in Nachtigall, 2002, p.105), for agricultural purposes (Kelly, 1868) or for fasteners (de Mestral, 1955).

Since then biomimetics was a valuable research area and found even more popularity at the invention of the electron microscope. In the area of material science the self-cleaning Lotus-Effect® (Barthlott and Ehler, 1977) as well as drag reduction mechanisms using sharks skin (Bechert, Bartenwerfer, Hoppe and Reif, 1986) are known examples of biomimicry. The reduction of drag using shark skin is accomplished by micrometer-sized scales with riblets in stream wise direction and is used for high-performance swimsuits. The Lotus-Effect® is used for wall paint, roofing shingles and rim polishing agents and takes advantage of hydrophobic nanometer-sized wax structures which reduce the friction of the surface allowing the water to collect dirt while pearling of. Another bio-inspired material is the dry adhesive derived from the surface found on gecko feet. They consist of setae on uniform arrays of lamellar pads at a density of 14,400 per mm^2. The tip of each setae branches into 200 nanometer thick hair (Spatulae) which generate Van-der-Waals forces, to the substrate (Autumn et al., 2000). Dry adhesives are self-cleaning (Hansen and Autumn, 2005), reusable and don’t use chemicals for their adhesive property.

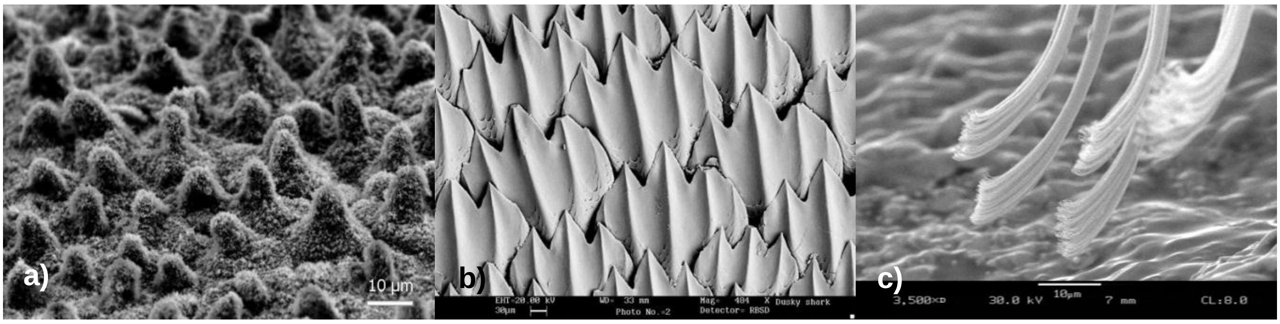

Figure 6: Scanning electron microscope (SEM) images of the a) wax structures of the lotus surface (Stratakis, Zorba and Barberoglou, 2009) b) scales an riblets of the shark skin (Lindsay, 2011) and c) the branching end of gecko setae (Autumn, Florance and Full, 2000)

Design optimization such as the CAO (Computer Aided Optimization) and SKO (Soft Kill Option) method by Claus Mattheck (1998) used by Adam Opel GmbH (Harzheim, 2008), Daimler AG (Daimler AG, 2008) as well as the Fin Ray Effect® (Bannasch and Kniese, 2011) used by Festo AG & Co. KG are examples for construction bionics. Biomimicry is used for passively self-regulating temperature control in buildings (Turner and Soar, 2008) and is used for a wide variety of sensors such as sonar (Rasmussen and Miller, 2004; Whiteley et al., 2010), electrical sensors (Schwarz, Hofmann and Von Der Emde, 2002) and fire detectors(Schmitz and Schuetz, 2000; Bleckmann, Mürtz and Schmitz, 1997).

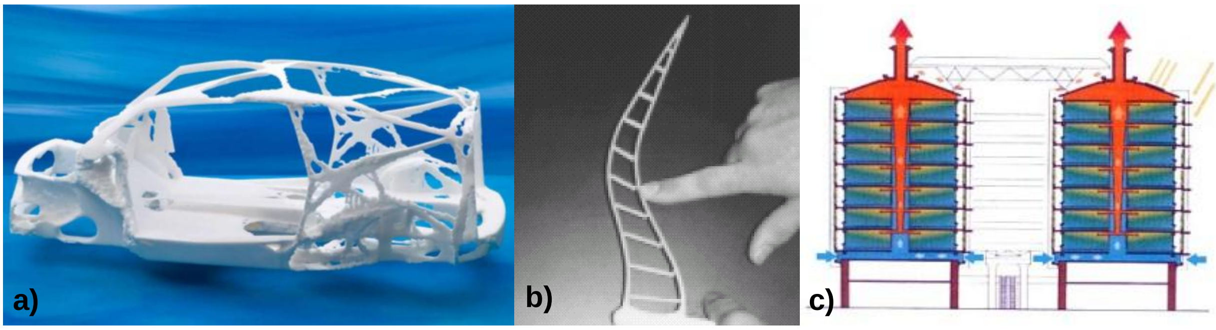

Figure 7: a) CAO Mercedes-Benz Bionic-Car (Mercedes-Benz Classic, 2008) b) Fin Ray Effect® (Wegener, 2007) c) Passive cooling Eastgate Center (Arquitetogeek, 2009)

The previous examples show that biomimetics has been in use for a long time and continues to gain importance for design and innovation processes. Even through these limited examples it can already be seen how diverse bio-inspired applications can be.

3.1.2 Overview of Subfields

Although nature was used as inspiration for centuries, biomimetics was established as an independent research area as recently as the 1950's. Since then an effort to define needed subcategories was made. A common way of classification by Werner Nachtigall is "structural-", "procedural-" and "informational" bionics (Nachtigall, 2002) and can be further differentiated into the following categories:

Category	Description
Structures bionics (Material bionics):	Biological structural elements, materials and surfaces
Device bionics:	Development of usable overall constructions
Structural bionics:	Biological constructions, closely related to above structural and device bionics
Anthropobionics (bionic robotics, bionic prosthetics):	Issues of human / machine interaction, ergonomics
Construction bionics:	Light constructions occurring in nature, cable constructions, membranes and shells, transformable constructions, leaf overlays, use of surfaces, etc.
Climate bionics:	Passive ventilation concepts, cooling and heating
Sensory bionics:	Detection and processing of physical and chemical stimulation, location and orientation within an environment
Locomotion bionics:	Walking, swimming and flying as primary forms of movement. Interaction with the surrounding medium
Neurobionics:	Data analysis and information processing
Evolutionary bionics:	Evolution techniques and evolution strategies, made useful for technology
Process bionics:	Photosynthesis, hydrogen technology, recycling
Organizational bionics:	Complex relationships of biological systems

Table 1: Subcategories of biomimetics (Gruber, 2011)

As a study of locomotion behavior of animals and its implementation in mobile robotics this master thesis falls into the category locomotion bionics.

3.2 Motion Analysis

A fundamental part of bionic research in locomotion behavior is the motion analysis. It can be divided in two categories: recording data and extracting data. For the recording aspect the biological trials the camera settings and software HiSpec Control Software (Fastec Imaging Corp.) and will be described. The data extraction is accomplished via the tracking software ProAnalyst (Xcitex, Inc.).

3.2.1 Data Recording

The camera model HiSpec 1 (specifications found in the appendix) from Fastec Imaging Corp. combined with a 25mm lens (Navistar, Inc.) was used to record the trials. The camera has an analog focus and aperture, a power cable with integrated trigger and is connected via Ethernet cable to a computer running the HiSpec Control Software. The Software GUI is separated into four sections as seen in Figure 8: the settings panel (1), the adjusted camera parameters panel (2), the video screen (3) and the recording controls (4).

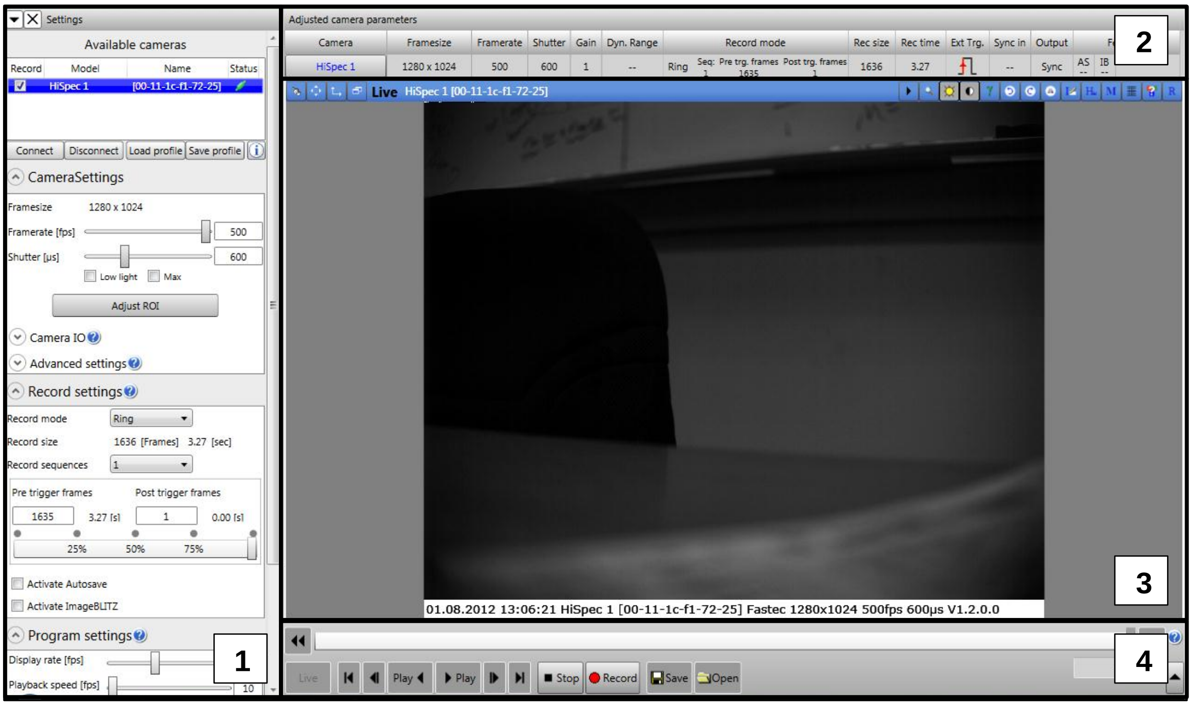

Figure 8: HiSpec Control Software GUI with setting panel (1), parameters panel (2), video screen (3) and recording controls (4)

The settings panel (1) can be divided into the camera connection field, which shows the connected cameras and the camera settings, which are used to define camera specific preferences. The camera settings include camera input and output preferences, where synchronization and triggers can be set as well as advanced camera setting. The settings panel also includes the record settings to define how the images are saved on the physical memory and which images are used in relation to the trigger. The program settings are manly video display and playback preferences as well as preferences of information displayed in the video description seen in the white line at the bottom of the video. Table 2 shows the important preferences for the project including their description:

Preference	Description
Frame Rate	Frequency at which consecutive images are produced (0-506)
Shutter-speed	Length of exposure time (2-1970 resp. 2-99994 in “low light” mode)
Frame dimensions	Dimensions of image (max. 1280x1024 changeable in “Adjust ROI”)
Blacklevel	Brightness of darkest part of image
Digital gain	Gain of video signal
Record Mode	Defines continuous recording where the oldest frame is overwritten by the newest frame, Record-On-Command (ROC) at the time of a user provided signal or Slip Sync. which operates with a frame rate defined by an external input signal (e.g. synchronized to tachometer)
Record Size	Defines the number of frames of the recording loop when record mode is set to continuous recording (max. 1636 frames)

Table 2: HiSpec Control Software: Main preferences

The adjusted camera parameter panel (2) in Figure 8 displays the current parameter and helps keep an over-view of different cameras and different camera profiles used. The video panel (3) shows the video in live mode, recording mode or video mode. A panel at the top of the video screen allows simple video interaction, such as zooming, rotating, flipping, changing gamma settings, adding comments to the info line, showing the histogram and many others. The recording controls (4) are used to switch display modes and interact with the recorded video such as cropping and saving.

When recording a trigger or other predefined input signal is used to stop the camera from recording. The video raw data is then sent from the physical memory of the camera to the HiSpec Control Software where the video can be reviewed, cropped and saved. If more than one interesting feature per video is recorded either two separate videos can be saved after being cropped or both cropped segments saved as one video file. The software provides an automatic labeling feature which includes date and time stamp in the video name.

3.2.2 Data Extraction

After the data acquisition is completed the data has to be extracted. To this end the tracking software ProAnalyst® by the company Xcitex, Inc., program specifically for tracking and video analysis in 2D or 3D space, is used. The GUI, as seen in Figure 9, consist of the toolbar panel (1) (Main Toolbar, Sync Play Toolbar, Annotations Draw Toolbar, Annotations Visibility Toolbar, Play All Toolbar), the video panel (2), the controls panel (3) and the play controls panel (4). The

Toolbars contain general functions to open, save, and print as well as functions to view or hide additional control and processing features such as graphs, calculations, histograms, timelines and various zoom options. The video panel shows the currently processed video. Additional features like rulers and showing the reticle can be applied. The controls panel features tabs for Image Processing, Image Filtering, Multi-Plane Calibration, Display Layers, Notes, Annotations, Line Tracking, Feature Tracking, Stabilization, Contour Tracking, Graph Configuration and gives the option to Save All Associated Toolkits.

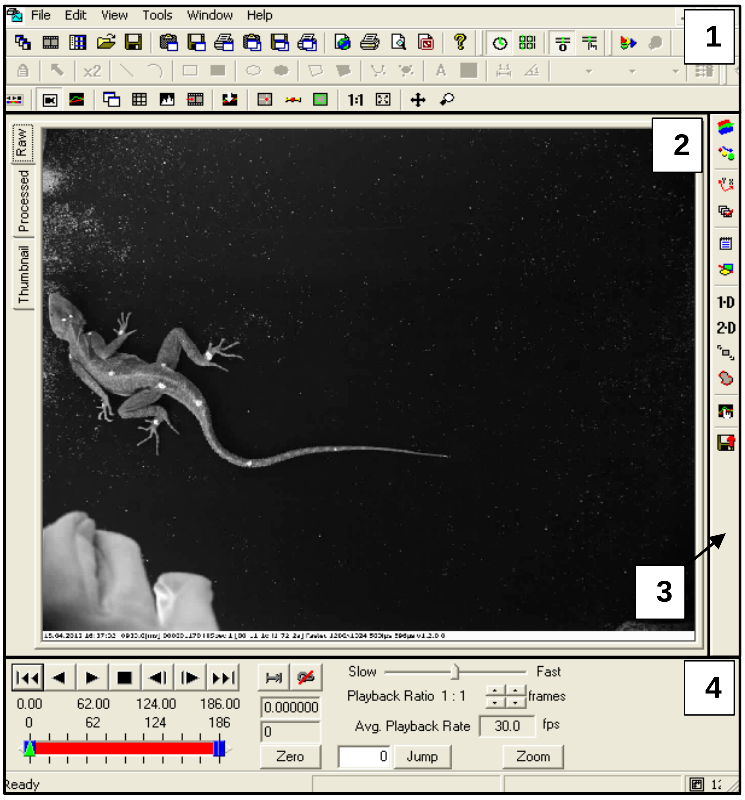

Figure 9: ProAnalyst GUI 1) Toolbar panel 2) Video panel 3) Controls panel 4) Play control panel

Before a video can be analyzed and saved correctly, a 2D resp. 3D calibration is necessary (Figure 10 - Multi-Plane Calibration). Next video manipulations can be realized by configuring the brightness, contrast, gamma correction as well as nonlinear input/output mapping. In Figure 10 the settings widow for Image Processing can be seen with the used image preferences for a specific trail. The Image Filtering Tab allows the user to apply many different filtering masks. The filtering features are categorized into Arithmetic, Common, Convolve, Histogram, LUT (lookup table), Morphology, Neighborhood and Lens filtering operations.

The general concept of the tracking software is the search for the previously defined image areas in every frame. The settings panel for feature tracking, seen in Figure 10 consists of basic controls as well as the currently defined parts of the lizard that should be tracked. The preferences for these points can be seen in Table 3. Depending on the tracking mode “Manual”, “Automatic” or “Delete”, further control options are enabled seen in Figure 10. The lower section of the panel enables export of acquired data.

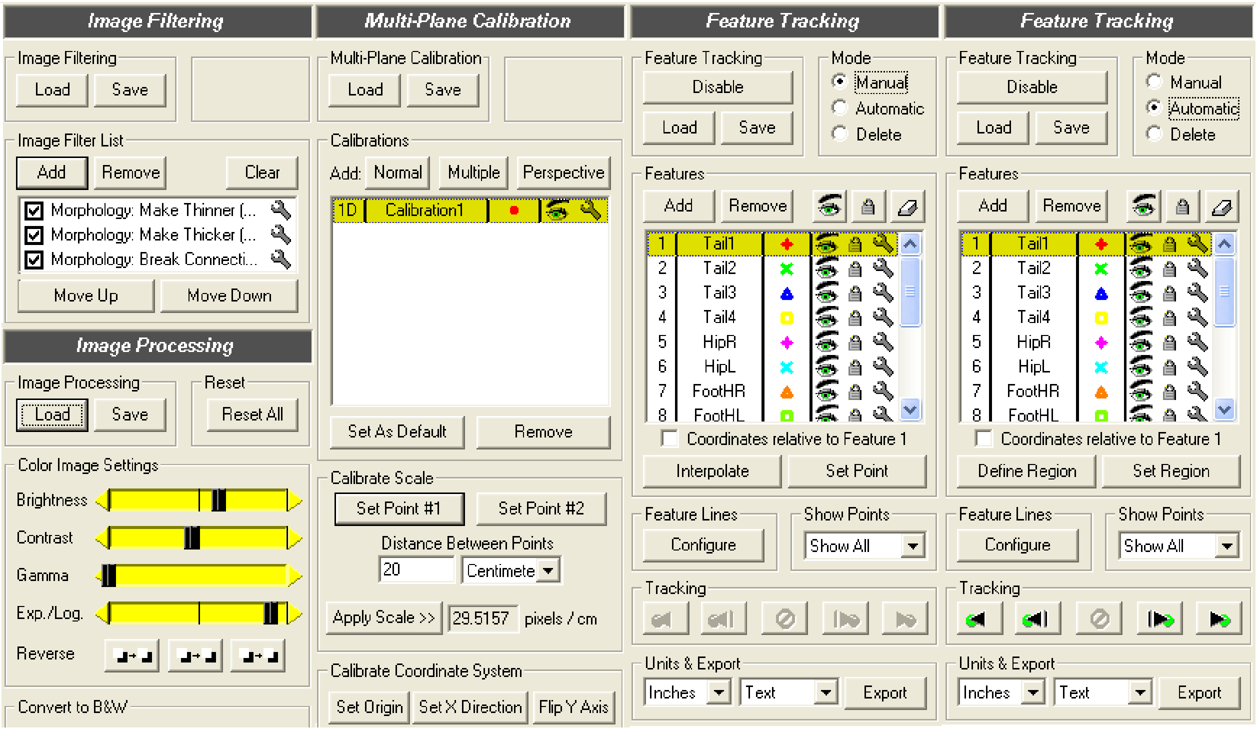

Figure 10: Setting panels for the Control Tabs of ProAnalyst®: Imaging Filtering, Image Processing, Multi-Plane Calibration and Feature Tracking for Manual and Automatic mode

To decrease tracking time while guaranteeing retrieval of defined tracking areas, following preferences can be set:

Preferences		Description
Search Region Multiplier (%)		Defines the region in which the data point should be searched for. Value is defined in percent where 100% is the same size as the defined tracking point.
Threshold Tolerance (0.0-1.0)		Defines the similarity between found region and predefined tracking point. At a value of 1 the program searches for identical regions.
Special Target Types		Defines if the tracking point is of constant shape. (e.g. white circular point on black background, 4-cell black and white chessboard pattern)
Feature Rotation	Angular Range (deg)	In case of a rotating region, this field defines the angle range the program will rotate the predefined tracking point to search for similar regions
	Step Size (deg)	Defines the step size of the rotation of the predefined tracking points to find similar regions.

Table 3: Feature tracking preferences

After defining all regions that should be tracked and their feature preferences the video data can be tracked. Depending on the tracking mode a manual or automated search for the following regions has to be conducted. If the automated tracking doesn't find similar regions or diverges from the tracking point, the original tracking point has to be redefined. If tracking points are temporarily covered or leave the image range an interpolation can be applied using the manual tracking setting. After completing the feature tracking the tracked data can be exported.

3.3 Inertia Measurement

When calculating dynamic properties of a given system, not only the data extracted from video recording is necessary but also physical attributes such as mass, center of mass (COM) and moment of inertia (MOI). The master thesis used measurements from cadavers to approximate these attribute for living animals.

The center of mass (COM) was measured using the plumb line method (Blackmail, 1925). This method, as seen in Figure 11 uses a plumb-line, a string with an attached weight, to generate a perfectly vertical line. By pinning the string to a location (P) on the segment the string shows a line that must pass the COM. The object is pinned in this way to two different locations, P1 shown as a blue dotted line and P2, depicted as black line. The intersection point of the resulting lines is the center of mass (red).

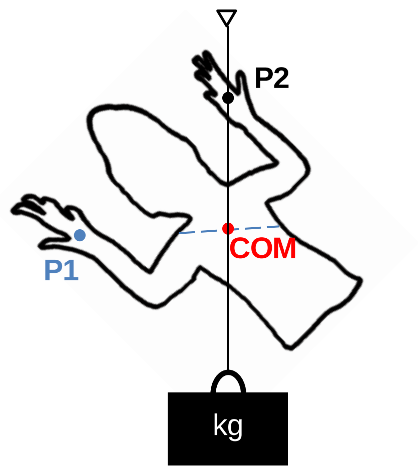

Figure 11: Diagram of the plumb line method

After the COM is obtained the measurement of the moment of inertia can be conducted. This measurement was realized using the pendulum method (Dowling, Durkin and Andrews, 2006) seen in Figure 12. The author shows that the precision of moment of inertia measurements is mainly influenced by the distance D between the axis of rotation and the center of mass. Dowling et al. (2006) state, that an iterative convergence of D toward the radius of gyration increases the precision of the MOI. The author describes how an object of any shape, of mass m, length l and radius r, can be hung at an axis with distance D to the center of mass and oscillated to calculate the moment of inertia. The initial value D is approximated and lies roughly at half distance between center of mass and either end of the object. By calculating the MOI and the associated ROG, a new distance D of the value of ROG can be achieved by repositioning the axis of rotation.

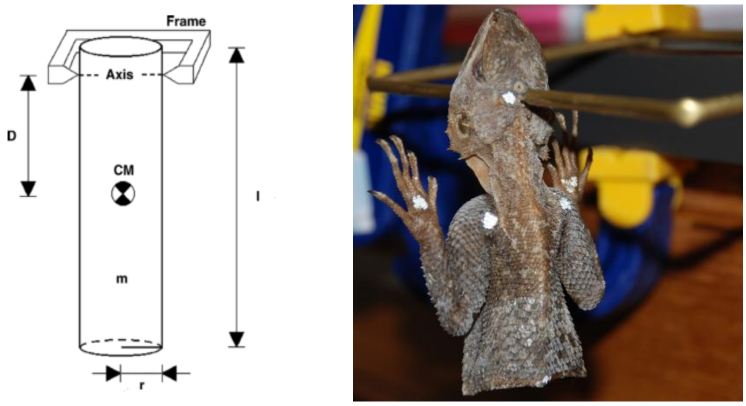

Figure 12: Pendulum method for measuring the moment of inertia

According to Dowling et al. (2006) the calculation of the inertia follows Formula (2) where I_{CM} represents the moment of inertia about the center of mass (kg*m^2), t the period of the oscillation in seconds, m equals the mass of the segment (kg), g represents the gravity (9.81 m*s^-2) and the distance D from the axis of rotation to the center of mass in meters.

$$I_{CM} = \frac{t^2 mgD}{4\pi^2} - mD^2 \tag{2}$$

Following the radius of gyration is calculated by:

$$ROG = \sqrt{\frac{I_{CM}}{m}} = D_{new} \tag{3}$$

3.4 Truncated Elliptical Cone

Measurements on cadavers are not the only way to approximate attributes such as center of mass and moment of inertia. Another method of approximation is the calculation of known geometries similar to the approximated objects.

An often used approximation of the human body is the truncated elliptical cone (Kwon, 1998). A truncated elliptical cone is described by two elliptical spheres with differing major and minor axes, which shape the base and top of a converging solid. Figure 13 shows the top major and minor axis as b_1 and a_1 and the base major and minor axis as b_0 and a_0. The height is depicted as L. Due to the similar shape of the lizard tail segments the truncated elliptical cone can be used as an approximation.

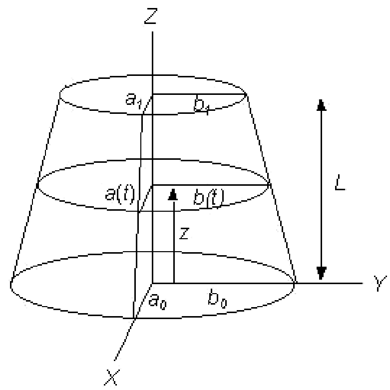

Figure 13: Truncated elliptical cone
(Kwon, 1998)

According to Kwon (1998) the mass, COM-distance and MOI of the truncated elliptical cone can be derived by:

$$m = \pi\rho L * G_{20}(a,b) \tag{4}$$

$$g_z = \frac{G_{21}(a,b)}{G_{20}(a,b)} L \tag{5}$$

$$I_{xx} = \frac{\pi}{4}\rho L * G_{40}(a,b,b,b) + \pi\rho L^3 * G_{22}(a,b) - m g_z^2 \tag{6}$$

where ρ is the density of the solid, the mass m, g_z the distance front the center of mass to the base of the elliptical frustum and I_{xx} the inertia around the x-axis of the center of mass. The replacement terms G_{20}, G_{21}, G_{22} and G_{40} can be reviewed in the appendix. The replacement functions are functions of a, the height of the lizard and b, the width of the lizard signifying relation to height and width of the bottom and top, a0, a1 and b0, b1 of the solid. These formulas were used to approximate the needed segments of the lizards.

3.5 Smart Composite Microstructures

The final section of the background gives a short overview of a novel fabrication method known as smart composite microstructure (SCM) as well as describes its advantages. This fabrication method was used to build physical demonstrators and robots being central to the design circle of the thesis.

A simple way to prove principles such as zero net angular momentum control (Libby et al., 2012) is by designing robots using the smart composite microstructures (SCM) fabrication method developed by Wood et al. (2008). The fabrication method combines a quick manufacturing process with easy methods of joint integration through a laser micromachining and lamination process. This fabrication method uses either carbon fiber or S-glass reinforced plastics in combination with compatible polymers to achieve millimeter-scale robots (Avadhanula, Wood, Campolo and Fearing, 2002). Further development of this fabrication method (Hoover and Fearing, 2008) enabled the use of SCM for macro-robotics using poster board and a polyethylene terephalate (PET) film. The fabrication process consists of five steps, which are depicted, in Figure 14. In the first step two poster board sheets (black) are layered above each other (1). Next the two sheets of poster board are laser-cut at the position of the predefined flexures (2). In the following step the two poster board sheets are coated one-sidedly with an adhesive polymer. The flexural polymer (PET) with high melting point is placed between the adhesives (3). The resulting layer assembly is then rolled through heat rollers to bond the individual layers (4). The final step of the fabrication (5) is the cutting of the outlines of the part to separate it from the sheet.

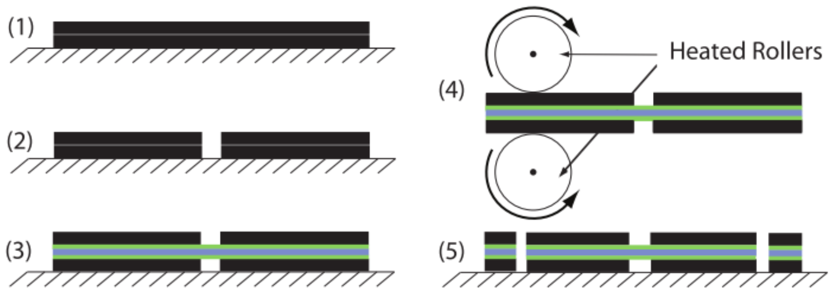

Figure 14: Step by step fabrication process smart composite microstructure (SCM) (Hoover and Fearing, 2008)

The resulting 2-dimensional robot parts are able to flex at the sections where both poster board sheets are removed while the polymer in combination with the adhesive sheets is intact. The flexure angle can be influenced by the thickness of the notch. To complete the robot the parts have to be folded and glued into place, leaving either rigid structures where flexures have been constrained or structures with movable flexures.

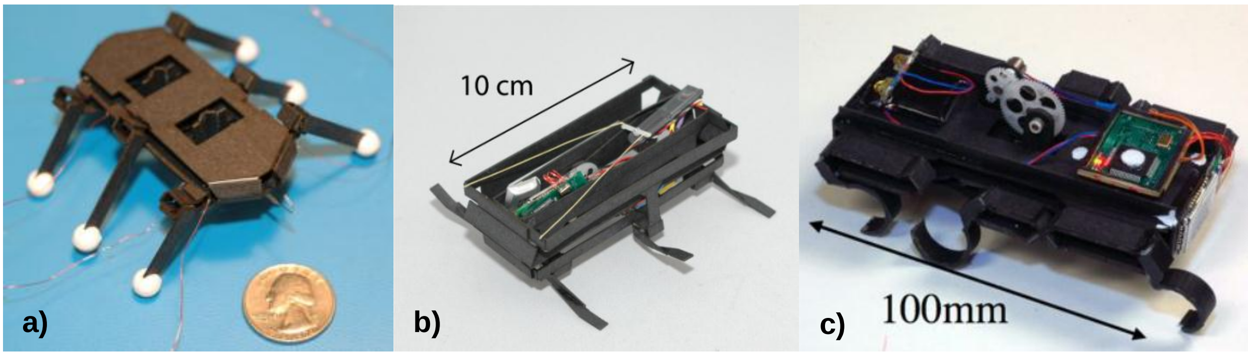

Figure 15: Robots using SCM a) RoACH (Hoover and Fearing, 2008) b) DASH (Birkmeyer, Peterson and Fearing, 2009) and c) DynaRoACH (Hoover et al., 2010)

This technique is used for many different types of robots as seen in Figure 15 including RoACH (Robotic, Autonomous, Crawling Hexapod) (Hoover, Steltz and Fearing, 2008; Hoover and Fearing, 2008; Wood et al., 2008), DASH (Dynamic Autonomous Sprawled Hexapod) (Birkmeyer, Peterson and Fearing, 2009) and DynaRoACH (Hoover et al., 2010) seen in the figure above.

Compared to other rapid fabrication processes used in mobile robotics such as rapid prototyping, SCM is a low cost solution combining cheap materials and integrated joints. Stability of the material can be increased or decreased via design solutions such as reinforcements or recesses. Furthermore the material and the integrated flexing solutions reduce weight of mobile applications Although this fabrication process require construction drawings in 2D which reduce the visualization, the rapid fabrication and construction increase effectiveness of the design circle (Hoover and Fearing, 2008).

4 Biological Studies

After introducing the thesis topic, presentation of the state of the art and giving an overview of fundamental principles, the biological aspects of the master thesis are described. The chapter describes the data acquisition concerning used equipment and procedure.

4.1 Animals and Habitat

The animals used in this research project are of the species *Agama Agama* also called Red Head Agamas. This lizard species can be distinguished by the reddish head and tail tip and the blue body of the males in mating season. The females and males when not in mating season have a brown body color. They can be found in Central Africa, the Ivory Coast as well as in Tanzania and Angola and southern parts of the United States of America. They can grow up to 41 cm and live in stony-sandy environments of 30-40°C at daytime and 24-30°C at nighttime. They eat mainly insects, worms and spiders. Males are very territorial (Madsen and Loman, 1987). The species was chosen due to their availability in California due to their compatibility with the climate as well as their survivability in captivity. The insect and small vertebrate facility at UC Berkeley at the Valley Life Sciences Addition – Basement (LSAB) held seven specimens. The population held two small lizards weighing up to 40g, four medium sized lizards between 40 and 80g and one big lizard weighing above 80g. The lizards were numbered from one to seven and marked with whiteout to be able to identify them for the trials.

The habitats of the lizards at the animal facility consisted of two smaller tanks of a capacity of 500 liters holding up to two Lizards and one big tank (1000 liters) holding up to five lizards. The separation of Lizards was established due to the territorial behavior of the animals. The tanks were fitted with a sand substrate as well as stones and pottery pieces for basking and a watering place and shelter. The room was heated to approx. 27°C, had a humidity of 10 - 20% and was fitted with full spectrum lighting (UV radiation) promoting calcium metabolism by vitamin D production (Coates, 2009, pp.69–71). The animals were fed crickets twice a week.

Due to inefficiency of former trial procedures conducted in the CiBER laboratory caused by distressed animals, the animal trials were conducted in the living habitat of the lizards. This approach was an attempt to standardize animal trials in their living habitat and was to be designed so that following trials could be done in the same way.

First the position of the cages was changed in such a way that all cages were on ground floor so that lighting and filming as well as the conducting of the trials resp. various stimuli could be easily performed. Second, as described in Chapter 4.2 the lighting and camera settings were adjusted according to the new environment. The habitat itself was changed initially that the agamas had to run trials on wooden slabs which were covered with sandpaper. Although this would guaranty a stone-sand like friction the idea proved unsuccessful due to bad cleaning properties of wood and sandpaper. Consequently the conditions for a suitable substrate were defined as washable or disposable, sufficient friction for enough foothold while not changing its form as e.g. sand. Furthermore it was deemed necessary to be easily removable from the cages and if possible unreflective to guaranty good video recording background. After investigating different anti-sliding-mats as well as anti-sliding-tapes used mainly for stairs, an ethylene-vinyl acetate (EVA) foam gym-matt (We Sell Mats) was chosen which fulfilled these properties. Preliminary test resulted in very good trial characteristics, giving good foothold and a good background for video analysis. After more mats were ordered and fitted to the tanks of the animals, the trials described in Chapter 4.2.4 were conducted. Later during the research period it became apparent that the mats out of natural caoutchouc were eaten or chewed on by the live food of the lizards, endangering the health of the animals. This resulted in removal of the mats which were consequently placed into the cages temporarily at trial phases.

As shelters for the animals, stone piles as well as pottery shards and plastic housing with one or more openings, depending on their size were used. As described in Chapter 4.2.3 the housings had to be changed in size, form and position. To this end cardboard tubes were cut lengthwise leaving on side open as an entrance and the other side closed ensuring no escape of the animals via the wrong side. These shelters were then used as escape holes for the lizards positioning then according to the trail procedure.

The habitat was changed at least one week prior to the trail to the arrangement necessary for the procedure. This way the animals could get accustomed to the new environment and could react fast to threatening stimuli. To be able to test individual animals the cages were divided using a cardboard sheet separating needed animals.

Additionally a habitat-change to accommodate two high speed cameras for 3-dimentional data acquisition was discarded due to the complex implementation and the fact that the conducted research aimed primarily on the capturing of the lateral movement of the animals. This reasoning lead to the conclusion, that an overhead high-speed camera, without the integration of a side-view window for additional recording was sufficient.

4.2 Data Acquisition

Following the adjustments of the habitat the data acquisition could be conducted. Necessary steps to for the recording of locomotion behavior of animals are the clarification which equipment is used, the arrangement of the used equipment and the trail procedure.

4.2.1 Equipment

The used equipment shown in Figure 16 consisted of lighting equipment, a high-speed camera and a computer with the necessary camera software provided by the camera manufacturer. Due to the high resolution and high-speeds at which the camera has to operate to capture the rapid movements of the lizards, the lighting of the trial setup has to be very bright and uniform. Additionally the light would have to be moved to the living habitat of the lizards and rearranged for different trial setups. To achieve these requirements 3 halogen lamps of the company Cooper Lighting (Cooper Industries plc.), two 250 Watt (PQS2504IN1) and one 500 Watt (SQS505QD) with UV filters, available in the laboratory were used. Previous animal trials (Mongeau et al., 2012; Libby et al., 2012) using these lighting solution proved successful. Due to their high power and the resulting heat generation the lamps had to be handled with caution these factors taken into account when arranging the equipment. As described in the background, the camera model HiSpec 1 (specifications found in the appendix) from Fastec Imaging Corp. combined with a 25mm lens (Navitar Inc.) was used to record the trials. The camera was mounted on a tripod for over-head view as seen in the arrangement section in Figure 16. After defining the Local Area Connection IPv4 as 192.168.3.1 and connecting the HiSpec camera via Ethernet cable the preferences of the HiSpec Control Software (Fastec Imaging Corp.) seen in Table 4 were set. A description of these features can be seen in Chapter 0.

Preference	Value
Frame Rate	500 fps
Shutter-speed	approx. 600 µs
Frame dimensions	1280x1024 (default)
Blacklevel	128 (default)
Digital gain	1 (default)
Record Mode	Ring (continuous)
Record Size	1636 frames (predefined)

Table 4: Fastec Camera - HiSpec Control Software Preferences

A frame rate was chosen to enable easy controllability of generated time-steps. The shutter speed was chosen depending on lighting condition and resulted in approx. 600 µs for the conducted trials. The frame size was set to maximum dimensions reducing the distance to the camera resulting in higher resolution. Continuous recording was enabled with maximum recording size resulting in 3.27 seconds of recorded video. An external trigger which reacted at the falling edge was used to stop the video stream after a locomotion behavior was observed. The pre-trigger frame function enabled the saving of the frames prior to the induced stop by the trigger. The chosen format for the video trials was the AVI (Audio Video Interleave) video format using Xvid codec compressing it to 90% of the original quality. This shrinks the raw video from up to 2GB down to under 20MB for each trial and guaranties a high resolution combined with fast video imaging and processing. All trials were saved in the following format:
RecordingDate\AnimalNo_TrialNo_FolderDate_FolderTime\AnimalNo_TrialNo_VideoDate_VideoTime_FolderDate_FolderTime.avi
Where folder resp. video date and time depict the date and time of creation resp. saving.

4.2.2 Arrangement

The equipment was arrangement according to uniformity of light in the area of the trial setup in the cage, to enable a sufficient range of camera view and also to allow for induction of stimuli. Additionally the equipment had to be arranged in a way that the stimulus could be induced without interfering with the behavior of the animal and the video recording of the trail.

There were two main setup models: free-standing cage and cage in scaffold. The scaffold posed a further influencing factor for the arrangement by preventing overhead accessibility. Figure 16 shows the two different arrangement settings.

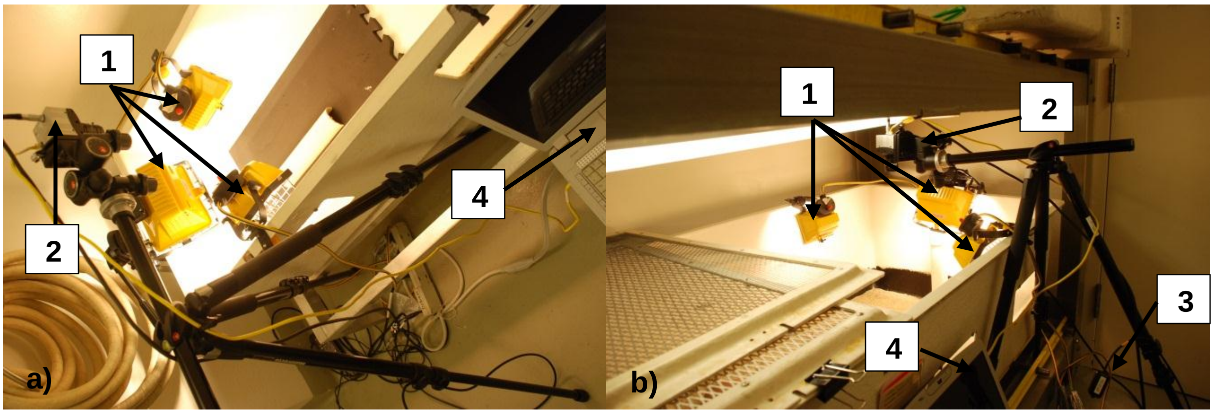

Figure 16: Equipment Arrangement a) free-standing cage b) cage in scaffold with spotlights (1), camera (2), trigger (3) and computer with HiSpec Control Software (4)

The choice of the arrangement was dependent on which cage held the lizard that had to be used for current trials. The first arrangement (Figure 16a) shows that the lights were directed towards the walls of the tank to reduce reflections in the video and to illuminate the trail setup uniformly. The 500 Watt light was mounted on the frontal side of the tank and directed towards the wall. The two smaller 250 Watt lamps were then fixed to the side of the tank pointing towards the tank wall to cancel out any shadows created by the bigger lamp and to illuminate the trial setup collinear with the lizard's movement. The cables of the lamps were wrapped around the lamp mounting to avoid cable burn. Due to its slow frequency, the regularly used full-spectrum UV light was unfavorable for the light quality of the video resulting in oscillating brightness. Despite this disadvantage it was kept in place due to the importance of ultraviolet light for the lizards. Also the alignment of the three halogen lights reduced this effect. The camera was mounted on a tripod with extension and was positioned on the side of the tank so that the camera would be suspended above of the trial setup. The stimulus was then induced by reaching over the 500 Watt lamp and would prompt the Agama to run in lengthwise direction of the recorded video as shown in Chapter 4.2.3.

The second arrangement as seen in Figure 16b incorporated the carrier scaffold of the tank in a way that the lamps were mounted onto the overhead beams. This arrangement as well used the

500 Watt lamp at the front side of the tank and the smaller lamps on the side to reduce the shadows. The lamps in this layout also looked at the tank wall resp. the room wall. The camera was positioned between the overhead beams and the tank. Stimuli were induced via the corner of the tank between the 500 Watt lamp and the camera tripod. In both arrangement settings the camera was arranged approx. 1 m above the tank substrate guaranteeing a big enough video frame while centering solely on the turn of the lizard. The position of the equipment was marked to decrease the preparation time and to make sure that the videos of each day were similar.

4.2.3 Trial Setup

Using the above mentioned equipment arrangements two sets of data collection were conducted. The first at the beginning of the project using full frictional substrate, the second after the first trials were analyzed, using a low friction underground.

The trial setup for the first trial-set consisted of two different types of shelters, named positioning shelter (1) and escape shelter (2), with openings pointing toward each other. The positioning shelter, aligned directly underneath the camera differed from the escape shelter by a pipe which was fixed in such a way that it would induce a certain position of the lizards in the shelter. This was important since early in the trials it was found that in a normal shelter the lizards would curl up in a corner which in turn wasn't a good initial position for the escape response. To avoid this position, as described in Chapter 4.1 a cardboard tube (3) was cut lengthwise and placed into the positioning shelter. The tube was small enough as to fit into the shelter and to make sure that the lizard would be aligned in a straight position, but not small enough to be uncomfortable for the animals. The second shelter, escape shelter (2), was used as a shelter that the lizards would recognize as a refuge and would escape into. The escape shelter was used to give direction to the escape response of the lizards towards a flight angle of 180°.

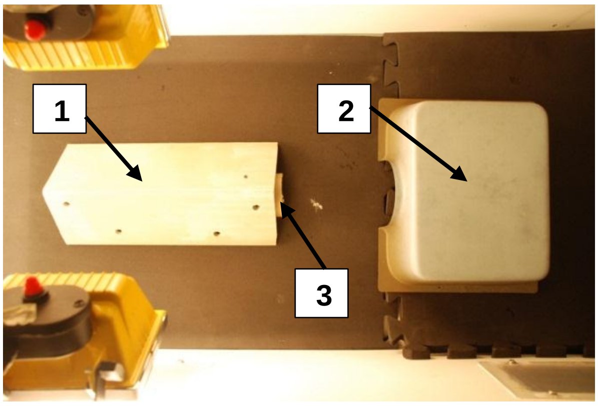

Figure 17: Cage arrangement for trial setup including positioning shelter (1) and escape shelter (2)

The second trial-set was conducted using an oil coated metal sheet to minimize the friction of the substrate. The metal sheet was placed underneath the camera position. Although the positioning shelter was not used at this set of trials the escape shelter was used to give the lizards a destination angle.

4.2.4 Trial Procedure

As mentioned before the first step of conducting the trails was the calibration of the high-speed camera. This was done using a ruler and taking a photo using the camera. When the videos are tracked as described in Chapter 5.1, the ruler will be used to define the coordinate system for the video.

The general systematic of the trail was to present a stimulus, inducing an escape response in the lizards. The optimal escape would entail a 180° turn and a following run towards the escape shelter. To achieve this motion the lizard was initially scared into the positioning shelter aligning the lizard with straight body and tail, looking in the opposite direction of the escape shelter. After a short pause to calm the animal the positioning shelter is lifted carefully so that the lizard stays in the aligned position. The lizard will watch the shelter lift of and out of sight, which will rotate its head into an upwards position. This position is necessary for the lizard to see firstly the escape shelter and secondly the stimulus. After a short pause that the Agama needs to orientate and evaluate the opening of the escape shelter as a possible hideout, the stimulus can be induced.

How the stimulus is induced is an essential part of the escape behavior. If the stimulus is induced to early the lizard will not escape towards to escape shelter, resulting in less than 180° of flight angle. If the pause before the stimulus is induced is to long the lizard will turn on its own accord to run into the shelter using motion which would not be defined as an escape response. The stimulus was conducted via gloved hand moving first slow towards the lizard, to capture the lizards attention and shortly before the lizard’s head accelerated into a grabbing motion. According to Hall et al. 1986 and Cooper et al. (2007) slow stimuli induce a turn of approx. 90° due to the fact that the lizard wants to keep the predator in its view. Faster induced stimuli provoke the agamas to escape directly away to increase the predator-prey distance (Domenici and Blake, 1997; Cooper, Pérez-Mellado and Hawlena, 2007).

After the stimulus is induced the escape response, described in Chapter 4.2.5 towards the escape shelter can be seen. A diagram seen in the appendix visualizes the trial procedure.

The resting of the animals throughout the animal testing had great significance for the conducted trials. It was deemed imperative that the animals didn’t get used to the stimuli which is why the animals were periodically left by themselves to return to their initial at-ease state thereby increasing the fear of being handled. An agama would be exposed to up to five trials in a row, depending on its reaction to the stimuli, and then left without physical presence for half an hour.

The number of trials to be conducted in a row depended on their level of escape response. A slower reaction to a stimuli was, due to the standardize stimuli process, interpreted as getting used to being handled. In this case a pause of approx. 30 min was initiated to increase their escape response. To further heighten their escape response behavior a period of 3 days testing was followed by 7 days of resting period. During the trials it was seen that the lizards, if scared too much would lose much of their orientation in the cage. This is why enough time had to be given to the lizards to orient and know their surroundings. The best way of chasing the agama into the positioning shelter was to scare them around the cage until the lizard was in a position in which he would see the opening of the positioning shelter. After a short orientation break, in which the lizard recognizes the opening and identifies it as an escape option a short stimulus would initiate an escape into the shelter. In general this method of handling the lizards would ensure good results.

As mentioned in Chapter 4.1 the behavior of the animals varied significantly if the environment in the cages changed shortly before the trials were conducted. The lizards would be confused and would not identify the shelters as escape possibilities. This is why the caoutchouc mats combined with the positioning and escape shelter had to be place at least two days prior to the execution of the trials. This method guaranteed an escape of the lizards towards the known hideout places.

4.2.5 Animal Motion

After inducing the stimulus the desired reaction of the agama is firstly bending its head, followed by an outwards push of the outer front foot, combined with a forward push of the hind legs as seen in Figure 18. Due to the push of the front foot the body starts bending. At the same moment the tail starts swinging in a planar trajectory towards the bending direction resulting in a trough-form of the body and tail. Next the front feet lift of the ground starting the aerial-phase of the front feet. The lizard uses tail and body motion to swig around using its hind feet as rotational center. At dropdown the tail and body will have already started their uncurling motion. In the optimal case the lizard then accelerates the tail towards its other side to using the stored up energy of its first curling motion to finalize its movement. Combined with a forceful stride of its outer hind leg, the lizard propels in the opposite direction of the stimulus.

The trials with reduced friction followed the same motion sequence. The reduction of the friction was used to minimize the ground reaction forces thereby maximizing the influence of the tail and body motion on the turning behavior of the animals. Under absolute absence of friction and the hypothesis that there is an exchange of angular momentum between tail and body as well as a total angular momentum of zero, the agama should curl und uncurl and regain its initial position. Reduced effects show the low friction trial sequence in Figure 18 when comparing body angle change of normal and low friction trial.

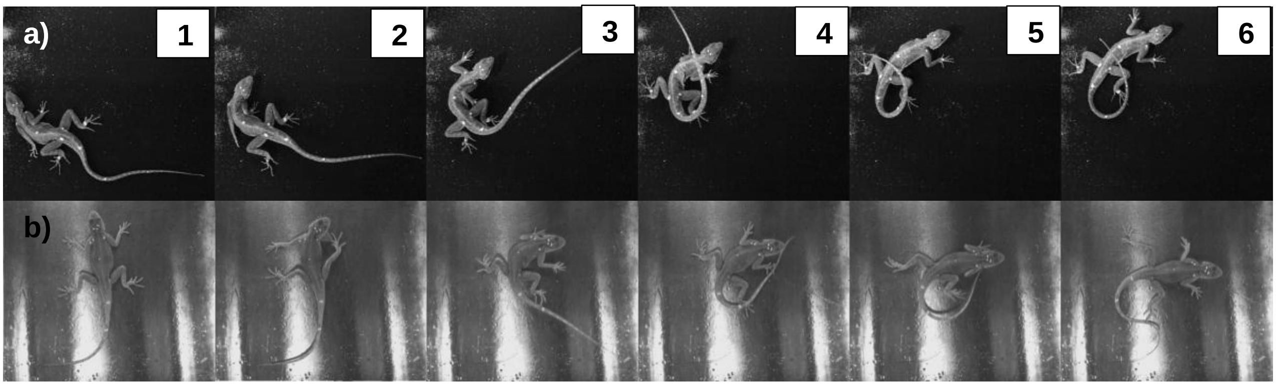

Figure 18: Trial Sequence a) Normal Friction b) Low Friction with start of move (1), pushing-phase (2), aerial-phase (3), curling-phase (5) and counter-swing-phase (6)

A complete Excel Spreadsheet (Microsoft Office) describes the phases of each trial. The phases can be categorized as follows:

- Start of movement (1)
- Curling-Phase
  - Pushing-Phase (2)
  - Aerial-Phase (3)
- Curling maximum (4)
- Uncurling-Phase (5)
- Counter-Swing-Phase (6)
- Running-Phase

Each phase was documented describing the time in the video recording. Furthermore as shown in Table 5 the body rotations are noted in degrees. Similar rotation angles and times can be extracted using this Spreadsheet to find comparable trials. The complete Excel Spreadsheet can be found in Appendix D.

			rotation		outer front foot				
Day	Animal	Trial	body	tail	start	lift-of	touch-down	curling start	uncurling end
24	1	1	90	-30	0.092	0.128	0.18	0.106	0.248
24	1	4	100	-15	0.052	0.072	0.134	0.068	0.204
25	1	2	-70	-45	0.034	0.054	NA	0.04	0.164
25	1	3	90	-15	0.032	0.056	0.142	0.042	0.166
25	1	5	90	-60	0.028	0.054	0.146	0.04	0.186
17	2	1	-135	10	0.064	0.086	0.14	0.092	0.188
18	2	1	-135	90	0.058	0.088	0.171	0.066	0.196
18	2	4	-125	50	0.056	0.094	0.15	0.1	0.26
18	2	9	-100	-30	0.158	0.182	0.236	0.184	0.258

Table 5: Phasing of Motion Sequence for all trials (Section)

Furthermore a rating of all trials was implemented to assess the quality of the trial and to filter out the trials which showed the needed motion for this study. These five indicators were as followed:

1. Tail influences the turn
2. Initially curled tail
3. Tail transverses to sagittal plane
4. Running after turn
5. All markers in view

For the analysis only the trials were used where an active tail motion could be detected. Of the 111 trials with normal friction, 40 trials and of the low friction trials, all 15 showed this behavior. The indicator of an initially curled tail could be found just once in the resulting 40 trials with friction. This indicates a relation between the influence of a turn and the initial state of the tail, since most of the trials (21 of 111) with initially curled tail were excluded with the first indicator. The indicator 3 describes if the tail motion is just planar or if the tail is swung in vertical direction as well. These trails, 19 of 40, were not sorted out since although there are also vertical forces acting on the lizard body the lateral forces still apply. The fourth indicator, running after the turn is completed, is optional for the trial quality and is correlated to a high level of stimulus reaction. The indicator number five was extracted using programing algorithms explained in Chapter 5.3.

4.3 Morphological Data

The morphometric data of the animals was important for the calculations of inertia, angular momentum and correct positions of the animals on the video recording. Due to the fact that the animals were depicted as a six segment system, tracking points necessary for the tracking software were painted on the lizard seen in Figure 19 to be able to define position and orientation of each segment at all times. The tracking points were painted with whiteout ensuring good adhesion properties as well as a good contrast for the tracking program. The marking-points were positioned on the center of the head at the amount of the lizard number. Further points were placed on the shoulder blades, the feet, the center of the lizard body as well as on the left and right side of the hip. The tail was marked with 4 point where the anterior point was placed at the transition of the bulge to the thinner part of the tail. The remaining points were painted in regular distance on the tail. Due to the method of calculation of the computer model, it was not necessary define exact position for the points on the animals. The attributes such as inertia and angular momentum were calculated for each lizard using their associated morphometric data set and the associated tracking data.

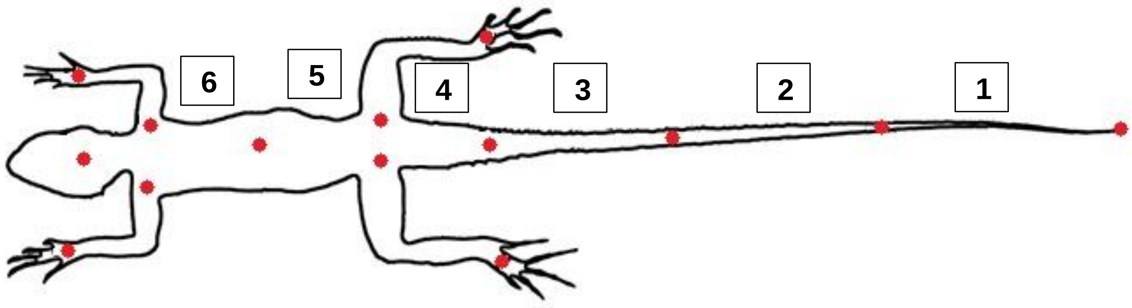

Figure 19: Agama Tracking Point Position subdividing the lizard into 6 segments, starting at tail tip ending at head.

After marking the lizards, the morphometric data of all points were measured specifically the width and the height of the animal using a caliber (Craftsman, Sears Holding Corp.). Furthermore the total mass was measured using a scale of Sartorius AG with an accuracy of 10^-2 g. The problem of measuring the morphological data from the living animals was that the animals when still alive would move as well as gain weight, width and height thereby making the measurement difficult. This is the reason why the living animals were measured more than once to ensure accurate values.

	Lizard 1						
	mass[kg]:	0.0794		Width incl Legs			
Morph Data [mm]	Length	Length incl. Cut	Width	90°	0°	Height	Diff
Snout	0		5.42			0.28	
Segment 6c		83.87		75.15	38.86		19.43
Head	19.43		16.53			8.32	
Segment 6b							26.51
Shoulders	45.94		16.72			12.52	
Segment 6a							39.86
Body	85.8		25.08			12.98	
Segment 5		44.83		88.05	45.56		42.51
Hip	128.31		11.84			8.93	
Segment 4							39.97
Tail 4	168.28		11.37			12.4	
Segment 3							53.97
Tail 3	222.25		6.23			9.27	
Segment 2							58.55
Tail 2	280.8		4.9			5.66	
Segment 1							62
Tail1	342.8		1.91			1.95	

Table 6: Morphological data of living agamas (section)

The approximation for the living lizards to calculate their segment inertia described in Chapter 5.2, was implemented by measuring seven dead lizards. The dead lizards were labeled after the date of death. They were used to approximate the two body segments of the living lizards, described as “Front”, for head to the center of the body and “Hind”, for body-center to hip. Due to the problem of changing inertia at different foot positions the lizards were measured in the following left/right foot constellations: 0°/0°; 90°/90°; 0°/90°; 0°/180°, where the angle describes the angle between lower and upper arm. At 0° the arm is pressed against the body and bent so that the foot is near the shoulder and the elbow lies flat to the lizard’s body. 180° describes the position where the arm is completely extended in perpendicular direction to the longitudinal axis of the body.

Lizard	length		Width							
	Front	Hind	0°/0°		90°/90°		0°/90°		0°/180°	
			Front	Hind	Front	Hind	Front	Hind	Front	Hind
08-26-11	72.0	40.9	31.6	43.5	61.6	69.9	45.1	51.7	58.8	72.4
09-25-11	87.2	48.7	45.9	49.8	77.2	85.2	52.8	59.0	71.8	84.7
09-15-11	88.6	55.0	52.3	44.7	76.4	87.9	56.1	67.8	70.2	91.3
04-20-12	80.1	42.9	44.7	51.2	73.2	81.8	52.0	56.7	62.2	81.5
09-14-10	81.4	47.4	37.9	49.9	74.6	82.8	51.3	58.6	68.5	79.3
06-25-11	66.9	30.5	27.9	32.4	60.3	69.8	42.4	48.7	57.5	68.9
06-04-12	75.1	38.2	35.2	48.0	66.2	77.0	48.7	55.3	58.5	77.2

Table 7: Morphological data of dead agamas for length and width in front feet postures (left/right) of 0°/0°, 90°/90°, 0°/90° and 0°/180°, degree from forearm to upper arm

The dead lizards were defrosted and pinned up at a certain position and refrozen. The lizards were then cut in their frozen state at the marker points of body, hip and tail segments, using a scalpel to achieve a clean cut and not to deform the lizard while cutting. The technical implementations will go into more detail which studies were done using these body parts.

5 Technical Implementation

After the conclusion of the biological aspects the technical implementation was conducted. The recorded data could be analyzed and the analytical results could be processed to develop a biological proposition for a technical application.

5.1 Data Tracking

After completing the trial-sets and the first preliminary analysis, stating which trails comply with the research's standards, data tracking was conducted. As described in Chapter 4.3 the lizards were marked with tracking points using whiteout. These markers could then be tracked using ProAnalyst® (Xcitex, Inc.) described in Motion Analysis of the Background.

To extract data from the recorded videos the tracking software is calibrated using a calibration image. For the discussed trials an image of a ruler was taken und used to define the coordinate system of the tracking software. To increase the visibility of the white markers on the animal, image processing and filtering was applied. Mostly used in the given trials were the Morphology-operations: Erode; Dilate; Close Connections and Break Connections. When applying filtering masks the order is very important. The erode filter causes the disappearance of noise or in regard to the trials, little sand corns on the mats. Combined with a following dilate operation, big enough white sections stay the same size whereas small white sections disappear as seen in Figure 20.

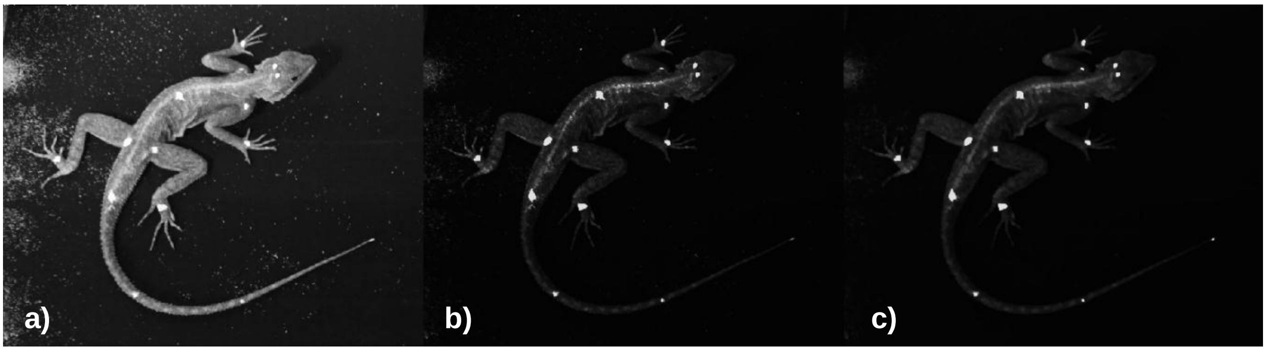

Figure 20: Image processing and filtering a) Original frame b) Frame after Image Processing c) Frame after image processing and filtering

After all filtering options are applied and the markers on the agama are clearly seen the tracking points were defined. Table 8 shows a list of defined tracking points including tracking preferences described in Chapter 20.

Feature	Search Region Multiplier (%)	Threshold Tolerance (0.0-1.0)	Special Target Types	Feature Rotation	
				Angular Range (deg)	Step Size (deg)
Tail1	350-550	0.65	No	10-15	2
Tail2	300-400	0.65	No	7-13	2
Tail3	350	0.65	No	10	2
Tail4	350	0.65	No	10	2
HipR	350	0.65	No(Yes)	10	2
HipL	350	0.65	No(Yes)	10	2
FootHR	350-400	0.65	No	10	2
FootHL	350-400	0.65	No	10	2
Body	350	0.65	Yes	(10)	(2)
ShouldersR	350	0.65	No	15	2
ShouldersL	350	0.65	No	15	2
FootFR	350-400	0.65	No	10	2
FootFL	350-400	0.65	No	10	2
Head	350	0.65	No	10-20	2

Table 8: Feature tracking preferences

Due to the fast motion of the lizards the values of the Search Region Multiplier are compared to the default of 250, increased. The threshold to find the correct tracking point was lowered from 0.75 to 0.65 because the points were drawn on a compliant material, the skin of the lizards, which would distort the points during motion. The target types where solely used in case the tracking point was an optimal circle. Parts of the body that rotate much have a higher rotational range. The step size was used in its default setting. Feature rotation is disabled when a circular target type is chosen symbolized by the brackets.

At the beginning of the data tracking the feet were also tracked. This was deemed later irrelevant for this early stage of research. To standardize the tracking template and to be able to integrate the leg tracking at a later phase of the research, the feet features FootHR, FootHL, FootFR and FootFL were left in the template but weren’t tracked.

After the tracked data is controlled it can be exported. For this research project the units of cm and file type .txt were chosen. This generates a txt-file with all tracked features described in coordinates (X/Y) for all frames. The text files of the 40 normal friction trials and of 3 low friction trials were then used for generating accurate model data.

5.2 Data Approximation and Validation

To be able to calculate angular momentum exchange of lizards, tracked data is used in combination with body attributes such as mass, center of mass and moment of inertia. To avoid measurements of the live lizards approximation methods are used. As described in Chapter 5.3

each lizard was defined as a six segment system correlating with the six lizard segments defined by the marker positions for the video tracking. The mentioned attributes have to be calculated for each of these segments. The lizard approximations can be separated into two general sections, the approximations for the lizard body and the approximations for the lizard tail. This categorization was applied due to the fact that contrary to the body the tail can be roughly assumed as a truncated elliptical cone. With this assumption in mind and the fact that the tail, in its form, stay generally very constant makes it easily calculable. A further discretization was not feasible due to the preliminary character and scope of the research done. The body segments on the other hand with varying limb constellations and irregular geometrical forms are more complex and have to be approximated using measurements of dead lizards to translate mass, COM and MOI.

Due to the high variance in behavior of the animals during the trials and the thereby resulting error for general statements, an error of 10% for the approximations of the attributes was deemed acceptable. Furthermore an additional error estimate can be concluded when considering the formula for the angular momentum, Equation (17). When judging the influences of these two terms on the total angular momentum, it becomes apparent that the $I_i\omega_i$-term is just influential if the center of mass of the specified lizard segment (segment COM) is close to the system center of mass (system COM) of the whole lizard. Therefore the second term $\mathrm{r_{i,COM}} \times \mathrm{m_i v_{i,COM}}$ increases its influence at increased distance ($\mathrm{r_i}$) between the segment COM and system COM. This leads to the conclusion that, for example errors of distance $\mathrm{r_i}$, mass $\mathrm{m_i}$ and velocity $\mathrm{v_i}$ are less influential for the hind body segment due to its proximity to the system center of mass. Table 9 shows 38.84% influence of the $\mathrm{I_i \omega_i}$ term to the total angular momentum. It also shows little influence of errors resulting in the approximation for the inertial $\mathrm{I_i}$ for segments with large distance to the system COM (tail segments) showing fractions of 0.77% to 3.01% of the total angular momentum. Although Table 9 shows values for a simplified case of lizard rotation a general tendency in the trials toward these fractions can be seen.

Lizard 2	$I_i\omega_i$	$\boldsymbol{r}_i \times m_i\boldsymbol{v}_i$	Fraction
Segment 1	6.33E-07	8.19E-05	0.77%
Segment 2	2.57E-06	1.84E-04	1.38%
Segment 3	7.63E-06	2.46E-04	3.01%
Segment 4	3.16E-06	1.52E-04	2.03%
Segment 5	1.61E-05	2.53E-05	38.84%
Segment 6	9.79E-05	5.40E-04	15.36%

Table 9: Fraction of $\mathrm{I_i \omega_i}$-component of angular momentum, in case of constant rotation around the hip of the lizard without body bending

5.2.1 Body Approximation

The approximation of mass, center of mass and moment of inertia, for the hind and font segments of the lizard body are used for the calculation of angular momentum. The general principle in approximating the body parts of the living lizards was to conduct morphological measurements of seven lizard carcasses and to find scaling factors. These scaling factors where applied on morphometric data measured from the living lizards to generate the needed body properties.

Body mass:

The mass approximation was implemented using the mass fraction of the body segments to the total mass of the dead lizards. The mass fraction can be calculated by dividing the actual body segment mass by the total mass of the lizard. Due to the fact that the total mass of the living lizards is known this approximation is applicable. Table 10 shows the result for the mass approximation. The masses for the body segments, front and hind as well as the total mass can be seen in the first data section. Then the fraction is calculated for hind and front body segments of all lizards. The average mass fraction (41.46% front, 37.78 hind) is then taken to calculate the approximated mass of the lizard segments. The resulting errors are shown in the last two columns, resulting in an average absolute error of 3.38%±4.50% for the front segment and 5.11%±8.57% error for the hind segment of the lizard body, falling below of the maximum error of 10%.

Lizard	mass			Fraction of Mass		Aprproximation		Error	
	Front	Hind	Total	Front	Hind	Front	Hind	Front	Hind
08-26-11	0.0126	0.0131	0.0326	38.70%	40.32%	0.0135	0.0123	-7.12%	6.30%
09-25-11	0.0286	0.0276	0.0701	40.88%	39.45%	0.0291	0.0265	-1.41%	4.22%
09-15-11	0.0352	0.0312	0.0831	42.33%	37.61%	0.0344	0.0314	2.06%	-0.46%
04-20-12	0.0210	0.0197	0.0518	40.42%	38.02%	0.0215	0.0196	-2.58%	0.61%
09-14-10	0.0188	0.0167	0.0445	42.25%	37.65%	0.0184	0.0168	1.86%	-0.36%
06-25-11	0.0102	0.0073	0.0229	44.72%	31.75%	0.0095	0.0086	7.29%	-19.01%
06-04-12	0.0125	0.0122	0.0306	40.92%	39.69%	0.0127	0.0116	-1.32%	4.81%
Average	0.0198	0.0183	0.0479	41.46%	37.78%	0.0199	0.0181	3.38%	5.11%
STDev	0.0092	0.0086	0.0221	1.88%	2.87%	0.0091	0.0083	4.50%	8.57%

Table 10: Body mass approximation by average mass fraction and calculated error to original value

Body COM:

The distance to the center of mass (COM) was calculated using the same method as in the mass approximation. The distance to the COM was measured in the dead lizards using the plumb line method (Blackmail, 1925) described as part of the Background. Table 11 shows the approximation for the COM distance. The first two data columns show the length of the front and hind segment of each animal. The second two columns show the distance between center of mass and the anterior end of the agama. After dividing the COM-distance by the length of the segments an average factor can be calculated. This average factor is used to calculate the approximation by multiplying it with the lengths of the lizard segments. The approximation method can be applied since the lengths of the body segments of the living lizards are known. The error of this approximation can be seen in the last two columns and result in an absolute average error of 8.32%±12.65% for the front segment and 16.19%±23.58% for the hind segment. Although the error of the hind segment exceeds the maximum error of 10% it was considered sufficient due to the proximity of the hind center of mass to the center of mass of the whole lizard. Additionally the average is influence significantly by a single lizard (08-26-11) with an error of -49.72%.

Lizard	Length		COM-Distance		COM-D/Length		Approximation		Error	
	Front	Hind	Front	Hind	Front	Hind	Front	Hind	Front	Hind
08-26-11	71.97	40.89	43.21	14.86	0.60	0.36	40.74	22.25	5.72%	-49.72%
09-25-11	87.22	48.66	51.46	23.9	0.59	0.49	49.37	26.48	4.06%	-10.78%
09-15-11	88.6	55.02	53.2	31.2	0.60	0.57	50.15	29.94	5.73%	4.05%
04-20-12	80.08	42.88	45.4	23.89	0.57	0.56	45.33	23.33	0.16%	2.34%
09-14-10	81.37	47.43	50.61	32.2	0.62	0.68	46.06	25.81	9.00%	19.86%
06-25-11	66.87	30.49	30.22	15.03	0.45	0.49	37.85	16.59	-25.25%	-10.38%
06-04-12	75.06	38.19	39.82	25.13	0.53	0.66	42.49	20.78	-6.69%	17.31%
Average	78.74	43.37	44.85	23.74	0.57	0.54	44.57	23.59	8.32%	16.19%
STDev	7.94	7.95	8.05	6.88	0.06	0.10	4.49	4.33	12.65%	23.58%

Table 11: Body COM-distance approximation by segment length fraction with calculated error of original value

Body moment of inertia:

For the approximation of the Moment of Inertia (MOI) about the center of mass of the two body segments, different methods for calculation were conducted. Through analyzing the different approximation methods, shown in the following tables the method for the least error was chosen. As seen in the following section the approximation factor have to relate to the unit of the moment of inertia (kg*m^2). Due to the fact that length scales proportionally to mass as length^3, the inertia can be written proportionally scaling to length^5 or mass^(5/3).

For approximation of moment of inertia of the living lizards, the inertia of the dead animals has to be measured to generate scaling factors using the morphometric data. the inertia was measured using the pendulum method (Dowling, Durkin and Andrews, 2006) described in the Background. To achieve an accurate measurement of the radius of gyration the period of the oscillation was measured in three trials per ROG calculation after which it was possible to calculate an average of the resulting inertia, giving an accurate ROG estimation. The new ROG is then used to calculate the new Inertia. After several iterations the exact moment of inertia can be calculated. The following table shows two iteration of this process. Since the error of the inertia decreases drastically if the distance from center of mass to the axis of rotation converging to the ROG

(Dowling, Durkin and Andrews, 2006) an error of 10% between the old and the new ROG was deemed sufficiently small.

Left=	0°	Right=	0°				
	mass	0.012					
	Seconds	Oscillations	Periode	D	Inertia	RoG	Error
Trial 1	12.27	30	0.4090	0.02355	5.274E-06	0.02060	
Trial 2	12.26	30	0.4087	0.02355	5.254E-06	0.02056	
Trial 3	12.27	30	0.4090	0.02355	5.274E-06	0.02060	
Average			0.4089	0.02355	5.268E-06	0.02059	-14%
	Seconds	Oscillations	Periode	D	Inertia	RoG	Error
Trial 1	11.98	30	0.399333	0.02061	4.872E-06	0.01980	
Trial 2	12.01	30	0.400333	0.02061	4.922E-06	0.01990	
Trial 3	12.03	30	0.401	0.02061	4.956E-06	0.01997	
Average			0.400222	0.02061	4.917E-06	0.01989	-4%

Table 12: Iteration process of inertia measurement for leg constellation 0°/0° until error <10%

After a precise moment of inertia was calculated different methods of approximation could be implemented. For the first method the simplest case of approximation was used, which was implemented by dividing the inertia by the segment length to the power of five. The average is used to approximate the new inertia. The error section shows that this method is too inaccurate with average absolute error values of 30.52%±36.75% for the front segment and 27.5%±33.89% for the hind segment exceeding the maximum error of 10%.

Lizard	Length		MOI (0°/0°)		I/L^5		Approximation		Error	
	Front	Hind	Front	Hind	Front	Hind	Front	Hind	Front	Hind
08-26-11	72.0	40.9	3.9E-06	3.4E-06	2.0	29.9	5.1E-06	4.4E-06	-29%	-28%
09-25-11	87.2	48.7	1.4E-05	9.9E-06	2.7	36.2	1.3E-05	1.0E-05	3%	-6%
09-15-11	88.6	55.0	2.0E-05	1.2E-05	3.7	24.7	1.4E-05	1.9E-05	28%	-55%
04-20-12	80.1	42.9	1.1E-05	6.7E-06	3.2	45.9	8.7E-06	5.5E-06	18%	17%
09-14-10	81.4	47.4	7.9E-06	5.9E-06	2.2	24.7	9.4E-06	9.2E-06	-20%	-55%
06-25-11	66.9	30.5	3.4E-06	1.7E-06	2.6	62.8	3.5E-06	1.0E-06	-3%	39%
06-04-12	75.1	38.2	4.9E-06	3.5E-06	2.1	43.7	6.3E-06	3.1E-06	-28%	12%
Average	78.7	43.4	9.2E-06	6.2E-06	2.6	38.3	8.7E-06	7.6E-06	19%	30%
STDev	7.9	8.0	6.1E-06	3.8E-06	0.6	13.7	4.1E-06	6.1E-06	23%	36%

Table 13: Body inertia approximation – length^5 with calculated error of original value

The second approximation with increased precision was a method using the segment mass to the power of 5/3. As mentioned before the inertia scales proportionally to length^5. Since the mass scales proportionally to the length^3 the length scales proportionally to mass^(1/3), resulting in a proportional scaling factor of the Inertia at mass^(5/3). The average of the inertia divided by mass^(5/3) is multiplied with the mass of the respective segment mass^(5/3). Since the segment masses of the living lizards are already approximated with an error of 3-5% this approximation is also not optimal. As seen in Table 14 the errors for this method exceed the maximum error at values of 11.93%±14.02% and 14.02%±17.01 without taking the approximation error of the segment mass into account. The combined error of mass approximation and inertia approximation amounts to 13.17%±17.24% and 12.18%±14.65%, showing just a slight increase of error average and standard deviation for the front and even a decrease of error for the hind segment.

Lizard	Mass		MOI (0°/0°)		I/m^(5/3)		Approximation		Error	
	Front	Hind	Front	Hind	Front	Hind	Front	Hind	Front	Hind
08-26-11	0.01	0.01	3.9E-06	3.4E-06	0.006	0.005	4.2E-06	3.6E-06	-7%	-5%
09-25-11	0.03	0.03	1.4E-05	9.9E-06	0.005	0.004	1.7E-05	1.2E-05	-20%	-25%
09-15-11	0.04	0.03	2.0E-05	1.2E-05	0.005	0.004	2.3E-05	1.5E-05	-16%	-22%
04-20-12	0.02	0.02	1.1E-05	6.7E-06	0.007	0.005	9.8E-06	7.0E-06	7%	-6%
09-14-10	0.02	0.02	7.9E-06	5.9E-06	0.006	0.005	8.2E-06	5.4E-06	-4%	10%
06-25-11	0.01	0.01	3.4E-06	1.7E-06	0.007	0.006	3.0E-06	1.3E-06	13%	20%
06-04-12	0.01	0.01	4.9E-06	3.5E-06	0.007	0.006	4.2E-06	3.1E-06	15%	11%
Average	0.02	0.02	9.2E-06	6.2E-06	0.006	0.005	9.9E-06	6.9E-06	12%	14%
STDev	0.01	0.01	6.1E-06	3.8E-06	0.001	0.001	7.5E-06	5.1E-06	14%	17%

Table 14: Body inertia approximation - mass^(5/3) with calculated error of original value

The next inertia approximation method used a combination of the length of the segment and the mass of the segment. Here the average of all the results of dividing the inertia by the mass times the length to the power of two of all segments was multiplied by the mass and length^2 of the segments. When calculating the error average, Table 15 shows results for the front of 14.32%±18.96% and for the hind segment of 15.26%±19.31% which made it more accurate than the length^5 method but less accurate than the previous approximation method using just the mass. The error, including the mass approximation results in an average for front and hind segment of 15.76%±20.80% and 12.54%±16.06%. This shows a decrease of error for the front and an increase of the hind error.

Lizard	MOI (0°/0°)		I/(m*l^2)		Approximation		Error	
	Front	Hind	Front	Hind	Front	Hind	Front	Hind
08-26-11	3.95E-06	3.42E-06	0.061	0.156	4.68E-06	4.20E-06	-18.46%	-22.81%
09-25-11	1.38E-05	9.87E-06	0.063	0.151	1.56E-05	1.25E-05	-13.37%	-26.77%
09-15-11	2.01E-05	1.24E-05	0.073	0.132	1.98E-05	1.81E-05	1.51%	-45.33%
04-20-12	1.06E-05	6.65E-06	0.079	0.184	9.63E-06	6.93E-06	9.45%	-4.19%
09-14-10	7.85E-06	5.93E-06	0.063	0.158	8.91E-06	7.20E-06	-13.48%	-21.39%
06-25-11	3.43E-06	1.65E-06	0.075	0.245	3.28E-06	1.29E-06	4.59%	22.03%
06-04-12	4.92E-06	3.55E-06	0.088	0.314	4.01E-06	2.16E-06	18.35%	39.12%
Average	9.24E-06	6.22E-06	0.072	0.191	9.42E-06	7.48E-06	11.32%	25.95%
STDev	6.09E-06	3.83E-06	0.010	0.065	6.27E-06	6.00E-06	13.74%	29.66%

Table 15: Body inertia approximation mass*length^2 with calculated error of original value

The last body moment of inertia approximation was implemented using unconstrained nonlinear optimization to find the minimum of a scalar function with the variable alpha and beta. The used function can be written as

$$I_{CM} = \alpha m l^2 + \beta m w^2 \quad (7)$$

where I_{CM} is the inertia (kg*m^2), m the mass (kg) and the length l and width w in meters, of the segment including the legs. Alpha and beta are two factors that describe the quantifier of each term. Using the fminsearch function in MATLAB® by MathWorks, Inc. alpha (x(1)) and beta(x(2)) could be calculated. Fminsearch opens the Matlab function (equ) which contains mass (m), length (l), width (w) and MOI (Icm) of the dead lizards. The scalar function e is then solved for all lizards and the average error (F) minimized by varying alpha (x(1)) and beta (x(2)).

```
for i=1:length(Icm)
    e(i)=x(1)*m(i)*l1(i)^2+x(2)*m(i)*l2(i)^2-Icm(i);
end
F=mean(abs(e./Icm));
```

As seen in Table 16 formula (7) was used to calculate the inertia approximation which results in an error of 6.98%±9.26% for the front segment and 6.99%±13.30% for the hind body segment. Combined with the mass approximation the average error calculates as 9.09%±11.84% and 6.37%±7.80%. The resulting error is the minimal error of all the approximation methods with a value of less than 10% satisfying the error limit.

Lizard	Width (0°/0°)		MOI (0°/0°)		Approximation		Error	
	Front	Hind	Front	Hind	Front	Hind	Front	Hind
alpha beta					0.0474 0.0729	0.068 0.0811		
08-26-11	31.60	43.47	3.95E-06	3.42E-06	4.01E-06	3.50E-06	-1.56%	-2.53%
09-25-11	45.87	49.83	1.38E-05	9.87E-06	1.47E-05	1.00E-05	-6.87%	-1.45%
09-15-11	52.30	44.67	2.01E-05	1.24E-05	2.01E-05	1.15E-05	-0.04%	7.70%
04-20-12	44.73	51.20	1.06E-05	6.65E-06	9.42E-06	6.65E-06	11.39%	-0.04%
09-14-10	37.88	49.86	7.85E-06	5.93E-06	7.86E-06	5.93E-06	-0.06%	-0.05%
06-25-11	27.92	32.36	3.43E-06	1.65E-06	2.75E-06	1.08E-06	19.99%	35.04%
06-04-12	35.22	47.96	4.92E-06	3.55E-06	4.48E-06	3.47E-06	8.94%	2.16%
Average	39.36	45.62	9.24E-06	6.22E-06	9.05E-06	6.02E-06	6.98%	6.99%
STDev	8.65	6.50	6.09E-06	3.83E-06	6.35E-06	3.73E-06	9.26%	13.30%

Table 16: Body inertia approximation alpha*mass*length^2+beta*mass*width^2 with calculated error of original value

After developing an approximation that would yield values of sufficient precision, measurements of the inertia of the dead lizards as well as the approximations for the inertia were conducted for all leg constellations. As described in Chapter 4.3 the width incl. the legs for all dead agamas using positioning of the legs (left/right) at 0°/0° 90°/90° 0°/90° 0°/180° was taken, followed by measuring the inertia of all dead lizards. This was necessary since the inertia of the agamas would change depending on the position of their feet. The pendulum method combined with the plumb line method to find the center of mass (Chapter 24), were used. Each foot combination was measured for all available dead agamas, followed by the calculation of alpha and beta and the approximation of the inertia. Table 17 shows the obtained alpha and beta values as well as the errors of approximation for each feet position including the mass approximation error.

Lizard	MOI (0°/0°)		MOI (90°/90°)		MOI (0°/90°)		MOI (0°/180°)	
	Front	Hind	Front	Hind	Front	Hind	Front	Hind
alpha	0.0474	0.0680	-0.0099	0.0185	-0.0270	0.0225	0.1124	-0.1137
beta	0.0729	0.0811	0.1151	0.0970	0.2618	0.1171	-0.0519	0.1193
08-26-11	-8.80%	3.93%	-7.28%	-5.29%	-14.84%	6.29%	-12.85%	1.99%
09-25-11	-8.38%	2.83%	-11.85%	-2.40%	-1.35%	-8.21%	-8.09%	4.24%
09-15-11	2.02%	7.28%	5.92%	4.97%	2.00%	-20.21%	1.98%	4.47%
04-20-12	9.10%	0.58%	-2.51%	-0.33%	-1.87%	9.48%	8.22%	-6.53%
09-14-10	1.81%	-0.41%	-15.33%	8.17%	-8.97%	0.32%	1.79%	7.98%
06-25-11	25.82%	22.69%	7.50%	9.33%	14.44%	-20.78%	23.24%	-8.82%
06-04-12	7.73%	6.87%	9.79%	4.82%	-1.27%	18.69%	6.46%	4.84%
Average	9.09%	6.37%	8.60%	5.05%	6.39%	12.00%	8.95%	5.55%
STDev	11.84%	7.80%	9.96%	5.52%	9.13%	15.04%	11.73%	6.32%

Table 17: Errors of moment of inertia approximation for all feet positions

The table shows that the approximations for the moment of inertia of the two body segments using the unconstrained nonlinear optimization are accurate for all feet constellations with an overall error of 7.75%±6.24%.

5.2.2 Tail Approximation

After describing the approximations for the lizard body, this section of the chapter will address the tail approximations. As for the body, the mass, distance of the center of mass to the anterior end of the body and the inertia will be described. The method for approximating the tail segments was accomplished by calculating an elliptical truncated cone (TEC) described in Chapter 3.4. The width and height of the living agamas (see Table 6) as well as the density of all segments were needed to calculate the mass, COM-distance and MOI (about COM) of each particular tail segment.

Due to uncertainty of validity of the formula used for the approximation by Kwon (1998) the formulas were verified by calculating the limits of the elliptical truncated cone. Firstly geometrical shapes possible by manipulating the minor and major axis values were calculated independently and verified using the actual truncated elliptical cone calculation and SolidWorks® (Dassault

Systèmes SolidWorks Corp.) to verify the findings. Table shows the achievable shapes with the a0, a1, b0, b1 and L values.

Geometrical shape	a0	a1	b0	b1	L
Cylinder	1	1	1	1	3
Cone	1	0	1	0	3
Elliptical Cylinder	1	1	2	2	3
Truncated circular cone	3	1	5	2	3

Table 18: Achievable geometrical shapes by values for the minor and major axes of base (a0, b0) and top (a1, b1)

These shapes were then calculated using their original formulas as well as modeled in SolidWorks and compared to the calculations by the truncated elliptical cone formula.

Moment of Inertia	Mass			MOI around COM (Ixx)		
	Calculation	TEC	SolidWorks	Calculation	TEC	SolidWorks
Cylinder	9424.778	9424.778	9424.780	9424.778	9424.778	9424.780
Cone	3141.593	3141.593	3141.480	1531.526	1531.526	1531.360
Elliptical Cylinder	18849.556	18849.556	18850.070	32986.723	32986.723	32990.010
Truncated Circular Cone	21991.200	21991.149	21990.840	29300.961	29300.961	29298.870

Table 19: Validation of geometric shapes for mass and moment of inertia using specific formula (Calculation), TEC method and SolidWorks

The table shows the calculated mass and MOI for the geometric specific formula (Calc), by the truncated elliptical cone formula (TEC) and SolidWorks. The used formulas for the specific geometric shapes can be seen in Appendix B.

Since the calculation didn't state if the major and minor axes as well as the Base and the top of the elliptical frustum are interchangeable, a function was written to avoid the problematic cases. A frustum was handled as a problematic case if the major (b0) and minor (a0) axes of the base and major (b1) and minor (a1) axes of the top were perpendicular to each other, resulting in a0>b0 and a1<b1 or a0<b0 and a1>b1. Cases of these constellations show at a certain distance (x) of the height (h) a circular cross-section where $a_{(x)}=b_{(x)}=r$. Using this approach the following calculations can be conducted. Figure 21 shows a diagram of the calculated case in side view.

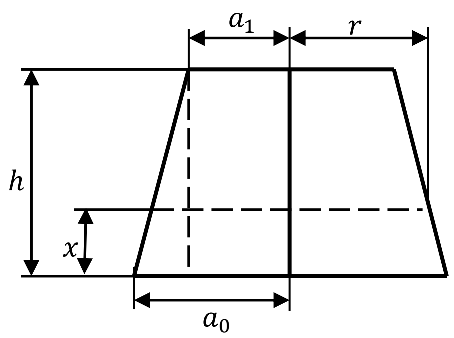

Figure 21: Diagram of truncated elliptical cone in side view

The distance x to the circular cross-section with radius r can be calculated by the method of proportional triangles for the minor axes as

$$\frac{h}{a_0 - a_1} = \frac{h - x}{r - a_1} \quad (8)$$

and for the major axes as

$$\frac{h}{b_0 - b_1} = \frac{h - x}{r - b_1} \quad (9)$$

By expressing r for each axis and equating the two terms, r and x can be expressed as

$$r = \frac{a_0 b_1 - a_1 b_0}{a_0 - a_1 - b_0 + b_1} \quad (10)$$

$$x = \frac{(a_0 - b_0)h}{a_0 - a_1 - b_0 + b_1} \quad (11)$$

The program would then split the segment in two parts, calculate the mass, COM-distance and inertia of these truncated elliptical cones with either circular base or top. After this calculation it would combine the resulting values. At a comparison of these parameters with the normal truncated elliptical cone calculation and SolidWorks it was found that the TEC calculation accounted for all possible cases and the corrected frustum function was not necessary seen in Table 20. Furthermore this comparison was used to assess the cases where a0,b0<a1,b1.

Values				Normal Calculation		Corrected Frustum		SolidWorks	
a0	b0	a1	b1	m	Ixx	m	Ixx	m	Ixx
3	5	1	2	7.07E+04	3.27E+05	7.07E+04	3.27E+05	7.07E+04	3.27E+05
1	2	3	5	7.07E+04	3.27E+05	7.07E+04	3.27E+05	6.98E+04	3.21E+05
5	3	2	1	7.07E+04	1.40E+05	7.07E+04	1.40E+05	6.89E+04	1.35E+05
2	1	5	3	7.07E+04	1.40E+05	7.07E+04	1.40E+05	7.05E+04	1.39E+05
3	5	2	1	7.38E+04	2.97E+05	7.38E+04	2.97E+05	7.20E+04	2.89E+05
1	2	5	3	7.38E+04	1.74E+05	7.38E+04	1.74E+05	7.32E+04	1.72E+05
5	3	1	2	7.38E+04	1.74E+05	7.38E+04	1.74E+05	7.26E+04	1.69E+05
2	1	3	5	7.38E+04	2.97E+05	7.38E+04	2.97E+05	7.08E+04	2.84E+05

Table 20: Validation of parameter dimensions

After the formula was assessed to be correct, the dead lizard tails were calculated using their morphometric and compared with measured data to assess this method of approximation. Table 21 shows the measured and approximated values for mass and Inertia. The lizard segments are numbered from one to four where one is the segment from tail tip to the first tail marker and segment six is the segment from the body center to the snout. This way of numbering the segments was implemented to have a standardized method for tracking as well as the morphometric data. The table shows a maximum mass-error of 44.64% and a maximum inertia-error of 35.13% for Lizard 2 (06/04/12), making the described approximation method not accurate enough. Segment five and six, body front and hind segments, seen in the table below are already calculated with the approximations of the previous section resulting in a minimal error.

Lizard 2	Mass [kg]			MOI [kg*m²]		
	Measured	Approximated	Error	Measured	Approximated	Error
Segment 1	0.00025	0.000287019	-14.81%	7.0985E-08	9.0038E-08	-26.84%
Segment 2	0.00101	0.000951448	5.80%	2.4277E-07	2.3977E-07	1.24%
Segment 3	0.00217	0.002945037	-35.72%	5.3956E-07	7.2909E-07	-35.13%
Segment 4	0.00269	0.003890776	-44.64%	2.3877E-07	2.4367E-07	-2.05%

Table 21: Tail mass and inertia approximation

Since the error of approximation was unreasonably high a density check was conducted using the liquid displacement method to decrease the obtained error. This method uses a measuring vial with milliliter makings. The vial is filled with water to a certain point. After the object that is measured is lowered into the water the new water level is recorded. To increase the accuracy the water displacement was measured by a caliber, using a scaling factor to calculate millimeter to milliliter. By submerging the object in the water the water displacement equals the volume of the object. The density can be calculated by dividing mass through volume. Table 22 shows the density calculation for two lizards.

Scaling factor	30	ml =		94.69	mm	
Lizards	Segments	mass [g]	water displacement [mm]		V [ml]	rho [kg/m³]
06/04/12	Segment 1	0.25		0.95	0.300982	830.614035
	Segment 2	0.99		2.63	0.833245	1188.12548
	Segment 3	2.13		5.57	1.764706	1207
	Segment 4	2.64		8.02	2.540923	1038.99252
04/20/12	Segment 1	0.51		2.06	0.652656	781.42233
	Segment 2	1.12		2.78	0.880769	1271.61631
	Segment 3	1.95		5.16	1.634808	1192.80039
	Segment 4	6.86		20.59	6.523392	1051.60013

Table 22: Tail density check

The average of the density of each segment was then used for calculating the new mass and inertia values for the agama tail approximation. The results in Table 23 show an increase in approximation error to a maximum error of 62.85% and an absolute average error of 34.34% for the mass of the tail segments and a maximum error of 62.14% for the moment of inertia.

Lizard 2	Mass [kg]			MOI [kg*m²]		
	Measured	Approximated	Error	Measured	Approximated	Error
Segment 1	0.00025	0.00023134	7.46%	7.0985E-08	7.2573E-08	-2.24%
Segment 2	0.00101	0.00117016	-15.86%	2.4277E-07	2.9489E-07	-21.47%
Segment 3	0.00217	0.00353375	-62.85%	5.3956E-07	8.7484E-07	-62.14%
Segment 4	0.00269	0.00406701	-51.19%	2.3877E-07	2.5471E-07	-6.68%

Table 23: Tail mass and inertia approximation including measured density average

The reason for the increased error and the bad approximation of the lizard tails were speculated to be connected to the fact that the shape of lizard tail has skin extensions at the dorsal side, and resembles more a teardrop than an ellipse. After new morphometric measurements concerning the weight, height and width of all segments excluding the dorsal ridge of the body were taken, a new estimation could be calculated. The estimate shows a maximum error of 26.47% for the mass and a 36.37% error for the Inertia.

Lizard 2	Mass [kg]			MOI [kg*m²]		
	Measured	Approximated	Error	Measured	Approximated	Error
Segment 1	0.00020	0.00015	26.47%	7.0985E-08	4.5169E-08	36.37%
Segment 2	0.00097	0.00077	20.88%	2.4277E-07	2.0890E-07	13.95%
Segment 3	0.00200	0.00182	8.99%	5.3956E-07	4.2643E-07	20.97%
Segment 4	0.00234	0.00227	3.20%	2.3877E-07	1.5468E-07	35.22%

Table 24: Tail mass approximation with density and new morphometric measurements excluding dorsal ridge

The previous tables demonstrate that the error of the frustum formula is highly sensitive for morphometric measurement errors. Furthermore the error of the two posterior segments could be reduced by taking the new measured morphometric data including the ridge to a mass-error of 4.17% and 5.48%. The approximation for the inertia was deemed sufficient for our purposes in light of the limited influence on the angular momentum described in Chapter 5.2.

5.3 Model

As shown in previous research (Jusufi et al., 2010; Libby et al., 2012) angular momentum exchange is used in aerial maneuvers of lizards for pitch control and dynamic self-righting. The generated models aim to prove that this kind of exchange has effects on terrestrial turning behaviors as well. Therefore the angular momentum, Equation (17) has to be calculated. After discussing the data acquisition, the morphometric data, the data tracking and the lizard approximations all needed information is available to implement the trial calculations in MATLAB (MathWorks, Inc.).

There are two models, one numeric and one analytic model, which will be explained in the following section. The models are interlinked by a cell array called agama_data including, among others, values such as certain morphometric data, angle data, the angular momentum for all segments over time, velocity and all distances from system COM to segment COMs (r_i). Although the two models can both calculate generated angular momentum of the lizard motion, the first model does this to show differences between tail and body influence. Furthermore the numeric model shows the difference to two specific cases of the movement of the lizard motion the “rigid stick” and the “varying inertia stick” model explained in the following Chapter. The second model focuses on the different effects of the two different components of the angular momentum. These components are effects due to body and tail bending (shape change) of the lizard and effects due to external impulses such as ground reaction forces.

The models are constructed as 6-link models in relation to the six lizard segments due to the number of markers on the lizard. The segment convention was chosen as segment 1 to 6 from tail tip to head due to the order of features extracted by the tracking program.

5.3.1 Numeric Model

The general principle of the numeric model is to analyze the lizard movement based on the kinematics extracted from the video analysis to calculate angular momentum of the lizard behavior. The general idea of this principle was generated to assess the tail swing of an Iguana (*Iguana Iguana*) with a two-link model (T. Libby, unpublished data) and was further developed (N. Kohut, unpublished data) for preliminary analysis on multi-link models. Due to different tracking data format, novel approximation methods and increase in level of detail and functionality, the calculation program was rewritten.

The model, depicted in Figure 22 calculates the angular momentum, Equation (17) using the extracted data of the animal trials and compares the resulting data with two special cases of the model. These two sub-models, named “Rigid Stick” and “Varying Inertia Stick” model are generated to point out the difference of the achieved rotation angle by the real lizard compared to a rigid stick (without shape change) with constant inertia and a rigid stick with varying Inertia. These sub-models will be described after the general process of the model is depicted.

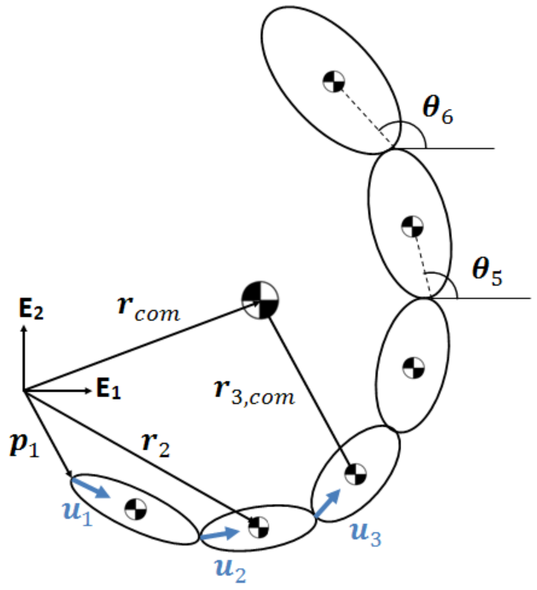

Figure 22: Numeric model – segment conventions

The coordinate system used for the numeric model was defined by the tracking software as a left handed coordinate system in the top left corner of the recorded images. This coordinate system was then changes to a right handed coordinate system in the computer program and is depicted here as the unit vectors E_1 and E_2. Furthermore the segments of the lizard are defined from one to six, starting at the tail of the lizard.

The angular momentum of a system can be attained by calculating the position of the center of mass $\boldsymbol{r}_i$ of segment i

$$\boldsymbol{r}_i = \boldsymbol{p}_i + \boldsymbol{u}_i g_i \qquad (12)$$

where the position vector of each segment $\mathrm{p_i}$, the approximated distance to the center of mass of said segment $\mathrm{g_i}$, and the unit vector of the segment $\mathrm{u_i}$ are used. This can be applied for

$$\boldsymbol{r}_{COM} = \frac{\sum_{i=1}^{j} m_i \boldsymbol{r}_i}{\sum_{i=1}^{j} m_i} \qquad (13)$$

calculating the position of the COM of the total system (system COM) where m_i depicts the mass of segment i and j the total number of segments. The distance between system COM and segment COM is calculated by

$$\boldsymbol{r}_{i,COM} = \boldsymbol{r}_i - \boldsymbol{r}_{COM} \tag{14}$$

and is used to calculate the velocity relative to the system COM $\boldsymbol{v}_{i,COM}(k)$ for each time frame k, taking two time steps dt for stabilizing effects into account.

$$\boldsymbol{v}_{i,COM}(k) = \frac{\boldsymbol{r}_{i,COM}(k+1) - \boldsymbol{r}_{i,COM}(k-1)}{2dt} \tag{15}$$

After the angle is calculated using the atan2 function (E_1 unit vector as 0°) on the position vectors the angular velocity can be calculated in the same manner.

$$\omega_i(k) = \frac{\theta_i(k+1) - \theta_i(k-1)}{2dt} \tag{16}$$

The resulting values are now used to calculate the angular momentum around the system COM

$$\boldsymbol{H}_{COM} = \sum_{i=1}^{j} I_i\omega_i + m_i\boldsymbol{r}_{i,COM} \times \boldsymbol{v}_{i,COM} \tag{17}$$

where I_i is the inertia of each segment around its segment COM. The angular momentum calculation consists of two separate terms. The term $I_i\omega_i$ takes the angular momentum of the specific segment into account, the second term the angular momentum of said segment about the center of mass of the system. This entails that a segment with low weight has little influence on the whole system unless it either has high angular velocity or a large distance to the system COM.

To quantify what effect the shape change component of the calculated angular momentum had, two rigid stick, single-segment models were established. The effect was shown by comparing resulting body angles of the lizard turn of all three models. The first model assumes that the lizard is a rigid stick, constraining shape change, resulting in simple calculation of the system inertia I_{COMR} using segment inertia I_i, mass m_i and distance between segment COM and system COM $\boldsymbol{r}_{i,COM}$ for all body segments j

$$I_{i,COM} = I_i + m_i\boldsymbol{r}_{i,COM}^2 \tag{18}$$

$$I_{COMR} = \sum_{i=1}^{j} I_{i,COM} \tag{19}$$

The angle of the rigid model can then be calculated by taking the first term of Equation (17), expressing ω and taking the time derivative resulting in

$$\theta_{rigid} = \frac{1}{I_{COMR}} \int \boldsymbol{H}_{COM}(t) \cdot \boldsymbol{E}_3 dt \qquad (20)$$

The angle of the first model shows which amount of degrees would have been possible to turn if the lizard would not change in shape.

The second model is calculated similarly, differentiating by using the calculated inertia of the lizard while changing its shape during the turn $I_{COMV}(t)$.

$$\theta_{varying} = \int \frac{\boldsymbol{H}_{COM}(t) \cdot \boldsymbol{E}_3}{I_{COMV}(t)} dt \qquad (21)$$

The changing inertia of the lizard is calculated as part of the numeric model and is passed to the varying rigid stick model for use. The resulting angle $\theta_{varying}$ shows the angle that can be achieved by a turning lizard with rigid body but varying MOI. It is comparable with a turning one-segment rod that can vary its length.

The described calculations were integrated in a program which would extract the needed tracking data and would generate all needed data for the analytical program. The code of the program can be seen in Appendix F.

The program folder contains eight function-files, combined with one main file and a folder containing the txt-files of the tracking software as well as an Excel (Microsoft Office) worksheet showing the trial phases as described in Table 5. The following listing shows the file-structure of the numeric model.

- Trials
  - animal1_trial1_20120424_162300_20120424_162859.txt
  - …
  - tracking_phases.xls
- Agama.m
- AnLizardData.m
- calcSegMOI.m
- getFilename.m
- getTrials.m
- LizardMorphData.m
- main.m
- MOI_calc.m
- search_File.m

When the main file of the program is started, the pathname of the folder that contains the txt-files of the tracking software has to be defined. This name is used to extract the file names of all tracking files. Following this operation, the name and path of the Excel Worksheet containing the trial phases is defined the data is extracted.
The next step of the program is the definition of the model configuration. To better assess the calculated data the program was written in a way that would allow for a definition of used segments. This means that if it becomes necessary to define the model as two segments, body and tail, instead of six, it can be implemented using this model configuration. This method makes it necessary to define a new term describing these configurations. Besides the term system which stands for the whole system and Segments which stand for a certain section of the lizard, the term subsystem was now defined to stand for combined segments. The definition of this model configuration is implemented as a cell array, by the name of ‘Segments’, where the cell is the system, the arrays are the subsystems and the segment numbers, 1 to 6, are the segments. To achieve a six-segment system the cell array is written as follows:

```
Segments = {[1 1],[2 2],[3 3],[4 4],[5 5],[6 6]};
```

The following cell arrays show a three segment model (two tail segments, one body segment), a two segment mode (one tail segment, one body segment) and a one segment model (one segment – rigid stick).

```
Segments = {[1 2],[3 4],[5 6]};
Segments = {[1 4],[5 6]};
Segments = {[1 6]};
```

After defining the above mentioned parameters the main file starts an iterative loop (for loop) with for all tracking data filenames, opening and passing the parameters filename of the tracking file, tracking phase data and the segment constellation to the function Agama.

The Agama function then uses the transferred filename to extract the data of the txt-files. Next the agama function extracts the lizard number from the filename and passes it together with the segment configuration to the calcSegMOI function. This function is used to extract the morphological data from the LizardMorphData function and to calculate the approximation of the mass, center of mass (COM) and the moment of inertia (MOI) of the sub-systems. Furthermore the function calcSegMOI is used to calculate the “rigid stick” model and the “varying inertia stick” model (referred in the code as magic_sick) if the array of the segment constellation is a string. This case will be discussed later in the description of the program.

The next step of the program is the extraction of the morphological data of the lizard which ran currently processed trial. The morphometric data consists of a height and width vector of 7 elements, a length and rho vector of 6 elements and an integer value of the total lizard mass. The height and width are halved to receive the major and minor axis of the base (a0, a1) and top (b0, b1) needed for the truncated elliptical cone method, as described in Chapter 3.4. These parameters, the length (L) and rho for each segment are passed to the function MOI_clac which calculates each segment inertia (I), mass (m) and distance to com (g) from the posterior end of the segment (the base of the frustum) while calculating from tail tip to head. The MOI_calc function was written to be able to calculate the Inertia about the base or the center of mass for all three axes (Ix, Iy, Ixx, Iyy, Iz=Izz).

The resulting parameters are used for the tail approximations. The next section will concentrate on the body approximations, described in Chapter 5.2.1. The mass approximation uses the fraction of the front (6) and hind (5) segment of the lizard in comparison to the whole body. It is implemented by multiplying the fraction with the whole body mass (mass_tot) received from LizardMorphData. The distance to the center of mass is approximated by the average distance from the anterior end to the COM of the dead lizards. The inertia approximation of the body segments is calculated by the formula (7) and needs the defined alpha and beta for the front and the hind segment as well as the mass, the length and the width to calculate the MOI of the body parts of the lizard.

```
I(6)=front_alpha*m(6)*L(6)^2+front_beta*m(6)*b(6)^2;
I(5)=hind_alpha*m(5)*L(5)^2+hind_beta*m(5)*b(5)^2;
```

After concluding the segment approximation, calcSegMOI calculates mass, COM and MOI in light of the segment configuration. Due to the fact that the sub-systems themselves are rigid entities, the Inertia of each sub-system can be calculated using Equation (18) and (19) of the rigid stick model. The center of mass is calculated by Equation (13) and the masses are summed and all values are passed back to the agama function. There phase data values for the current trial are extracted and the calculation of the angular momentum is started by calling the AnLizardData-function.

AnLizardData manipulates the data array of the tracking txt-file to be able to calculate the angular momentum. The tracking file is a matrix of values where the columns are x/y coordiantes for the tracking features such as head, hipR or tail2. The rows of the matrix are the time steps of the tracking. After the tarcking data is converted into a right-handed coordinate system, two different procedures for both columns and rows are realized to manipulate amount or order of the data.

Columns:

- Arranging order of tracking features
- Integrating sub-system configuration

Rows:

- Including tracking phases
- Excluding not fully tracked data sections

The columns are first rearranged according to the model convention where the posterior tail segment is segment 1 and the anterior body segment is segment 6. The second manipulation is the arrangement due to the segment constellation. This would order the tracked data according to the defined sub-systems. If the lizard was defined as one sub-system, a 1-link model, the tracking data of the tail tip and the shoulder would be positioned sequentially and the remaining data discarded. The rows, coordinates for each time steps of the trial, are cropped to a specified data range using the data of the trail phases. This could e.g. be implemented for the time of the “curling start” to the “uncurling end”. Next the data is controlled for any untracked data points, shown as -1 in the tracking data. Since the total angular momentum can just be calculated if all segments are available, sections where a part of the lizard left the camera view cannot be used.

The next step of the program is the calculation of the angular momentum, and can be seen in the source code in Appendix F, following the Equations (12) to (17). The angular momentum for tail and body are calculated by summing the angular momentum of the separate segments. In light of the variety of sub-system constellations the convention was made that all sub-systems that are posterior or include the segment form hip to tail 4 (segment 4) are added to the tail angular momentum. This would solely affect systems such as {[1 3] [4 5] [6 6]}. After the function AnLizardData passes the calculated values, as seen in the source code, back to the Agama function, the rigid stick models can be calculated.

As described previously there are two different rigid stick models, one evaluating a rigid stick with constant segment inertia using the angular momentum to calculate the angle change, Equation (20). The second model describes a stick model with varying inertia about the center of mass as seen in Equation (21). The implementation in the program of these functions is achieved by overloading the getSegMOI function and was done because large parts of the same data are calculated for both functions. To override the normal function getSegMOI the segment cell array has to be exchanged for a string stating either “stick”, for the rigid model or ‘magic_stick’ for the model using the varying lizard inertia. Furthermore input arguments for the length of a time step (dt), the angular momentum (H) and the inertia relative to the system center of mass have to be passed to the function. In comparison to the rigid stick, where the constant inertia of a rigid lizard is used, the “varying inertia stick” model uses the MOI generated by the lizard during the trial (sum of I_rel_com) for each time step. Equation (20) and (21) calculate the angle of each specific time step (angle change). Continuous summation of these values reveals the achieved body rotation over time.

As last step the Agama function saves the calculated variables into a cell array named agama_data. Agama_data is used as a connection between the numeric and the analytic model and consists of the variables:

- Mass (m)

- Anterior COM-distance (d)
- Length of the segments (L)
- Inertia of the segments around their COM (I)
- Segment angles (A)
- Angular momentum of all segments (H)
- Distance between the segment COM and the system COM (R_rel_com)
- Velocity of segment COM relative to system COM (V_rel_com)
- Segment Inertia at COM relative to system COM (I_rel_com)
- MOI of the rigid stick model (I_stick)
- Index of tracking start (start_idx)

The program then returns to the main file and calculates these values for all existing trials, saving all received values into a cell array. There the agama_data file, consisting of all information for all trials, is saved and can be used for the analytical model. The main file then displays the partial results.

To verify the validity of the model a program was written to generate a set of tracked test data of a lizard rotating with constant velocity around a selectable axis. In this case the angular momentum has to be constant where the angular momentum of body and tail are in defined relations. As a second verification of the program the second model was used to analytically calculate the angular momentum and was compared to the numeric model showing matching results.

5.3.2 Analytic Model

The analytical chain model was written (T. Libby, unpublished data) to combine the results of the numeric model with a zero angular momentum model. The zero angular momentum model revealed body rotation of the trial if the lizard would have no external impulses such as ground reaction forces. Furthermore the analytical model was able to calculate the angular momentum for the lizard trial by receiving the segment angles of the numeric model and was able to verify the results. It furthermore extended the functionality as well as the visualization possibilities of the results. Due to the simultaneous development of the two models and the fact that the previously described model acts as a foundation to this model, the model is described as part of the master thesis and not as part of the background. Due to the fact that there was only partial involvement of the author of this master thesis in the developing process of this model, the basic design and functionality alone will be described. The general principle of the program is deriving the analytical expressions for the angular momentum using the center of mass of the system as coordinate system origin. The terms are calculated by expressing the vector term for all distances from segment COM and system COM (r_i) and insert these terms into the term of the assumption that distance from system center of mass to the origin (d_c) is zero. This generates a term that is only dependent on the segment angles (θ), segment velocities ($\dot{\theta}$) and known constants. It is then possible to express the angular momentum formula in a form where the angular momentum is the sum of all segment scalar terms (a_i) multiplied by the angular velocities ($\dot{\theta}_i$) of the segments by fracturing out the angular velocity. The angular velocities are then written as shape angle velocities, so velocities relative to the velocity of the first angle. The formula can be transformed to show the resulting angle of the first segment, dependent on all other segment angles. The following figure shows the six segment model and the needed vectors and angles. As seen in the figure the convention for the segment constellation is first segment starting at the head to the 6 segment being the last segment of the tail. Furthermore the model was designed to be able to compute the model with a variable segment number.

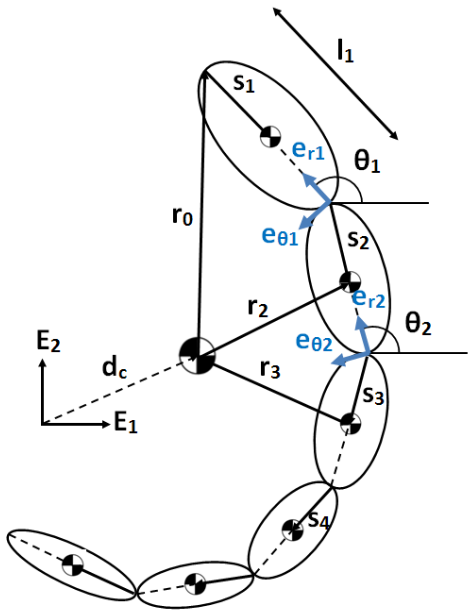

Figure 23: Analytical chain model - segment conventions

The figure shows that $\boldsymbol{r_0}$ is the vector from the center of mass of the system to the anterior end of the first segment, si are the vectors from the anterior end of the segment to the segment COM and li the lengths of the segments. The unit vectors $\boldsymbol{e_{ri}}$ and $\boldsymbol{e_{\theta i}}$ are the Cartesian basis vectors $\boldsymbol{E_1}$ and $\boldsymbol{E_2}$ turned by the angle of θ. According to T. Libby (unpublished data) the calculation of the vector $\boldsymbol{r_2}$ can now be described as

$$\boldsymbol{r_2} = \boldsymbol{r_0} - l_1\boldsymbol{e_{r1}} - s_2\boldsymbol{e_{r2}} \tag{22}$$

This leads to the general term of describing the vectors from the system center of mass to each segment center of mass ($\boldsymbol{r_i}$) as

$$\boldsymbol{r_i} = \boldsymbol{r_0} - \sum_{k=1}^{i-1} l_k\boldsymbol{e_{rk}} - s_i\boldsymbol{e_{ri}} \tag{23}$$

When describing the center of mass of a system, it can be described as the sum of all masses with the distance $\boldsymbol{d_c}$ from the origin of the coordinate system equaling the sum of masses (m_i) with the COM-system to COM-segment distance of $\boldsymbol{r_i}$.

$$\left(\sum_{i=1}^{6} m_i\right)\boldsymbol{d_c} = \sum_{i=1}^{6} m_i \boldsymbol{r_i} \tag{24}$$

When defining the COM as the origin of the coordinate system $d_c = 0$, and inserting $\boldsymbol{r_i}$ of equation (23) into the formula of the center of mass, the term

$$0 = \sum_{i=1}^{6}\left(m_i\left(\boldsymbol{r_0} - \sum_{k=1}^{i-1} l_k \boldsymbol{e_{rk}}\right) - s_i \boldsymbol{e_{ri}}\right) \tag{25}$$

is obtained (T. Libby, unpublished data). Now it is possible to write the formula defining $\boldsymbol{r_0}$ which can then be inserted to equation (23) to define $\boldsymbol{r_i}$

$$\left(\sum_{i=1}^{6} m_i\right)\boldsymbol{r_0} = \sum_{i=1}^{6} m_i\left(s_i \boldsymbol{e_{ri}} + \sum_{k=1}^{i-1} l_k \boldsymbol{e_{rk}}\right) \tag{26}$$

$$\boldsymbol{r_i} = \frac{\sum_{i=1}^{6} m_i\left(s_i \boldsymbol{e_{ri}} + \sum_{k=1}^{i-1} l_k \boldsymbol{e_{rk}}\right)}{\sum_{i=1}^{6} m_i} - \sum_{k=1}^{i-1} l_k \boldsymbol{e_{rk}} - s_i \boldsymbol{e_{ri}} \tag{27}$$

The velocity can be written in the same manner, exchanging the unit-vector $\boldsymbol{e_{ri}}$ for its derivative $\frac{d}{dt}(\boldsymbol{e_{ri}}) = \dot{\theta}_i \boldsymbol{e_{\theta i}}$ due to following calculation.

$$\boldsymbol{e_{ri}} = \cos\theta_i\, \boldsymbol{E_1} + \sin\theta_i\, \boldsymbol{E_2} \tag{28}$$

$$\frac{d}{dt}(\boldsymbol{e_{ri}}) = -\dot{\theta}_i \sin\theta_i\, \boldsymbol{E_1} + \dot{\theta}_i \cos\theta_i\, \boldsymbol{E_2} \tag{29}$$

$$\frac{d}{dt}(\boldsymbol{e_{ri}}) = \dot{\theta}_i(-\sin\theta_i\, \boldsymbol{E_1} + \cos\theta_i\, \boldsymbol{E_2}) = \dot{\theta}_i \boldsymbol{e_{\theta i}} \tag{30}$$

The velocities $\boldsymbol{v_i}$ can then be written as

$$\boldsymbol{v_i} = \frac{\sum_{i=1}^{6} m_i\left(s_i \dot{\theta}_i \boldsymbol{e_{\theta i}} + \sum_{k=1}^{i-1} l_k \dot{\theta}_k \boldsymbol{e_{\theta k}}\right)}{\sum_{i=1}^{6} m_i} - \sum_{k=1}^{i-1} l_k \dot{\theta}_k \boldsymbol{e_{\theta k}} - s_i \dot{\theta}_i \boldsymbol{e_{\theta i}} \tag{31}$$

Now all needed terms to calculate the angular momentum

$$HE_3 = \sum_{i=1}^{6} I\dot{\theta}_i + \sum_{i=1}^{6} \boldsymbol{r_i} \times m_i \boldsymbol{v_i} \tag{32}$$

are defined. After expressing these terms symbolically, the unpublished data by T. Libby shows that $\dot{\theta}_i$ can be factored out giving the term

$$H = \sum_{i=1}^{6} a_i \dot{\theta}_i \tag{33}$$

where a_i is a function of θ_1 to θ_6. When defining the shape angles and velocities as being the angles or velocities of all segments in relation to the first angle or velocity,

$$\dot{\varphi}_i = \dot{\theta}_i - \dot{\theta}_1 \tag{34}$$

the angular momentum can be written as a function of $\dot{\theta}_1$ and the shape angle velocities $\dot{\varphi}_i$ where c_i is a function of φ_1 to φ_6.

$$H = a_1 \dot{\theta}_1 + \sum_{i=2}^{6} c_i \dot{\varphi}_i \tag{35}$$

According to T. Libby, Equation (35) shows that in the case of a rigid stick $\dot{\varphi}_i = 0$ the second term of the equation equals zero, leaving a_1 to be the Inertia of the stick (I_S) and $\dot{\theta}_1$ its angular velocity. It is now possible to calculate angle θ_1 by integrating the angular velocity. The two terms describe now also the different components of the angle change. The first being the angle change due to impulse to the system (so the angle change the "varying inertia stick" model is calculating), the second term is the angle change due to the shape change of the lizard. This means that the second term is the angle change in zero angular momentum conditions.

$$\theta_1 = \int \frac{H(t)}{I_S} dt - \int \sum_{i=2}^{6} \frac{c_i}{I_S} \dot{\varphi}_i(t) dt \tag{36}$$

The formula was described in such a way, to calculate the effects of all body angles changes on the first body segment. This means that the effects of the segment angle changes show in the first angle θ_1. This can be depicted either for the angle changes due to impulse generated from ground-reaction forces, the first component of the calculation, or for angle changes due to shape changes of the body itself. In Chapter 6.2 the results will show which angle changes due to which forces are most prominent at every phase of the trial, stating how important shape change are for escape responses of lizards.

Following the description of the principle of the chain model a short overview of the programming structure is given. The full code was deemed too long to integrate in the master thesis and can be viewed in the code folder contained in the electronic version of the master thesis hand in. The code structure is as follows.

- agama_data.mat
- H_models.mat
- AngMo_snake.m
- AnimateChain.m
- Chain_H.m
- draw_chain.m
- Eval_H_poly.m
- EvalModels.m
- SimulateChain.m

To run the program, agama_data from the numeric model has to be present in the program folder. The next step of executing the model is the symbolic derivation of the analytical expression for the angular momentum seen in Equation (32) using Equation (27) and (31). This part of the program is executed by AngMo_snake and the results saved as H_models.mat. With agama_data and H_models it is possible to start the function EvalModels which is responsible to evaluate the model and acts as a main function. After defining the variables, path names and Excel phase data. Then the function will call Eval_H_poly where the symbolic formulas of the angular momentum are exchanged for numeric values. To start the chain simulation the function SimulateChain is called. It calls Chain_H which passes back the angular velocity $\dot{\theta}_1$ and integrates it to receive the resulting first angle of the body θ_1. After the angle is passed back the AnimateChain function is called, which together with the draw_chain function animate the model. Results of the program will be shown in the results section of this master thesis.

5.4 Robot Design

To prove the model results and to be able to design and construct a robot in reasonable time, the Smart Composite Microstructure (SCM) fabrication method developed by Wood et al. (2008) was used as described in the background. To fabricate a robot based on this method, the robot has to be designed in 2D space, which on one hand makes the designing process harder due to a lack of visualization of the end product itself, on the other hand the robot can be built in short time, during the design process. Due to these characteristics the design was conducted by using an iterative process. The aim of the design process was not only the feature redesign but also the reduction of the motors and to rely on passively moved legs and body motion. The design process was divided into six design steps which can be categorized into morphological changes and movement changes:

- Morphology:
    - Reducing robot size
    - Reduce foot number

    - Connect two segments
- Movement:
    - Including tail motion
    - Passive motion of segments
    - Feet motion
    - Passive motion of feet

The design steps were each seen as separate version of the robot and were built to be able to visualize the next design step and to detect possible designs errors.
As a basis for the robot a new version of RoACH (Robotic, Autonomous, Crawling Hexapod) (Hoover, Steltz and Fearing, 2008), the TAYLRoACH (Tail Actuated Yaw Locomotion RoACH) (Kohut et al., 2012) was used to implement changes in relation to the results found in this master thesis.

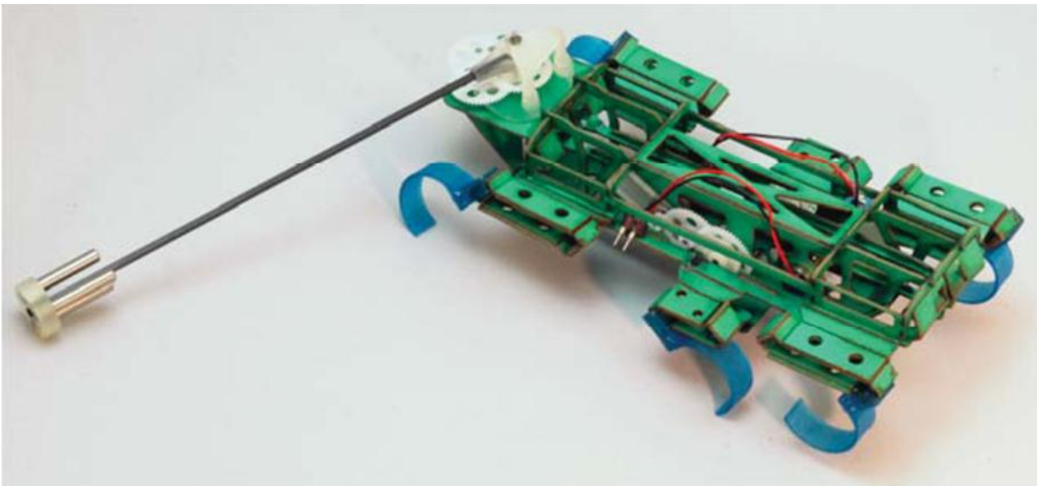

Figure 24: TAYLRoACH Robot excluding baterie and electronics for better overview (Kohut et al., 2012)

The robot was chosen due to its stability and the fact that the left and right sets of legs are actuated separately. Although this separation would have to be redesigned so that the feet move relative to each other, the independent movement was necessary to start out without constraints. A further advantage of this robot version was the fact that a possible tail connection was already designed and implemented in the robot.

For designing the robot, AutoCAD® by Autodesk, Inc. was used, due to the good 2D capabilities. To construct 2D models for the SCM fabrication method in AutoCAD, three different line types can be differentiated. The black lines depict the outer lines of the features, which will be cut in the last step of the fabrication process. The red lines describe the flexures, so the lines which will be cut before the PET is merged with the cardboard. The lines are cut into both cardboard sheets which are then merged with the PET sheet in between. The third line type (yellow) is construction lines, which are used to define feature centers and limits. This line type will have no effect on the fabrication process and are only for design purposes.

5.4.1 Morphology

In comparison to previously designed robot models of this kind, the new design would incorporate two separate sections, connected by a rotational joint. To implement lateral body bending in the robot, it had to consist of two separate sections. Since the two separate sections had to be fully functional the robot TAYLRoACH had to be decreased in size to act as a single segment of the new design. Together with its decrease in size less legs had to be implemented. After the successful implementation of these two features, two body segments of the same structure were combined using a rotational joint flexure.

The first design change to the TAYLRoACH was a change of size combined with a change of leg number. The total length of approx. 100 mm was reduced to 63.8 mm. To change the overall length of the robot, all lengths of features parallel to the longitudinal axis of the robot had to be shortened the same distance. As seen in Figure 25 this includes the main body parts, the feet mountings and the stabilizing shafts of the synchronizer. The features perpendicular to the longitudinal body axis, such as the synchronizers themselves parts for supporting the foot mounting could be left in the same configuration.

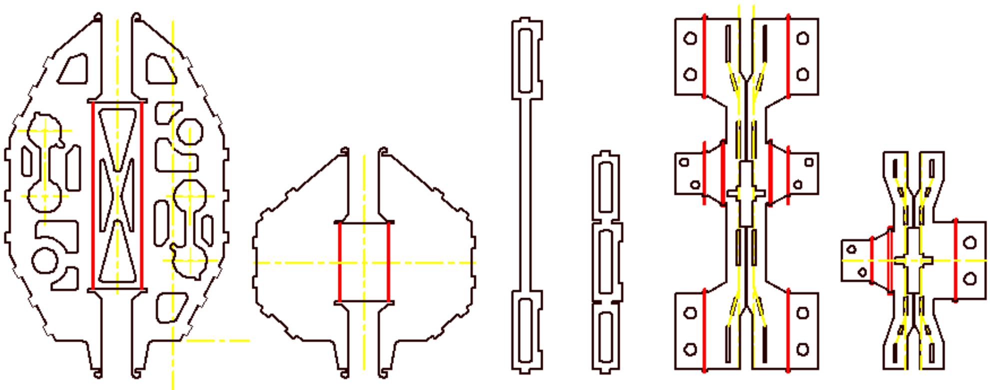

Figure 25: Upper main body part, upper leg mounting, middle leg mounting of TAYLRoACH in comparison to frist version of new design

While changing the size of the whole body size the feet number was reduced. The new back-bending model was designed to have two feet for each segment. This means the reduction of from three feet for each side, of the old model, to one foot, in the new model. The feet were designed in such a way that a connection of the left and right side of the foot would result in an asynchronous movement, meaning that the mounting on each side had to be different, one connecting to the bottom mounting one to the top mounting. With the change of the feet number and positions the mounting had to be changed accordingly.

The next change in the design was the connection of two robot bodies as segments with a rotational joint. Different methods of rotational joint were assessed, including methods similar to hinges using bearings to connect the two segments with each other. This method was assessed as not advantageous due to the weight increase at a position of the robot that was assessed to be already under stress due to torques acting perpendicular to the joint in latitudinal direction of the body. Furthermore the fabrication process was extra designed for stiff lightweight solutions combined with the possibility of flexures as joints. The final solution was the implementation of a flexure in vertical direction at the middle line of the robot segments. The body segments were extended at the main body parts and reinforced with plates to uphold the stiffness. Then a part was constructed that would extend to both main body parts with a flexure vertically to robot allowing for yaw movement. Figure 22 shows a comparison of the first version to the second version of the new robot including the stiffness plate (4) and the connection flexure (5) with the joint. The build robots can be seen in Figure 37 in Chapter 6.2.

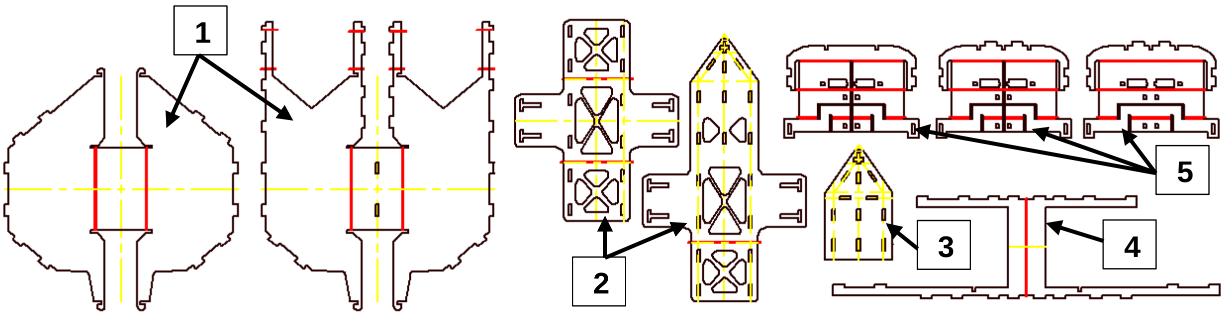

Figure 26: Version 1 in comparison to version 2 of new design upper main body part (2), lower main body part (2), stiffening plate (3), segment connection (4) and synchronizers (5) with additional synchronizer of robot version 3.

5.4.2 Movement

The second set of proposed design modification addresses the implementation of the movement for the robot. The three proposed changes concern the movement of the tail, body bending and the legs. As described in the results section the process of assessing various methods of implementing the body movement for the lizard robot could not be completed.

Due to the fact that the robot design was based on the results of the master thesis the reasoning for many of the possible implementations will be described in length in the result section of the master thesis.

To understand the principles, involved in lizard motion, the movements of the lizards in the trials as well as the results have to be studied. The following section of the design chapter will give a short overview of the motions-sequence for normal gait of the lizard and for the escape response.

The first observation was the feet position of the lizards during their gait. At full bending of the lizard body during a step, the outer front leg extends as far forward as possible while the hind leg is extended backwards. The inner legs are pointing toward each other, front leg in backwards direction, and hind leg in forward direction. At the next step the lizard moves its inner front foot and outer hind foot forwards bending in the other direction.

When dealing with escape responses in lizards the front feet push in outwards direction of the bending while the tail accelerates towards the bending direction. The front feet of the lizards leave the ground, coupled with an induction of torque by the hind feet and in some cases with a traversal of the tail into the sagittal plane. The tail stops curling inwards and starts curling in the opposite direction. After the lizard touches down the first step of the running phase is initiated finalizing the turn. When comparing the feet movement of the normal lizard gait and the escape response the same movement of hind feet can be seen. The front feet differ in their movement. Where the feet movement of hind and front of the gait is asynchronous the feet movement of the escape response is unrelated to each other.

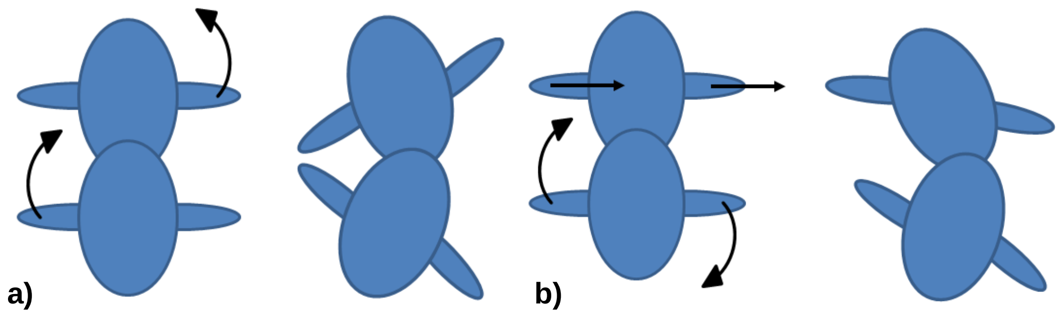

Figure 27: Lizard feet movement during a) Running gait b) Escape response

Tail

As described in the results of the thesis the tail motion concerning its role as lift off help in the aerial phase of the lizard turn has yet to be assessed. What can be said is that there is an aerial phase of the lizards when turning, giving them one center of rotation, their hind legs. There are two possibilities of including the tail into the lizard. Firstly the tail is connected as in TAYLRoACH, in plane with the body. In this configuration the robot relies on the feet movement to execute the necessary ground interaction for a possible turn. The feet are moved perpendicular to the longitudinal axis of the body, away from the robot to initiate the turn. The second possibility is to mount the tail at an angle to the robot, enabling a traversal of the tail into the sagittal plane. When positioning the tail mounting at an angle of 0° to 90° seen from the longitudinal axis upwards, the tail swing in a circular motion from one side to the other. In this case, the tail moves from the transversal plane of one side, over the sagittal plane at a displacement specified by the angle, to the traversal plane of the other side. It is believed that trough this exchange of angular momentum between tail and body, the friction forces for the front segment of the lizard will be reduced, thereby enabling the turn.

Segments

By implementing the tail in the robot, the included motor can be used to passively move the body motion. Using an eccentric wheel, a shaft is used to translate the rotary movement into linear movement. This linear movement is then used to steer the body rotation of the front segment. A possible solution for the implementation of the passive segment movement is seen as top view in Figure 28. On the right side of the figure the tail motor block is seen in light grey. As in the TAYLRoACH the motor block consists of several gears, shown in blue to achieve the necessary tail angels and velocities. The robot segments are depicted in middle gray. Due to the fact that the two possibilities, of a planar motor section and a tilted motor section persist, the gears consist of an additional gear on the robot itself. This gear (6) is used to influence the amount of linear motion and, in the case of a tilted motor solution to be able to translate the rotary movement from the tilted plane to a horizontal plane using a bevel gear. The gear, connected to the robot body is driving a rod (5), which trough an eccentric mounting on the gear and supporters in longitudinal direction (4), translates the rotational movement into a linear movement. The rod is connected to a lever (3) which is connected by a rotary link to the robot. The lever translates via another rod the motion of the tail to the frontal segment of the robot. This enables a relative motion of the frontal segment to the hind segment and results in the desired back bending motion. The rods are connected by either free moving rotational joints, depicted as empty white circles (2), or stationary rotational joints connected to the robot, with rotation axis outward of the figure plane.

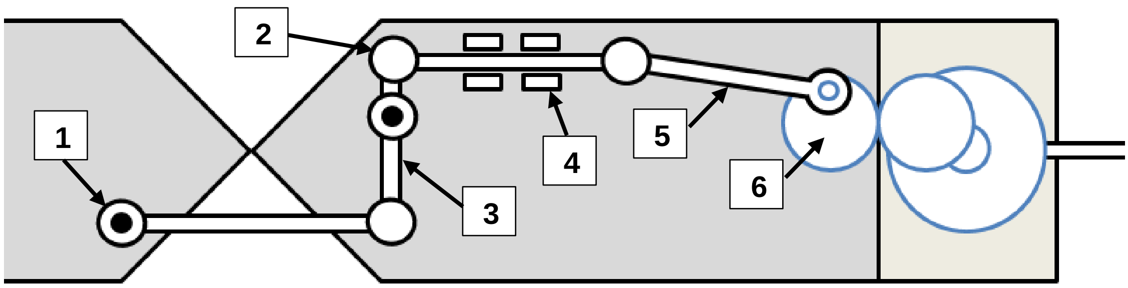

Figure 28: Top view of proposal for passive front segment motion by rotational joint connected to the robot (1), rotary joint not connected to robot (2), lever (3), supporters (4), connection rod (5) and (bevel) gear with eccentric mounting (6)

Feet motion

The feet motion can be divided into three different constraints. Firstly the relative motion of the feet pair on one segment, secondly the connection of the feet motion of the two segments and thirdly the aspect of passive feet motion. This motion constrains have to be considered for two different movement types. The movement the robot executes when moving forwards and the motion the robot needs to execute at the escape response.

The asynchronous motion of the feet pair for one segment was implemented using different leg mountings on both sides of the robot. This made a connection between the two movable sections of the synchronizers possible, while upholding the asynchronous movement characteristic of the feet. The left and right side of the synchronizers were connected above and below the horizontal cut as seen in the upper right corner of Figure 26, enabling synchronized movement of the middle leg mounting.

To combine the gait motion of the feet as well as the escape response movement, the front feet have to be able to move in a lateral direction. When thinking about the lateral movement of the front feet one has to consider that at any moment just two feet of the whole robot are in contact with the surface. This leads to two obvious effects. On one hand the robot itself is unstable when walking on the other hand to achieve lateral movement just one leg has to be actuated. These effects give rise to either let the tilting behavior of the robot account for the lateral movement while turning, or to the possibility of including an actuated longitudinal flexure in the lower body parts that are connected to the bottom foot mounting. An actuation of this flexure would tilt the leg in contact with the surface in lateral direction, accounting for the necessary movement. Furthermore due to the relative low weight of the front segment and the partly tail-induced aerial phase the possibility of inducing a lateral movement of the front feet by shifting the phase for the front feet motion was considered. This movement would help turn the robot into the right direction. The movement of the hind legs during the aerial phase of the lizard turn can be accomplished by inducing a step during the turning behavior. To achieve the necessary motion the outer hind foot pushes backward while the inner hind foot pushes forward. This induced torque helps the lizard to uphold positive impulse throughout the aerial phase of the turn. The tilting behavior of the robot plays in this case a vital role to guarantee a tripod stance of the robot, where the two hind legs, due to the higher weight of the hind segment and one front leg are on the ground.

As with the motion of the robot segments the feet motion was tried to be implemented as passively driven components. This was assessed for front and hind legs. When transmitting motion to the hind feet of the robot a simple gearing solution can be implemented, connecting the tail motion to the leg motion. A more difficult part is the translation to the front feet set. A solution for implementing a passive motion as it was done with the hind legs was researched. In the case of a gearing solution that would connect the hind feet with the front feet it would be hard to separate the body bending behavior from the leg movement. Bevel gears are used to divert the motion into the sagittal plane and are connected to a gearing solution defining the needed ratio. This can then be used to drive the middle feet mounting, depicted red in Figure 29. For the front segment of the robot the rotary linkage to the segment can be changed to a gear. The relative motion of the connecting beam to the segment can be used to drive the gears turning the foot mounting. Different gear ratios can be used to achieve the relative motion of front and hind legs.

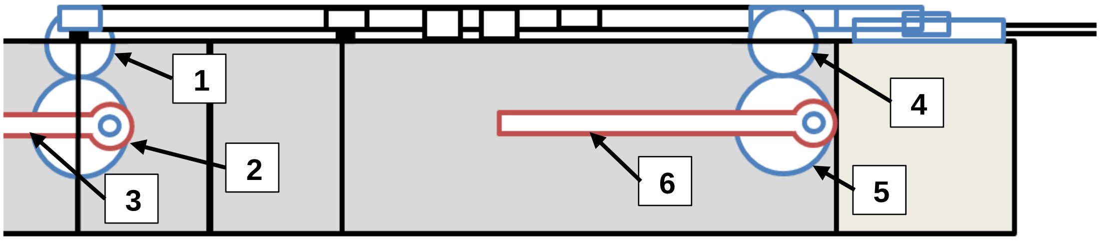

Figure 29: Side view of proposal for passive front and hind feet movement with bevel gear for motion translation to sagittal plane for front and back (1, 4), ratio gears front and back (2, 5) and rotary middle mounting for the feet (3, 6)

Another possibility for designing the leg movement is to drive the front feet with a cable that would translate body movement independent motion by exposing the cable to torsion. The easiest way of implementing frontal leg movement is the implementation of a motor on the front segment of the body with the disadvantage of weight increase.

5.5 Robot Construction

As soon as one design step, as described in the previous chapter was finalized, the robot was printed. To be able to apply the used fabrication process correctly it was necessary to follow the conventions of the laser printing software. The software is designed to differentiate between different layers resp. colors of a 2D SolidWorks or AutoCAD drawing. Since the flexures and the outlines are laser-cut at different steps of the fabrication process they were drawn in different layers.

The first step of fabrication was the rough cut of the sheets of poster board in the dimensions of 230x200 mm. The rough-cut differentiated by 20mm for height and width to the original dimensions of 210x180mm to pin the sheet down with weight to avoid displacement during the cutting process. As soon as the sheets were cut an adhesive sheet was attached to the cardboard. This compound was then fed into a lamination machine to guaranty a solid connection. The sheets were then fitted after each other into the laser cutter (VersaLaser VL200) and were pinned down with weights to cut the first layer of the drawing, the flexures. The cardboard sheets would be stuck together adhesive sheets facing each other, which is why the compound had to be cut one with the adhesive sheet facing up and once with the sheet facing downwards. After all flexures were cut, seen in Figure 30a the protective foil of the adhesive sheets could be removed. One of the cardboard sheets was then attached to a 1µm thick layer of PET. After aligning the sheets perfectly using the newly cut dimensions and alignment holes the two cardboard sheets with one layer of PET in the middle were stuck together. After the resulting layers of cardboard-adhesion-PET-adhesion-cardboard were merged using the laminate machine the compound was fitted of the finalizing cut into the laser cutter. After ensuring that the sheet was fitted the right way and weighing down, the outlines of the robot parts were cut.

Thereafter the parts could be extracted from the rest material. The parts were then fitted and glued together in the designed for way.

Figure 30 shows one of the two poster board sheets after the flexures have been cut out to the left. In the middle the resulting parts of the first version can be seen and to the right the constructed robot of version 2.

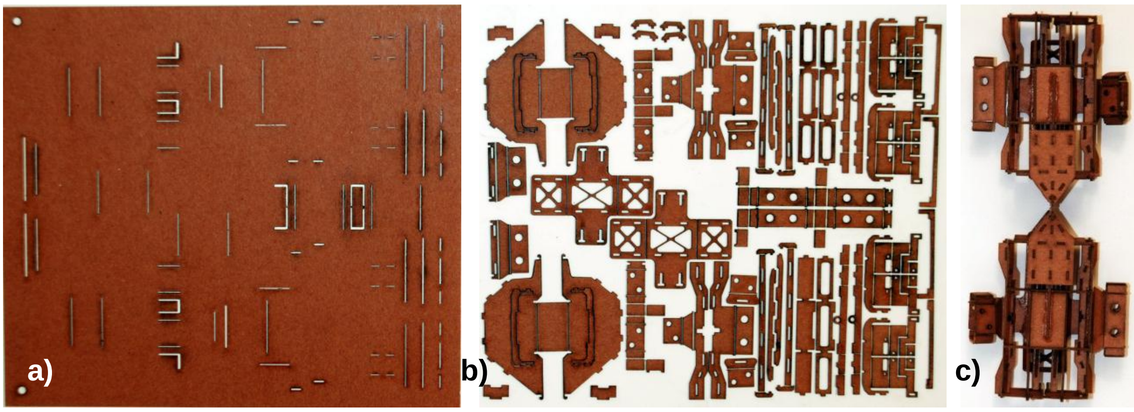

Figure 30: Construction steps a)Cardboard sheet with cut flexures – version 1 (left) b) final laser-cut parts – version 1 (middle) c) complete robot – version 2 (right)

After the current version is built the robot is assessed and used as a visualization help for further design steps.

Due to the early stage of the design process the tail had not been fitted to the current model. The tail addition would include the motor. Battery and microcontroller would be placed at the hind segment of the robot.

6 Results

Following the successful data acquisition, extraction and implementation, the results can be discussed. They will be divided into the same subcategories as the previous chapters, biological and technical to enable a clear overview. Due to the novel character of this research topic, much of the research time was invested in the biological aspect of the research and the evaluation of the morphometric and approximated values. It is also clear that further studies are needed to assess implications of the results of this thesis.

6.1 Biological

The results for the biological aspects are shown below and discuss the data acquisition. Many of the described results such as animal behavior are derived from observations of the author. To be able to generalize these behavioral characteristics further studies are needed.

6.1.1 Habitat and Standardization

The habitat was, as described in Chapter 4.1 rearranged and equipped to be able to conduct animal trials. For this reason three high power spotlights were positioned to reflect against the walls of the lizard cages. The housing was furthermore fitted with caoutchouc mats to act as a non-reflective background for the high speed cameras while upholding the surface friction for the lizards. These mats had to be removed again due to the fact that the natural rubber was eaten by the crickets which were provided as food for the lizards and might have caused digestion problems for the lizards. The camera was arranged so that videos could be taken from an overhead view. The equipment was left in the room that the lizards would be not distressed by the overhanging lights and camera when taking trails. Furthermore the shelters of the lizard housing tank were arranged in a way that the trials could be conducted. It was deemed important that the shelters would be put into place a week before the trials to make sure that the lizards would know where to escape to. Two shelters, the positioning shelter and the escape shelter were positioned in a way that the entrances would point towards each other. The positioning shelter was place under the camera, the escape shelter outside of the field of view. The arrangement of the equipment for the trials proved to be advantageous since it was possible to shine out the whole trial area, while upholding accessibility. The camera position was deemed to near to the trail setup. The negative effect can be seen in many trials where a part of the lizard leaves the field of view. Furthermore a negative aspect of handling and arrangement of the equipment for the trials is the distance of the animal facility from the laboratory as well as the small premises of the lizard facility. When evaluating the new method of conducting trials in their living environment, it can be said that it was possible to increase the trial rate drastically. The assumption that the lizards would be more receptible to stimuli in an environment they are familiar with could be confirmed. Furthermore a change in lizard behavior over the course of the trials could be identified, where the lizards after several trials were unwilling to go back into the shelters. As described in Chapter 4.2.4 the lizards were chased into the shelters to position them in respect to the camera. After the lizard went successfully into the shelter the shelter was lifted to be able to induce the escape response via the stimuli. It was noticed that the lizards would take longer each trail to return to the shelter. In some cases the lizards were unwilling to go back into the shelter after numerous trials. This behavior would suggest a learning behavior that could interfere with a standardized trial setup. Another disadvantage to a standardized trial is the problem of the lizards getting accustomed to a certain type of stimulus, while using different stimuli could interfere with the scientific validity of a general statement about the movement of lizards. In the conducted trails the stimulus was presented as a slow hand motion at the beginning, to catch the lizard's attention and an acceleration combined with a grabbing motion when coming closer to the lizard. The stimulus was presented from the front to achieve escape responses of high angles.

6.1.2 Animal Behavior

During the trial the lizard motion sequence varied in small degrees from the expectations. It could be seen that when a stimuli was induced to early that it was more likely that the lizard would turn less than 135° to either keep the predator in view or due to lack of orientation after the shelter was lifted. For this reason the positioning shelter was rotated to enable a sight of line from the lizard to the escape shelter. Additionally the time between the removal of the shelter and the presentation of the stimuli was lengthened to accommodate the lizard to the new surroundings. Another dominating aspect of the lizard motion was a traversal of the tail into the sagittal plane at the lizard turn after the stimulus was presented. This motion was considered to be executed due to a possible reduction of ground reaction forces for the front feet of the lizard enabling an easier lift of for the aerial phase. Another possibility why this behavior was executed was the fact that the stimuli had to be presented from the top of the lizard tank downwards due to the shape of the habitat. The reaction could be interpreted as a defense mechanism against the stimuli. A combination of these two possible advantages might be the reasons for this behavior.
In many of the conducted trials the lizard, although executing the turn would stay at the position of the touch down after the areal phase. This behavior can be possibly ascribed to an adaption to the stimulus, a high degree of distress or a lack of orientation. Trails with this behavior could only be used for evaluating the turn phase, but had to be excluded from evaluations of the running phase.

The trials with reduced friction increased the insight of the forces acting at the lizard turn. The most prominent aspect of the lizard movement when analyzing the low-friction trials was the great displacement of hind legs. At the start of the turn the outer hind leg pushes outward laterally and the inner hind leg pushes forwards generating a torque in direction of the turn, about the hind legs. This behavior could not be seen in the normal friction trials which suggest that the back legs play a great role for the turning behavior of the lizard.

The overall number of trails conducted is 126 where 111 where conducted with normal friction and 15 with low friction. The trials showed an average turning angle of 112° showing that either the lizards were too familiar with the trial situation and thereby showed a decreased escape response or the animals were still to unfamiliar with the environment. Another possibility of such a small turning angle could be to short resting phases for the animals.

6.2 Technical

Although many biological aspects had to be addressed, due to the novelty of the research topic, the technical aspects were planned to be the significant part of the research and combine data extraction and implementation.

6.2.1 Tracking

Of the 126 trials 40 trials with normal friction and 3 trials with low friction were tracked. Below a sequence of figures, extracted from the tracking software are seen. Resulting text files with exacted coordinates of the tracked markers were then used in the numeric model.

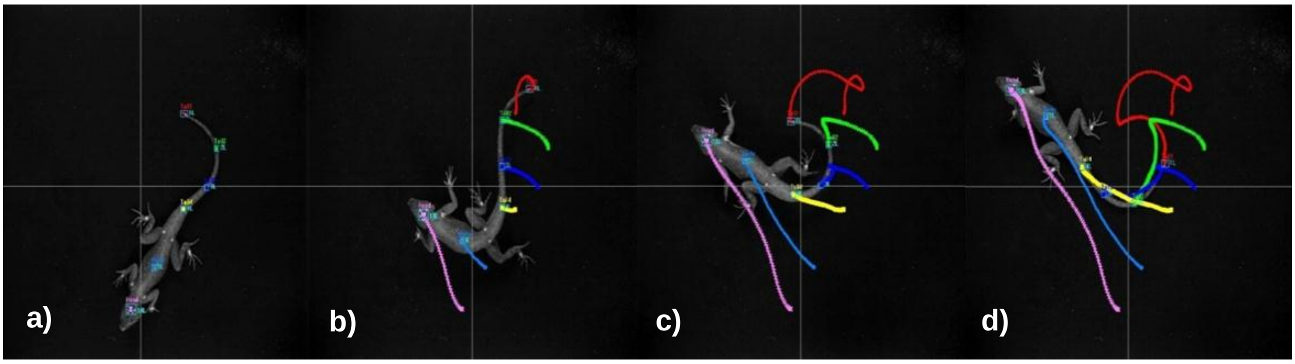

Figure 31: Sequence of tracked video a) movement start b) curling phase – aerial phase c) curling maximum d) uncurling phase

The tracking was conducted mainly by automatic tracking. After the automated tracking had stopped, the consistency of the tracking was controlled. Sequences that were too far from the marked point on the lizard, or sequences where the point was completely lost were done manually. Due to the high value of the search area multiplier and the low threshold the tracking was quite stable but increased the time in tracking.

6.2.2 Approximation

The approximations of the living lizards were conducted separately for the body of the lizard and the tail. The body approximations for mass and the center of mass distance were calculated using the average fraction of seven dead lizards. This resulted in average mass-errors lower than 10% and COM-distance errors of 8.32% for the front and 16.19% for the hind segment of the body. The inertia for the body was calculated using unconstrained nonlinear optimization for equation 4. This resulted in an average error lower than 7%. The methods used for the body approximations proved to be accurate enough for our trials. Although the center of mass distance had a higher error than we hoped for, a reduction of influence, as described in chapter 5.2.1 could be proven.

The mass, COM-distance and Inertia of the tails of the living lizards was approximated using a truncated elliptical cone method. After validating the formula to be correct and usable for all cases the results showed significant error for mass and inertia of approx. 60%. After excluding the dorsal ridge from the morphometric measurements the maximum error could be reduced to approx. 30%. Furthermore the case was made that the inertia for the posterior segments of the tail were of little influence for the total angular momentum resulting in fraction of 0.77% to 2.03%. It was also made the case that the total error of the model is less influential than the variations of the individual trials.

6.2.3 Numeric and Analytic Model

The numeric model was verified using simplified model data which was generated by rotating a rigid body around a specified position. The angular momentum in this case is constant and was verified by independent calculation. Furthermore the data of the numeric model was transferred to the analytical model and recalculated, showing equal results thereby validating the numeric model. The analytical model was then used to simulate and extract results from the data generated by the numeric model. The results will be presented by explaining two different trials, Trial-A with no running phase after the turn and Trial-B where a running phase was executed.

Tail influence

The first achieved result was a comparison between the actual executed body rotation and the body rotation that would have been achieved if no external torques are acting on the system (total angular momentum is zero). It can be stated that the angle achieved is solely a result of shape changes without any external impulses. Furthermore the effect of the tail segments on this zero-angular-momentum model was plotted to show how the length of the tail would influence the body rotation. In the following figure the actual body angle is depicted as blue line showing a single slope for Trial-A. For Trial-B the beginning of the oscillatory effect of the running gait on the lizard’s body angle can be seen. From the green line to the ochre line zero-angular-momentum models are depicted with decreasing segment size from 6 to 2, starting the reduction of the segments at the posterior end of the lizard.

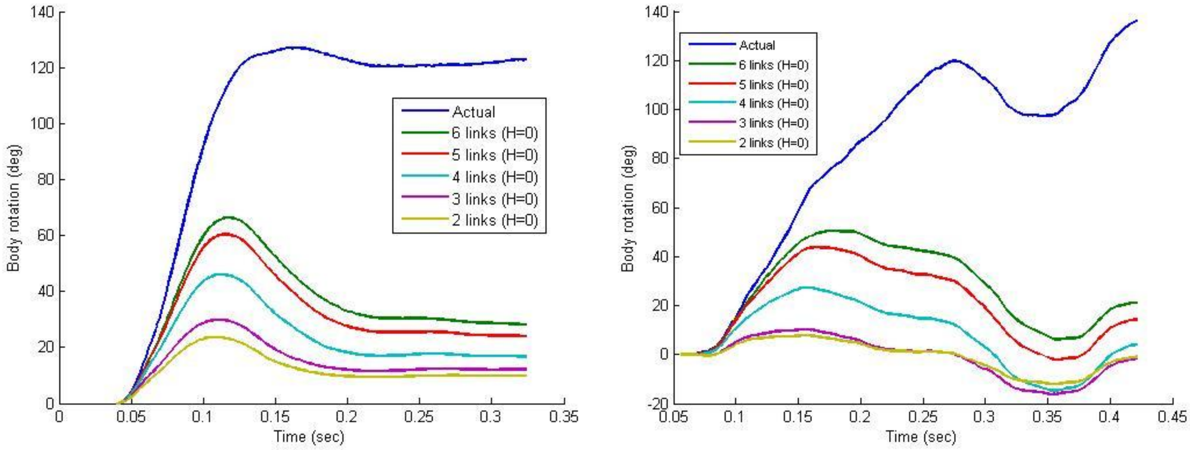

Figure 32: Angular change of actual body angle and body angles of reduced zero-angular-momentum models

The figure shows clearly that the initial angle change of the actual trial and the zero-H model are very similar in magnitude. At approx. 65 degree for Trail-A and 50 degree for Trial-B the zero-H model starts to turn back. The reductions of the first three tail segments have a high impact on the achieved angle which is remarkable considering that the tail has 20% of the total lizard mass. If all tail segments are remove and the shape change of the two body segments are the only inputs for the turn the body angle decreases to 20°(Trial-A) or 10° (Trial-B). This shows the high importance of the tail during the turn of the lizard.

Body angle

The next comparison shows the actual body angle (blue), zero angular momentum body angle (cyan), the body angle achieved by the rigid stick model (green) and the body angle achieved by the varying inertia stick model (red). The stick model depicts the angular change of a rigid object with the same morphometric data and angular momentum of the lizard excluding the inertia change. The varying inertia stick is the model that depicts the angular change including the change of inertia over time. Due to the fact that the segments themselves don't change position in relation to each other these two models show the body angle change excluding the shape change of the lizard. The figure also shows the phases of the trial. The phases are categorized by outer foot contact (dark blue) and the phase when the outer front foot is in the air (light blue). The dark red – light red bar at the bottom of the graph show the tail curling behavior from start, to maximum, to uncurling end of the motion

It can be clearly seen that in the initial phase, where the lizard's front feet are still in contact with the floor, the angle changes due to shape change dominate. In the second phase, where the front feet of the lizards are lifted off of the ground, the forces due to impulse gain importance. These two effects where surprising at first, since the lizard seems to be pushing in the first phase (generating impulse forces) and shape changing in the second phase (generating forces by exchange of angular momentum). An explanation for the data could be found when looking at the frictionless trails. As explained before an exaggerated movement of the hind feet during the initial phase could be seen generating a torque about the body's hind section. Combined with the fact that the front feet seem to just follow the movement of the displacement passively the data is plausible. In this phase, after the lizard has touched down again the forces due to external impulses keep the lizard from rotating backwards.

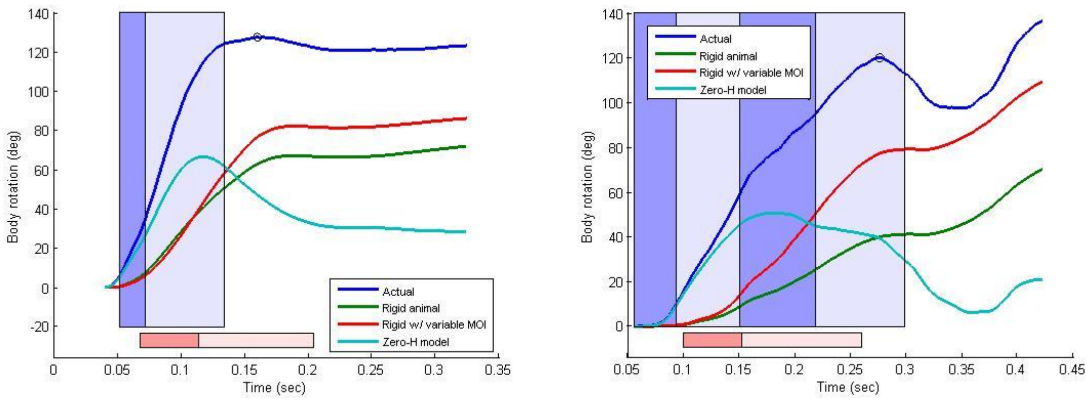

Figure 33: Angular change in comparison of actual body angle (blue) to zero-angular-momentum (cyan), stick model (green) and varying inertia stick model (red) angle change

The figure shows the body rotation due to shape change and body rotation due to external impulses very clearly and how these two influence the total body angle. Another clearly seen feature is how both body angle aspects play a vital role for the total body angle change. What can also be seen is that as soon as the body angle would go backwards due to the uncurling of the tail, the body angle change due to impulse forces gain importance and keeps the total body angle from decreasing.

Body velocity

A clearer picture of the involved forces is shown by Figure 34 which shows velocities of all the models from the previous figure: Actual model (blue); Zero-angular-momentum model (cyan); Stick model (green); Varying inertia stick model (red).

The generated torques equal the slopes of the graphs and when compared to the Figure 33 have to be applied before any change of angle can be seen. As expected this show a rapid incline of the graph depicting the zero-H model in the initial phase. Due to the regular slope of the velocities of the models depicting the external impulses, it can be said that the resulting generated torque about COM is constant during the first phase and reaches into the second phase. As explained before the difference between the stick model and the varying inertia stick model is the changing of the moment of inertia around the center of mass. As seen in the figure the red line extends further than the line depicting the stick model. This means that although the velocity due to the angular momentum falls of, the velocity of the varying inertia stick can be increased by decreasing the moment of inertia with the curling behavior. This shows the well-known effect of a rotating figure skater pulling his arms in to increase the angular velocity. In the second phase of the turn, where the front legs of the lizard are in the air, a decrease of the velocity due to the shape change can be seen. This decrease is counteracted by an increase of velocity due to external impulses. This is the reason why the total velocity can be seen as a relative constant coasting behavior during the second phase of the turn.

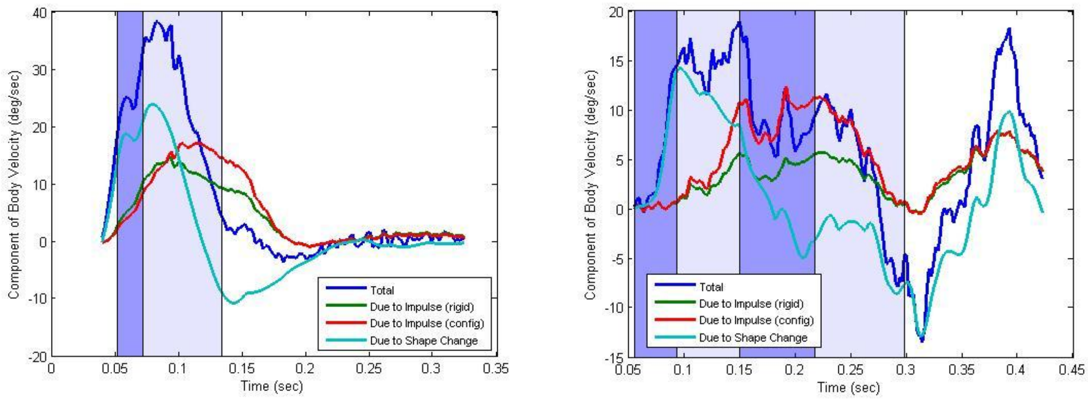

Figure 34: Angular velocity of actual trial (blue), zero-angular-momentum (cyan), stick model (green) and varying inertia stick model (red)

Rotation fraction

The previously seen figures were evaluated for all trials. To quantify the results for all trials a plot was generated to show the relation of the body angle components for all trials for each phase. Figure 35 shows the first two phases of the turn for all shape change influenced angle change (blue circles) and for all impulse influenced angle change (red circles). The plots show the components of the angle change in relation to the actual shape change. In the first phase, the phase, where the front feet are on the ground, an average of 68.8% of actual angular change are due to forces generated by shape change. In the second phase these forces are still slightly dominant with 57.4%. Another interesting fact in the following plot is that in the first two phases the values can be linearized and are both in the positive area of the plot. This means that firstly the fraction of the components are not related to the turn. This implies that no matter which angle is achieved by the turn the fractions of the angle components shape change and impulsive are the same. Secondly the positive value speaks for a contribution of both values towards the swing.

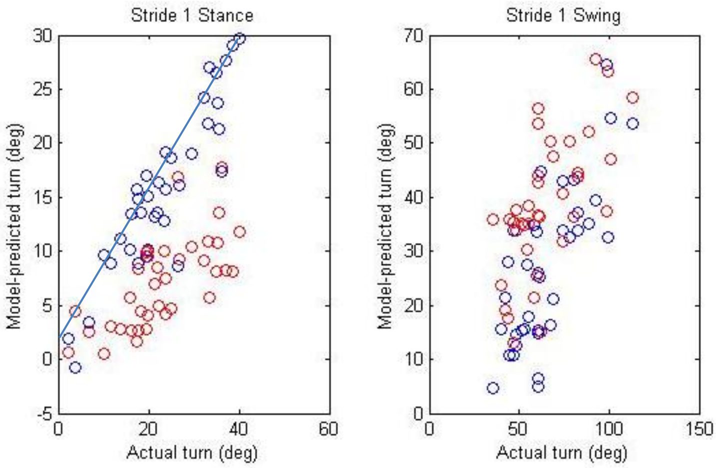

Figure 35: Components of the angle change (shape change - blue; impulse - red) in relation to the actual shape change for phase 1 and phase 2 of the turn

The third and fourth phase show opposing angles due to the fact that rotational effects caused by the shape change and those caused by external impulses mostly chancel each other out.

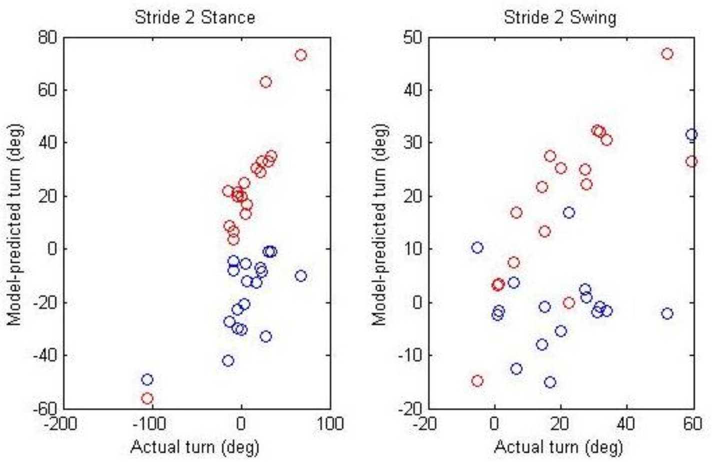

Figure 36: Components of the angle change (shape change - blue; impulse - red) in relation to the actual shape change for phase 1 and phase 2 of the turn

6.2.4 Robot Proposal

The results for the concerning the proposal for the robot implementation of the found biological principles combine the first two built versions of the robot and sketches for the implementation of the motion implementation. The robot seen in Figure 37 was built as a segmented version of TAYLRoACH with the capability of body bending using the smart composite microstructure (SCM) fabrication method.

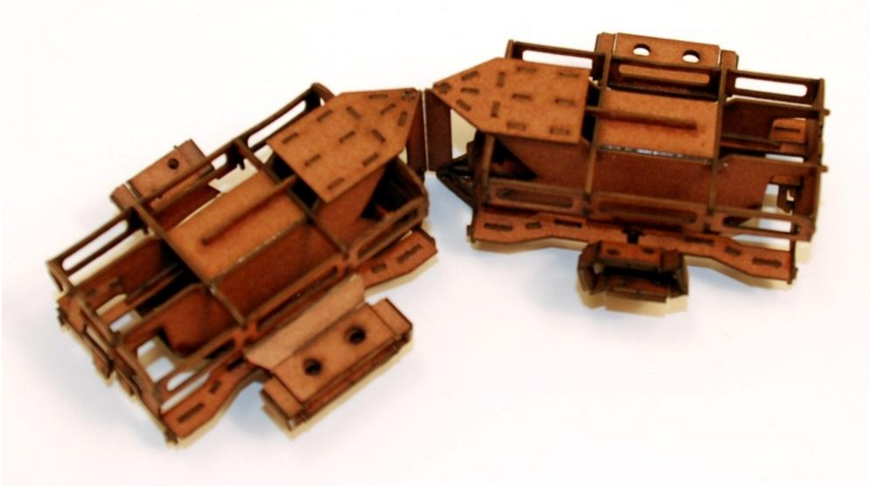

Figure 37: Robot built as part of the biological inspired robot proposal (version 2)

The synchronized motion of the leg pairs on each segment was proposed to be implemented by connecting the synchronizers of the robot. The tail of the robot was proposed to be connected to the robot at an angle to enable an aerial phase of the front feet. Furthermore the hind feet motion and bending motion was proposed to be connected to the motor moving the tail of the robot. The motion of the front feet was proposed either to be implemented connected to the body motion or to be actuated by a separate motor. Due to the phase shift of the feet motion when looking at the normal gait and the turning behavior, the motor implementation is seen as a more likely implementation to succeed. When looking at the results of the models it can be seen that the robot has to firstly make a step at the lizard’s first stride of the turning behavior. Secondly the robot has to move its tail at the first phase of the turn.

The results in light of the hypothesis of the master thesis contradict the null hypothesis. Shape change during the lizard motion does influence the turning behavior of the lizard. It could be proven that the shape change of the lizard increases the body angle by 68.6% in the first phase and 57.4% in the second phase of the turn. The second stride is dominated by external impulses to counteract the back swing of the tail proving hypothesis three.

7 Conclusion

The goal of the thesis was to conclude if the shape changes in lizard escape responses influence the velocity and angle of the turn and to propose a robot design which would incorporate this movement. Escape responses are vital for the survival of a species which is why the motion sequence is a highly refined and optimized process. Due to previous research that showed that lizards use exchange of angular momentum for aerial maneuvers it was deemed adequate to presume a similar exchange for terrestrial maneuvers. To prove this hypothesis, trials on living lizards of the species *Agama Agama* was conducted. In the trials the agama was presented frontally with a stimulus to induce an escape response. To increase the trail number and reduce the time necessary for conducting the trials, they were conducted in the lizard facility using their housing tanks as research setup. The trial setup consisted of two shelters, the escape shelter and the positioning shelter. The lizard would be chased into the positioning shelter, which would guarantee a stretched position of the lizard. After the shelter was lifted off and the stimulus presented, the lizard would execute an escape response into the escape shelter. The escape response consists of several phases of which the first one is an outward pushing of the front feet combined with a curling of body and tail towards the escape direction. The next phase consists of the lift-off of the front feet to generate a rotational axis around the hind legs which at this point push forward and outward to generate a torque that would help to increase the total turning angle. Approximately halfway through the turn the tail starts to uncurl. At the touch down of the first stride the lizard initiates the running phase in the second stride the tail uncurls fully. The trials were recorded with a high speed camera, were assessed, tracked and exported as text files. Of the 126 conducted trials 40 normal friction trials and 3 trials with low friction could be used to input into the generated models and be processed. The models consisted of a numeric model, which calculated the inertia, angular velocity and angular momentum. To be able to calculate the angular momentum the living lizards had to be approximated. For the approximation of the front and hind body segment of the lizards, 7 dead lizards were measured and an average fraction used to specify the mass and the distance to the COM of the lizard segments. The body moment of inertia was approximated using unconstrained nonlinear optimization resulting in an average error of less than 10%. The tail was approximated using a truncated elliptical cone which was found to be sensitive to measurement errors. After the angular momentum was calculated the analytical model could calculate the zero-angular-momentum case and could compare it to the rigid stick model and the rigid stick model with changing inertia. This then was used to show angle and velocity for each component of the actual behavior where the zero-angular-momentum case depicted the component for changes due to shape changes and the stick models changes due to external impulses. The robot proposal could be concluded with a segmented robot with a flexible joint and proposals for the implementation of actuation solutions.

The thesis can be concluded as successful since all goals were achieved. The results of the trials could show that 68.8% to 57.4% of the first stride of the lizard turn was due to shape change as well as be implemented in the proposal of the robot.

The results of the master thesis will built the basis for research in the coming years. Further projects could include force platforms to evaluate ground reaction forces, and 3D laser scans for calculating the morphometric data. Lizard housing, possibly with integrated light and cameras could help to increase the trial number. For future trials two stimuli at 45° could increase the escape response. Also trials for escape responses while the lizards are running would further the understanding of the roles of the feet while turning. Furthermore trials with more camera views should be conducted to be able to calculate tail swings into the sagittal plane. For future work the models could include different inertia at different foot stances and could be expanded for 3D data information.

The conducted proposal of the robot could be implemented and assessed to prove if similar values for the components of shape change and external impulses could be achieved.

Bibliography

Arquitetogeek, 2009. *biomimética e arquitetura*. [online] Available at: <http://arquitetogeek.com/2009/11/15/biomimetica-arquitetura-2/> [Accessed 10 Sep. 2012].

Autumn, K. et al., 2000. Adhesive force of a single gecko foot-hair. *Nature*, [online] 405(6787), pp.681–5. Available at: <http://www.ncbi.nlm.nih.gov/pubmed/10864324> [Accessed 22 Mar. 2012].

Autumn, K., 2005. Robotics In Scansorial Environments. *Proceedings of SPIE*, [online] 5804, pp.291–302. Available at: <http://link.aip.org/link/?PSI/5804/291/1&Agg=doi>.

Autumn, K., Florance, E. and Full, R.J., 2000. *Publication Images*. [online] Available at: <http://geckolab.lclark.edu/private/u38j47a0t/images.html> [Accessed 10 Sep. 2012].

Avadhanula, S., Wood, R.J., Campolo, D. and Fearing, R.S., 2002. Dynamically tuned design of the MFI thorax. In: *Proceedings 2002 IEEE International Conference on Robotics and Automation Cat No02CH37292*. [online] Ieee, pp.52–59. Available at: <http://ieeexplore.ieee.org/lpdocs/epic03/wrapper.htm?arnumber=1013338>.

Baker, M., 1590. *Fragments of Ancient Shipwrightry*.

Bannasch, R. and Kniese, L., 2011. *Flexible Impact Blade with Drive Device for a Flexible Impact Blade*. 281479.

Barthlott, W. and Ehler, N., 1977. Rasterelektronenmikroskopie der Epidermisoberflächen von Spermatophyten. *Tropische und subtropische Pflanzenwelt*, 19, pp.367–467.

Bechert, D.W., Bartenwerfer, M., Hoppe, G. and Reif, W.E., 1986. Drag reduction mechanisms derived from shark skin. In: *15th ICAS Congress*. International Council of the Aeronautical Sciences, pp.1044–1068.

Birkmeyer, P., Peterson, K. and Fearing, R.S., 2009. DASH : A Dynamic 16g Hexapedal Robot. In: *Proceedings 2009 IEEE International Conference on Intelligent Robots and Systems*. pp.2683–2689.

Blackmail, A.E., 1925. The Plumb-line Method of Centring a Lens. *The Australasian Journal of Optometry*, [online] 7(7), pp.180–185. Available at: <http://dx.doi.org/10.1111/j.1444-0938.1925.tb00731.x>.

Bleckmann, H., Mürtz, M. and Schmitz, H., 1997. *Detektor für Infrarotstrahlung*. DE19718732.

Boston Dynamics Inc., 2012. *Cheetah - Fastest Legged Robot.* [online] Available at: <http://www.bostondynamics.com/robot_cheetah.html> [Accessed 12 Sep. 2012].

Brown, R.M., Taylor, D.H. and Gist, D.H., 1995. Effect of caudal autotomy on locomotor performance of wall lizards (Podarcis muralis). *Journal of Herpetology*, [online] 29(1), pp.98–105. Available at: <http://www.jstor.org/stable/1565091>.

Chang-siu, E., Libby, T., Tomizuka, M. and Full, R.J., 2011. A Lizard-Inspired Active Tail Enables Rapid Maneuvers and Dynamic Stabilization in a Terrestrial Robot. *Science And Technology*, pp.1887–1894.

Coates, J., 2009. *Lizards*. 2nd ed. New Jersey: OTTN Publishing, p.112.

Cooper, W.E., 1998. Risk factors and emergence from refuge in the lizard Eumeces laticeps. *Behaviour*, 135(135), pp.1065–1076.

Cooper, W.E., Pérez-Mellado, V. and Hawlena, D., 2007. Number , Speeds , and Approach Paths of Predators Affect Escape Behavior by the Balearic Lizard , Podarcis Lilfordi. *Society for the Study of Amphibians and Reptiles*, 41(2), pp.197–204.

Daimler AG, 2008. *Design and technology inspired by nature: Mercedes-Benz bionic car at The Museum of Modern Art in New York.* [online] Available at: <http://www.emercedesbenz.com/Feb08/21_001037_Mercedes_Benz_Bionic_Car_To_Appear_As_Part_Of_A_New_Yorks_Museum_Of_Modern_Arts_Exhibition.html> [Accessed 10 Sep. 2012].

Domenici, P., 2002. The Visually Mediated Escape Response in Fish: Predicting Prey Responsiveness and the Locomotor Behaviour of Predators and Prey. *Marine and Freshwater Behaviour and Physiology*, [online] 35(1), pp.87–110. Available at: <http://www.tandfonline.com/doi/abs/10.1080/10236240290025635>.

Domenici, P. and Blake, R.W., 1997. THE KINEMATICS AND PERFORMANCE OF FISH FAST-START SWIMMING. *Journal of Experimental Biology*, [online] 1178(8), pp.1165–1178. Available at: <http://jeb.biologists.org/content/200/8/1165.short>.

Dowling, J.J., Durkin, J.L. and Andrews, D.M., 2006. The uncertainty of the pendulum method for the determination of the moment of inertia. *Medical engineering & physics*, [online] 28(8), pp.837–41. Available at: <http://www.ncbi.nlm.nih.gov/pubmed/16442329> [Accessed 12 Mar. 2012].

Gillis, G.B., Bonvini, L.A. and Irschick, D.J., 2009. Losing stability: tail loss and jumping in the arboreal lizard Anolis carolinensis. *Journal of Experimental Biology*, [online] 212(Pt 5), pp.604–609. Available at: <http://www.ncbi.nlm.nih.gov/pubmed/19218510>.

Gruber, P., 2011. *Biomimetics in Architecture: Architecture of Life and Buildings*. [online] Springer Vienna Architecture, p.245. Available at: <http://www.amazon.com/Biomimetics-Architecture-Life-Buildings/dp/3709103312>.

Hall, S.J., Wardle, C.S. and MacLennan, D.N., 1986. Predator evasion in a fish school: test of a model for the fountain effect. *Marine Biology*, 91, pp.143–148.

Hansen, W.R. and Autumn, K., 2005. Evidence for self-cleaning in gecko setae. *Proceedings of the National Academy of Sciences of the United States of America*, [online] 102(2), pp.385–9. Available at: <http://www.pubmedcentral.nih.gov/articlerender.fcgi?artid=544316&tool=pmcentrez&rendertype=abstract>.

Harzheim, L., 2008. *Bionische Otimierung bei der Konstruktion technischer Bauteile in der Automobilindustrie*. [online] Bionik-Wirtschaftsforum. Available at: <http://www.bionik-wirtschaftsforum.de/media/1405080508147b2d.pdf> [Accessed 10 Sep. 2012].

Hoover, A.M. et al., 2010. Bio-inspired design and dynamic maneuverability of a minimally actuated six-legged robot. In: *Proceedings 2010 3rd IEEE RAS & EMBS International Conference on Biomedical Robotics and Biomechatronics*. pp.869–876.

Hoover, A.M. and Fearing, R.S., 2008. Fast scale prototyping for folded millirobots. In: *Proceedings 2008 IEEE International Conference on Robotics and Automation*. pp.886–892.

Hoover, A.M., Steltz, E. and Fearing, R.S., 2008. RoACH: An autonomous 2.4 g crawling hexapod robot. In: *Proceedings 2008 IEEE/RSJ International Conference on Intelligent Robots and Systems*. [online] pp.26–33. Available at: <http://ieeexplore.ieee.org/xpls/abs_all.jsp?arnumber=4651149> [Accessed 19 Mar. 2012].

Jusufi, A., Goldman, D.I., Revzen, S. and Full, R.J., 2008. Active tails enhance arboreal acrobatics in geckos. *Proceedings of the National Academy of Sciences of the United States of America*, [online] 105(11), pp.4215–9. Available at: <http://www.pubmedcentral.nih.gov/articlerender.fcgi?artid=2393739&tool=pmcentrez&rendertype=abstract>.

Jusufi, A., Kawano, D.T., Libby, T. and Full, R.J., 2010. Righting and turning in mid-air using appendage inertia: reptile tails, analytical models and bio-inspired robots. *Bioinspiration biomimetics*, [online] 5(4), p.045001. Available at: <http://www.ncbi.nlm.nih.gov/pubmed/21098954>.

Jusufi, A., Zeng, Y., Full, R.J. and Dudley, R., 2011. Aerial righting reflexes in flightless animals. *Integrative and Comparative Biology*, [online] 51(6), pp.937–43. Available at: <http://www.ncbi.nlm.nih.gov/pubmed/21930662>.

Kelly, M., 1868. *Improvement in Fences*. 74379.

Kim, S. et al., 2007. Whole body adhesion: hierarchical, directional and distributed control of adhesive forces for a climbing robot. *Proceedings 2007 IEEE International Conference on Robotics and Automation*, [online] pages(April), pp.1268–1273. Available at: <http://ieeexplore.ieee.org/lpdocs/epic03/wrapper.htm?arnumber=4209263>.

Kohut, N.J. et al., 2011. MEDIC : A Legged Millirobot Utilizing Novel Obstacle Traversal. In: *Proceedings 2011 IEEE International Conference on Robotics and Automation*. [online] pp.802–8. Available at: <http://robolab.cse.unsw.edu.au/conferences/ICRA-2011/data/papers/1622.pdf>.

Kohut, N.J., Haldane, D.W., Zarrouk, D. and Fearing, R.S., 2012. EFFECT OF INERTIAL TAIL ON YAW RATE OF 45 GRAM LEGGED ROBOT. In: *Proceedings of the Fifteenth International Conference on Climbing and Walking Robots and the Support Technologies for Mobile Machines*. pp.157–164.

Kwon, Y.-H., 1998. *BSP Equations*. [online] Available at: <http://www.kwon3d.com/theory/bspeq/bspeq.html> [Accessed 14 May 2012].

Lewis, M.A., Bunting, M.R., Salemi, B. and Hoffmann, H., 2011. Toward Ultra High Speed Locomotors: Design and test of a cheetah robot hind limb. *2011 IEEE International Conference on Robotics and Automation*, [online] pp.1990–1996. Available at: <http://ieeexplore.ieee.org/lpdocs/epic03/wrapper.htm?arnumber=5979812>.

Libby, T. et al., 2012. Tail-assisted pitch control in lizards, robots and dinosaurs. *Nature*, [online] 481(7380), pp.181–184. Available at: <http://www.nature.com/doifinder/10.1038/nature10710>.

Lilienthal, O., 1889. *Der Vogelflug als Grundlage der Fliegekunst*. Berlin.

Lindsay, S., 2011. *The Australian Museum - Dusky Shark denticles, Carcharhinus obscurus*. [online] Available at: <http://australianmuseum.net.au/image/Dusky-Shark-denticles-Carcharhinus-obscurus> [Accessed 10 Sep. 2012].

Lüneberg, H., 2003. *Geschichte der Luftfahrt: Band 2: Luftschiffe*. Mannheim: Reinhard Welz Vermittler Verlag.

Madsen, T. and Loman, J., 1987. ON THE ROLE OF COLOR DISPLAY IN THE SOCIAL AND SPATIAL ORGANIZATION OF MALE RAINBOW LIZARDS AGAMA-AGAMA. *AmphibiaReptilia*, [online] 8(4), pp.365–372. Available at: <http://0-search.ebscohost.com.library.unl.edu/login.aspx?direct=true&db=boh&AN=BACD198885088095&loginpage=Login.asp&site=ehost-live>.

Martin, J. and Avery, R.A., 1998. Effects of tail loss on the movement patterns of the lizard, Psammodromus algirus. *Functional Ecology*, [online] 12(5), pp.794–802. Available at: <http://doi.wiley.com/10.1046/j.1365-2435.1998.00247.x>.

Mather, T.W. and Yim, M., 2009. Modular configuration design for a controlled fall. *2009 IEEE/RSJ International Conference on Intelligent Robots and Systems*, [online] pp.5905–5910. Available at: <http://ieeexplore.ieee.org/lpdocs/epic03/wrapper.htm?arnumber=5354027>.

Mattheck, C., 1998. *Design in Nature*. [online] *Nature*, Springer, p.217. Available at: <http://www.springerlink.com/index/10.1007/978-3-642-58747-4>.

Mercedes-Benz Classic, 2008. *Bionic Car*. [online] Available at: <http://blog.mercedes-benz-passion.com/bionic-car/> [Accessed 10 Sep. 2012].

Merriam-Webster Dictionary, 1960. *Bionics*. [online] Available at: <http://www.merriam-webster.com/dictionary/bionics> [Accessed 20 Jul. 2012].

de Mestral, G., 1955. *Velvet Type Fabric and Method of Producing Same*. 2717437.

Mongeau, J.-M. et al., 2012. Rapid Inversion: Running Animals and Robots Swing like a Pendulum under Ledges. *PLoS ONE*, [online] 7(6), p.e38003. Available at: <http://dx.plos.org/10.1371/journal.pone.0038003>.

Nachtigall, W., 2002. *Bionik: Grundlagen und Beispiele für Ingenieure und Naturwissenschaftler*. 2nd ed. Heidelberg: Springer-Verlag.

Pullin, A., Kohut, N., Zarrouk, D. and Fearing, R.S., 2010. *Dynamic turning of 13 cm robot comparing tail and differential drive*. [online] *robotics.eecs.berkeley.edu*. Available at: <http://robotics.eecs.berkeley.edu/~ronf/PAPERS/pullin-icra12.pdf> [Accessed 19 Mar. 2012].

Rasmussen, M.H. and Miller, L.A., 2004. Echolocation and social signals from white-beaked dolphins, Lagenorhynchus albirostris, recorded in Icelandic waters. In: J.A. Thomas, C.F. Moss and M. Vater, eds., *Echolocation in bats and dolphins*. University of Chicago Press, pp.50–53.

Schmitz, H. and Schuetz, S., 2000. Waldbrandortung durch Melanophila acuminata Die spezialisierten Sinnesorgane des Feuerkäfers. *Biologie in Unserer Zeit*, 30(5), pp.266–273.

Schwarz, S., Hofmann, M.H. and Von Der Emde, G., 2002. Weakly electric fish as a natural model for industrial sensors. *Computer Methods and Programs in Biomedicine*, 67, pp.55–66.

Stratakis, E., Zorba, V. and Barberoglou, M., 2009. Laser structuring of water-repellent biomimetic surfaces. *SPIE Newsroom*. [online] Available at: <https://spie.org/documents/Newsroom/Imported/1441/1441_5423_0_2009-01-16.pdf> [Accessed 10 Sep. 2012].

Tobin, J., 2004. *To Conquer the Air: The Wright Brothers and the Great Race for Flight*. New York: Simon&Schuster.

Turner, J.S. and Soar, R.C., 2008. Beyond biomimicry : What termites can tell us about realizing the living building . (May), pp.14–16.

da Vinci, L., 1505. *Sul volo degli uccelli*. Firenze.

Wegener, K., 2007. *Ein flexibles Greifsystem für Roboterassistenten im Haushalt*. [online] Universität Stuttgard, p.122. Available at: <http://elib.uni-stuttgart.de/opus/volltexte/2007/3178/> [Accessed 22 Mar. 2012].

Whiteley, S.M. et al., 2010. Wireless recording of the calls of Rousettus aegyptiacus and their reproduction using electrostatic transducers. *Bioinspiration biomimetics*, [online] 5(2), p.026001. Available at: <http://dx.doi.org/10.1088/1748-3182/5/2/026001>.

Wood, R.J. et al., 2008. Microrobot Design Using Fiber Reinforced Composites. *Journal of Mechanical Design*, [online] 130(5), p.052304. Available at: <http://link.aip.org/link/JMDEDB/v130/i5/p052304/s1&Agg=doi>.

List of Figures

List of Tables

List of Abbreviations

2D, 3D	Two-dimensional, Three-dimensional
AVI	Audio video interlace
CAO	Computer aided optimization
CiBER	Center for Integrative Biomechanics in Education and Research
COM	Center of mass
DASH	Dynamic Autonomous Sprawled Hexapod
EVA	Ethylene-vinyl acetate
GB	Gigabyte
GUI	Graphic User Interface
LUT	Lookup table
MB	Megabyte
MOI	Moment of inertia
PET	Polyethylene terephalate
Poly-PEDAL	Poly- Performance, Energetics, and Dynamics of Animal Locomotion
RoACH	Robotic, Autonomous, Crawling Hexapod
ROC	Record on demand
ROG	Radius of Gyration
SCM	Smart composite microstructure
SEM	Scanning electron microscope
SKO	Soft kill option
TAYLRoACH	Tail Actuated Yaw Locomotion RoACH
TEC	Truncated elliptical cone
TXT-Files	Text-file
UV	Ultraviolet

A: HiSpec 1 – Fastec Imaging Corp.

FASTEC IMAGING™
HIGH SPEED IMAGING IN THE PALM OF YOUR HAND

HiSpec 1 Innovative Low-Light High-Speed Camera

Fast Facts

- Excellent Light Sensitivity: 3,200 ISO monochrome, 1,600 ISO color
- Outstanding Image Quality: Up to 506 frames per second at 1280 x 1024 resolution
- Extremely Fast: Adjustable frame rate up to 112,000 frames per second
- Well Connected: GiGE compatible for easy remote camera control
- Fits Anywhere: Only 63mm H x 63mm W x 65mm D and .28 kg
- GiGE Vision: Industry standard control interface

Easy to use Camera Control Software

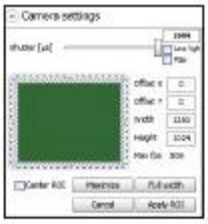

ImageBLITZ® Auto Trigger feature based on selectable region of interest

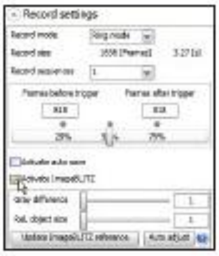

Key Features

- **Forget About Bright Lights** – Until now, lighting has sometimes been a challenge with high-speed imaging. No more! The photo-sensitivity of the HiSpec 1 enables high speed recordings at 1.3 megapixels under normal lighting conditions.
- **ImageBLITZ® Auto Trigger** – Now it's easy to capture those elusive random events. Simply define a "region of interest" in the field of view and let the ImageBLITZ® trigger take over. Any change in the pre-set image area will stop the recording and save the event sequence. No special hardware or intrusive wiring is required.
- **Multi-Sequence Record Mode** - The Multi-Sequence Record Mode allows the recording of multiple events by partitioning the memory into 2, 4, 8 or 16 individual recordings. And with the HiSpec 1's unique Burst Trigger Mode, you can capture hundreds of separate image sequences in the memory without downloading.
- **Use it Everywhere** – The HiSpec 1's Gigabit Ethernet interface allows the user to operate multiple cameras from any standard Notebook / PC up to a distance of 100 meters. The HiSpec 1 is designed for easy operation in virtually any industrial or laboratory environment.

See what you've been missing

Fastec HiSpec 1

Camera Specifications

Standard Features

System Design	Scaleable and network-compatible with standard and/or notebook PCs Synchronous processing of multiple cameras
Sensor	CMOS sensor, 1280 x 1024 pixels, 10-bit monochrome or RGB color with BAYER filter Active pixel area 22.9mm diagonal
Pixel Size	14 x 14 µm
Light Sensitivity	3,200 ISO monochrome, 1,600 ISO color
Spectral Bandwidth	400 - 900 nm
Record Rate	Up to 506 fps at full resolution, up to 112,183 fps at reduced resolution
Image Memory	2GB, Optional upgrade to 4GB.
Recording Time	3.2 seconds at full resolution Longer record times with variable resolution and frame rates
Shutter	Global electronic shutter from 2µsec to 1second
Lens Mount	C-Mount or F-Mount
Frame Format	BMP, TIF, DNG, JPG or AVI file format
Camera / PC Interface	1000/100 Ethernet interface (Gigabit Ethernet)
Phase Lock	Multiple cameras can be synchronized to a master camera or to an external source
Trigger	Contact closure, external TTL signal or software trigger (ImageBLITZ® Auto Trigger)
Multi-Sequence Record Mode	2, 4, 8 or 16 individual recording partitions
Camera Size	63mm H x 63mm W x 65mm D with C-Mount lens. 63mm H x 63mm W x 92.5mm D with F-Mount lens
Camera Weight	.28 kg. without lens
Operating Environment	+5° to +35°C (to +45° with cooling option)
Power Supply	10 - 30V DC external power supply
Power Consumption	7.5W maximum

Software Specifications

Camera Control Software	HiSpec Director 2 Software for Windows 7/ Vista / XP
Image Amplification	Digital gain from 1 to 4 in 8 steps
Optional SDK	GiGE Vision compatible

Options Available

Memory	4GB

Sample Frame Rates and Resolutions

Maximum Frame Rate	Resolution	2GB Standard Recording Time @ Maximum Frame Rate	2GB Standard Total Frames	4GB Option Recording Time @ Maximum Frame Rate	4GB Option Total Frames
506 fps	1280 x 1024	3.2 sec.	1,636	6.5 sec	3,274
718 fps	1280 x 720	3.2 sec.	2,327	6.5 sec	4,656
1,008 fps	1280 x 512	3.2 sec.	3,272	6.5 sec	6,548
1,319 fps	768 x 600	3.5 sec.	4,654	7.1 sec	9,313
2,312 fps	480 x 480	4.0 sec.	9,309	8.1 sec	18,627
5,672 fps	320 x 240	4.9 sec.	27,926	9.9 sec	55,879
13,540 fps	144 x 144	7.6 sec.	103,436	15.3 sec	206,967
112,183 fps	128 x 2	74.7 sec	8,378,368	149.4 sec	16,756,736

FASTEC IMAGING 17150 Via Del Campo, Ste. 301 • San Diego • CA 92127 • CA USA
1.858.592.2342 • www.fastecimaging.com

R1-HiSpec1-04/12

B: Truncated elliptical cone – (Kwon, 2008)

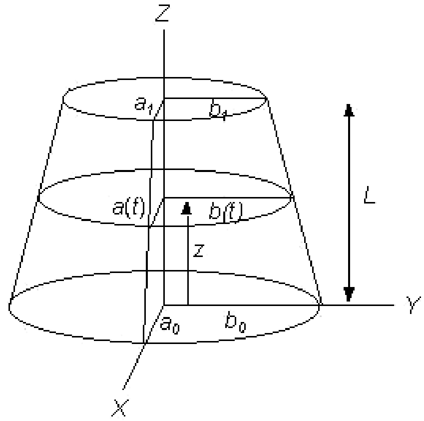

$$F_{22}(a,b) \equiv (a_1 - a_o)(b_1 - b_o)$$
$$F_{21}(a,b) \equiv a_o(b_1 - b_o) + (a_1 - a_o)b_o$$
$$F_{20}(a,b) \equiv a_o b_o$$

$$F_{44}(a,b,c,d) \equiv (a_1 - a_o)(b_1 - b_o)(c_1 - c_o)(d_1 - d_o)$$
$$F_{43}(a,b,c,d) \equiv a_o(b_1 - b_o)(c_1 - c_o)(d_1 - d_o) + (a_1 - a_o)b_o(c_1 - c_o)(d_1 - d_o)$$
$$+(a_1 - a_o)(b_1 - b_o)c_o(d_1 - d_o) + (a_1 - a_o)(b_1 - b_o)(c_1 - c_o)d_o$$
$$F_{42}(a,b,c,d) \equiv a_o b_o(c_1 - c_o)(d_1 - d_o) + a_o(b_1 - b_o)c_o(d_1 - d_o) + a_o(b_1 - b_o)(c_1 - c_o)d_o$$
$$+(a_1 - a_o)b_o c_o(d_1 - d_o) + (a_1 - a_o)b_o(c_1 - c_o)d_o + (a_1 - a_o)(b_1 - b_o)c_o d_o$$
$$F_{41}(a,b,c,d) \equiv (a_1 - a_o)b_o c_o d_o + a_o(b_1 - b_o)c_o d_o + a_o b_o(c_1 - c_o)d_o + a_o b_o c_o(d_1 - d_o)$$
$$F_{40}(a,b,c,d) \equiv a_o b_o c_o d_o$$

$$G_{20}(a,b) = \frac{F_{22}(a,b)}{3} + \frac{F_{21}(a,b)}{2} + F_{20}(a,b)$$

$$G_{21}(a,b) = \frac{F_{22}(a,b)}{4} + \frac{F_{21}(a,b)}{3} + \frac{F_{20}(a,b)}{2}$$

$$G_{22}(a,b) = \frac{F_{22}(a,b)}{5} + \frac{F_{21}(a,b)}{4} + \frac{F_{20}(a,b)}{3}$$

$$G_{40}(a,b,c,d) = \frac{F_{44}(a,b,c,d)}{5} + \frac{F_{43}(a,b,c,d)}{4} + \frac{F_{42}(a,b,c,d)}{3} + \frac{F_{41}(a,b,c,d)}{2} + F_{40}(a,b,c,d)$$

$$m = \pi\rho L \cdot G_{20}(a,b)$$

$$g_z = \frac{G_{21}(a,b)}{G_{20}(a,b)} L$$

$$I_{xx} = \frac{\pi}{4}\rho L \cdot G_{40}(a,b,b,b) + \pi\rho L^3 \cdot G_{22}(a,b) - m \cdot g_z^{\,2}$$

C: Trial Procedure Diagram

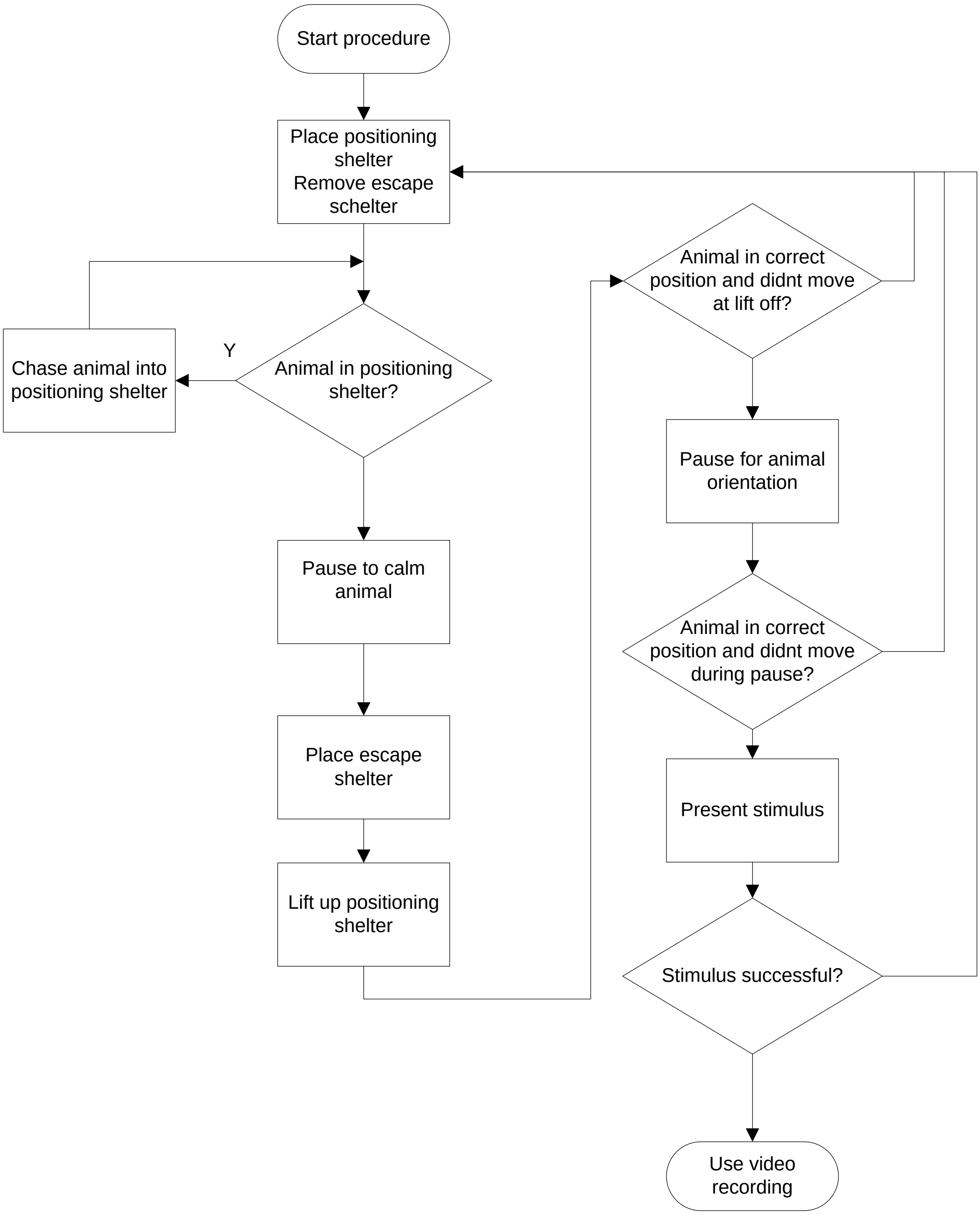

D: Trial Phases

Day	Animal	Trial	Body Rotation	relative Tail angle	start move	start outer front foot move	outer front foot lift-of	outer front foot touch-down	Outer front second LO	Outer front second TD	curling start	curling max	uncurling end
24	1	1	90	-30	0.088	0.092	0.128	0.18	0.31	NA	0.106	0.17	0.248
24	1	4	100	-15	0.04	0.052	0.072	0.134	0.226	0.3	0.068	0.114	0.204
25	1	2	-70	-45	0.016	0.034	0.054	NA	NA	NA	0.04	0.07	0.164
25	1	3	90	-15	0.016	0.032	0.056	0.142	NA	NA	0.042	0.078	0.166
25	1	5	90	-60	0.014	0.028	0.054	0.146	NA	NA	0.04	0.084	0.186
17	2	1	-135	10	0.044	0.064	0.086	0.14	0.196	0.26	0.092	0.112	0.188
18	2	1	-135	90	0.046	0.058	0.088	0.171	NA	NA	0.066	0.112	0.196
18	2	4	-125	50	0.056	0.056	0.094	0.15	0.218	0.298	0.1	0.152	0.26
18	2	9	-100	-30	0.15	0.158	0.182	0.236	0.345	0.356	0.184	0.202	0.258
18	2	11	-110	70	0.002	0.004	0.026	0.104	NA	NA	0.03	0.058	0.162
19	2	2	-75	40	0.21	0.219	0.26	0.322	0.41	0.476	0.246	0.296	0.366
19	2	4	-110	30	0.032	0.044	0.072	0.142	NA	NA	0.076	0.122	0.194
19	2	5	-135	-10	0.028	0.038	0.058	0.14	0.22	0.288	0.064	0.104	0.178
19	2	6	140	40	0.016	0.022	0.056	0.121	NA	NA	0.052	0.096	0.168
19	2	7	110	0	0.116	0.126	0.15	0.232	0.28	0.336	0.152	0.164	0.256
18	3	1	-100	30	NA	NA	NA	0.158	NA	NA	NA	0.142	0.26
5	5	7	-50	90	0.016	0.018	0.036	0.084	NA	NA	0.032	0.068	0.114
5	5	8	-75	100	0.006	0.008	0.03	0.07	NA	NA	0.026	0.06	0.114
5	5	10	-85	60	0.036	0.038	0.06	0.104	NA	NA	0.056	0.092	0.138
24	5	2	180	-55	0.126	0.132	0.15	0.19	0.222	0.27	0.158	0.236	0.328
24	5	3	135	-35	0.102	0.124	0.144	0.19	NA	NA	0.122	0.174	0.226
24	5	5	130	-45	0.56	0.572	0.588	0.64	0.678	0.728	0.588	0.642	0.762
25	5	5	180	-90	0.022	0.038	0.058	0.096	0.126	0.16	0.044	0.074	0.232
25	5	6	95	-25	0.002	0.022	0.034	0.072	0.116	0.156	0.022	0.06	0.098
25	5	7	135	-80	0.012	0.02	0.044	0.082	0.108	0.15	0.032	0.072	0.176
25	5	8	-100	30	0.014	0.242	0.284	0.312	NA	NA	0.03	0.068	0.114
25	5	9	55	-60	0.01	0.02	0.046	0.088	0.344	0.376	0.044	0.08	0.116
12	6	1	90	-90	0.204	0.214	0.235	0.29	NA	NA	0.226	0.248	0.34
23	6	1	90	-40	0.234	0.242	0.261	0.316	NA	NA	0.26	0.288	0.388
23	6	3	55	-10	0.082	0.096	0.117	0.218	NV	NV	0.109	0.154	0.222
23	6	4	120	-45	0.114	0.132	0.161	0.219	0.288	0.36	0.161	0.188	0.272
25	6	1	70	-45	0.024	0.032	0.052	0.122	NA	NA	0.044	0.092	0.162
12	7	4	-100	15	0.014	0.016	NA	0.117	NA	NA	0.052	0.076	0.116
12	7	5	145	-15	0.023	0.03	0.063	0.135	0.176	0.236	0.07	0.111	0.204
12	7	6	-70	-10	0.048	0.055	0.074	0.13	NA	NA	0.074	0.094	0.154
12	7	7	-75	0	0.038	0.056	0.076	0.135	NA	NA	0.068	0.102	0.178
23	7	1	95	0	0.052	0.059	0.084	0.138	0.17	0.234	0.082	0.108	0.146
23	7	4	-60	30	0.042	0.052	0.072	0.122	NA	NA	0.076	0.098	0.146
23	7	6	-80	0	0	0.008	0.036	0.114	NA	NA	0.024	0.06	0.126
25	7	1	-85	10	0.006	0.018	0.042	0.118	NA	NA	0.028	0.07	0.154
25	7	3	-85	25	0.002	0.014	0.038	0.1	0.284	0.376	0.018	0.052	0.108
25	7	4	-100	20	0.02	0.028	0.056	0.112	NA	NA	0.042	0.082	0.144
25	7	5	-125	10	0.018	0.026	0.048	0.086	0.128	0.238	0.038	0.078	0.184

E: Geometric Formulas

Cylinder	Formula	Source
v	pi a^2 h	http://www.wolframalpha.com/input/?i=cylinder+volume
Iy	m*(1/3*l^2+1/4*a0^2)	http://bp1.blogger.com/_oF_1Qcfku_w/R5q-yiAnbaI/AAAAAAAAAZw/Y_PjNmn1kf0/s1600-h/rectangle-moment-inertia.gif
Ix	m*(1/3*l^2+1/4*a0^2)	http://bp1.blogger.com/_oF_1Qcfku_w/R5q-yiAnbaI/AAAAAAAAAZw/Y_PjNmn1kf0/s1600-h/rectangle-moment-inertia.gif
Iyy	m*(3*a0^2+l^2)/12	http://bp1.blogger.com/_oF_1Qcfku_w/R5q-yiAnbaI/AAAAAAAAAZw/Y_PjNmn1kf0/s1600-h/rectangle-moment-inertia.gif
Ixx	m*(3*a0^2+l^2)/12	http://bp1.blogger.com/_oF_1Qcfku_w/R5q-yiAnbaI/AAAAAAAAAZw/Y_PjNmn1kf0/s1600-h/rectangle-moment-inertia.gif

Cone	Formula	Source
v	1/3 pi a^2 h	http://www.wolframalpha.com/input/?i=cone+volume
Iy	m*(3*a0^2+2*l^2)/20	http://www.wolframalpha.com/input/?i=cone+moment+of+inertia
Ix	m*(3*a0^2+2*l^2)/20	http://www.wolframalpha.com/input/?i=cone+moment+of+inertia
Iyy	m*(3/80*l^2+3/20*a0^2)	http://bp1.blogger.com/_oF_1Qcfku_w/R5q-yiAnbaI/AAAAAAAAAZw/Y_PjNmn1kf0/s1600-h/rectangle-moment-inertia.gif
Ixx	m*(3/80*l^2+3/20*a0^2)	http://bp1.blogger.com/_oF_1Qcfku_w/R5q-yiAnbaI/AAAAAAAAAZw/Y_PjNmn1kf0/s1600-h/rectangle-moment-inertia.gif

Elliptical Cylinder	Formula	Source
v	pi a b h	http://www.wolframalpha.com/input/?i=ellyptical+zylinder
Iy	m*(1/4*a0^2+1/3*m*l^2)	http://www.efunda.com/math/solids/solids_display.cfm?SolidName=EllipticalCylinder http://www.engrasp.com/doc/etb/mod/util1/solidprop/solidprop_help.html
Ix	m*(1/4*b0^2+1/3*m*l^2)	http://www.efunda.com/math/solids/solids_display.cfm?SolidName=EllipticalCylinder http://www.engrasp.com/doc/etb/mod/util1/solidprop/solidprop_help.html
Iyy	m*(1/4*a0^2+1/12*l^2)	http://www.efunda.com/math/solids/solids_display.cfm?SolidName=EllipticalCylinder
Ixx	m*(1/4*b0^2+1/12*l^2)	http://www.efunda.com/math/solids/solids_display.cfm?SolidName=EllipticalCylinder

Truncated Circular Cone	Formula
v	1/3 pi h (a b+a^2+b^2)
Iy	pi*l^3*rho*((a1*(a0 - a1))/2 + a1^2/3 + (a0 - a1)^2/5) + (pi*l*rho*(a0^5 - a1^5))/(2*(10*a0 - 10*a1)) + (pi*l*rho*(l - (l*(3*a0 - 3*a1)*((2*a1*(a0 - a1))/3 + a1^2/2 + (a0 - a1)^2/4))/(a0^3 - a1^3))^2*(a0^3 - a1^3))/(3*a0 - 3*a1) - (pi*l^3*rho*(3*a0 - 3*a1)*((2*a1*(a0 - a1))/3 + a1^2/2 + (a0 - a1)^2/4)^2)/(a0^3 - a1^3)
Ix	pi*l^3*rho*((a1*(a0 - a1))/2 + a1^2/3 + (a0 - a1)^2/5) + (pi*l*rho*(a0^5 - a1^5))/(2*(10*a0 - 10*a1)) + (pi*l*rho*(l - (l*(3*a0 - 3*a1)*((2*a1*(a0 - a1))/3 + a1^2/2 + (a0 - a1)^2/4))/(a0^3 - a1^3))^2*(a0^3 - a1^3))/(3*a0 - 3*a1) - (pi*l^3*rho*(3*a0 - 3*a1)*((2*a1*(a0 - a1))/3 + a1^2/2 + (a0 - a1)^2/4)^2)/(a0^3 - a1^3)
Iyy	pi*l^3*rho*((a1*(a0 - a1))/2 + a1^2/3 + (a0 - a1)^2/5) + (pi*l*rho*(a0^5 - a1^5))/(2*(10*a0 - 10*a1)) - (pi*l^3*rho*(3*a0 - 3*a1)*((2*a1*(a0 - a1))/3 + a1^2/2 + (a0 - a1)^2/4)^2)/(a0^3 - a1^3)
Ixx	pi*l^3*rho*((a1*(a0 - a1))/2 + a1^2/3 + (a0 - a1)^2/5) + (pi*l*rho*(a0^5 - a1^5))/(2*(10*a0 - 10*a1)) - (pi*l^3*rho*(3*a0 - 3*a1)*((2*a1*(a0 - a1))/3 + a1^2/2 + (a0 - a1)^2/4)^2)/(a0^3 - a1^3)

F: Matlab code – Numeric model

```
% Master Thesis Project: "AgamaTurning", 2012
% Written by Viktor Gudenus

% Main ----------------------------------------------------------------------

clear
clc
close all

% Files for analysis
folder_name='Trials';
filename = getFilename(folder_name);
filename = sort(filename);

% Define Excel-Worksheet Phases Name and Path (same path as trials!) & Read
filename_xls='Trials/tracking_phases.xls'; % Path/filename.xls
xls_data=struct;
[xls_data.num,xls_data.text,xls_data.all] = xlsread(filename_xls);

% SubSystem description {[Seg1 Seg2]} from Seg1 to Seg2 of subsystem
% where:  1=Tail1-Tail2; 2=Tail2-Tail3; 3=Tail3-Tail4;
%         4=Tail4-Hip; 5=Hip-Body; 6=Body-Head

Segments = {[1 1],[2 2],[3 3],[4 4],[5 5],[6 6]}; % Six-Segemnt Model
% Segments = {[1 2],[3 4],[5 6]}; % Three-Segment Model
% Segments = {[1 4],[5 6]}; % Two-Segment Model
% Segments = {[1 6]}; % One-Segment Model
% Segments = {[1 1],[2 2],[3 3],[4 4],[5 5]}; %without front body :) perfect


 for i = 1:length(filename)
    % Outputs time, Angular momentum, MOI of links about system center of
    % mass, etc
    [time{i}, H_tot{i}, I_rel_com{i}, body_angle{i}, magic_angle{i},
stick_angle{i}, I_tot{i}, H_tot_body{i}, H_tot_tail{i}, R_com{i},
R_rel_com{i}, R{i}, A{i}, H{i}, omega{i},agama_data{i},H_fraction{i}] =
Agama(filename{i},xls_data,Segments);
    % Total MOI about system COM
    I_overall{i} = sum(I_rel_com{i}')';
    max_I(i) = max(I_overall{i});
    min_I(i) = min(I_overall{i});
    I_ratio(i) = min(I_overall{i})/max(I_overall{i});
 end

mean(I_ratio);
std(I_ratio);

% Calculate influence of I*omega term on angular momentum Fraction
h_frac_tmp={[] [] [] [] [] [] []};
for i=1:length(H_fraction)
    h_frac_tmp{eval(filename{i}(14))}=[h_frac_tmp{eval(filename{i}(14))}(:,:);
H_fraction{i}];
end
clear H_fraction
H_fraction=[];
```

```
for i=1:length(h_frac_tmp)
    h_frac_tmp{i}=mean(h_frac_tmp{i},1);
    H_fraction=[H_fraction(:,:);h_frac_tmp{i}];
end
H_fraction=mean(H_fraction,1);


save('ChainModel\agama_data.mat','agama_data');

%% Plot output from one file
Day=25;
Animal=5;
Trial=8;
ind=search_Trial(filename,Day,Animal,Trial);
fprintf('Displayed file:\n%s\n',filename{ind})

figure
plot(time{ind}, H_tot{ind}, 'r', 'Linewidth', 3)
hold on
plot(time{ind}, H_tot_body{ind}, 'b--', 'Linewidth', 3)
hold on
plot(time{ind}, H_tot_tail{ind}, 'g-*', 'Linewidth', 3, 'MarkerSize', 7)
title(filename{ind})
legend('Total Angular Momentum', 'Angular Momentum of Body', 'Angular Momentum
of Tail', 'Location', 'Best')
xlabel('Time, sec')
ylabel('Angular Momentum, kg-m^2/sec')

color=['g*';'r*';'b*';'c*';'k*';'y*'];
figure
G = axes;
set(G, 'FontSize', 12)
for i=1:size(A{ind},2)
    plot(time{ind},(180/pi)*(A{ind}(:,i)-A{ind}(1,i)),color(i,:),'MarkerSize',
7)
    hold on
end

legend('Segment 1', 'Segment 2', 'Segment 3', 'Segment 4', 'Segment 5',
'Segment 6')
xlabel('Time, sec')
ylabel('Angle, deg')

% Main end -----------------------------------------------------------------
% Agama --------------------------------------------------------------------


function [time, H_tot, I_rel_com,  body_angle, magic_angle, stick_angle,
I_tot, H_tot_body, H_tot_tail, R_com, R_rel_com, R,  A, H, omega,
agama_data,H_fraction] = Agama(filename,xls_data,Segments)

%script for calculating angular momentum

% Extract data from text file:
data=importdata(filename);
if data.data(1,2)==0
    fprintf('Wrong time line tracking in file:\n%s\n',filename)
```

```
end

% Strip path from filename:
[p,filename]=fileparts(filename);

%Determines which lizard to pull morphometric data for
%number of letters of Folder + 1 (/) + 7 (Animal) + 1 (wanted value)
lizardnum = eval(filename(7));

%calculation of Inertia(I), Mass(m), distance to com from posterior-(g) and
%anterior(d) end, length(L) and density(rho) (all values are tail-to-head
%direction)
[I,m,g,d,L,rho,L_act]=calcSegMOI(lizardnum, Segments);


%% Excel-worksheet phase data
% ['filename','Day','Animal','Trial','Controlled','Body Rotation',
% 'relative Tail angle','start move','start outer front foot move',
% 'outer front foot lift-of','outer front foot touch-down','curling start',
% 'curling max','uncurling end',
% 'outer front foot moves before inner front foot','notes']
xls_phase_data=[];
for i=2:size(xls_data.all,1)
    if strcmpi(filename,xls_data.text{i,1})
        xls_phase_data=xls_data.num(i-1,5:end);
    end
end
%for cases where no phases data is available (dummydata)
if isempty(xls_phase_data)
    xls_phase_data=[360 0 0 0 0 1000 0 0 1000];
end
%for cases where phase data is incomplete
if sum(isnan(xls_phase_data))~=0
    tmp_data=[360 0 0 0 0 1000 0 0 1000];
    col=find(isnan(xls_phase_data));
    xls_phase_data(col)=tmp_data(col);
end

%%
 dt = 1/500; %1/frame rate
 % Outputs: Angular momentum of each link, Inertia relative to system
 % center of mass of each link, position of each link relative to system
 % center of mass, position of each link relative to origin
[time, H_tot, I_rel_com, body_angle, H_tot_body, H_tot_tail, R_com, R_rel_com,
R,  A, H, omega,V_rel_com,start_idx,H_fraction] =
AnLizardData(filename,data.data,xls_phase_data,I,m,dt,g,Segments);

% Determines the inertia of the lizard when it is fully extended
%Outputs the angle of a rigid stick subjected to the same angular momentum
[I_stick,z,x,y,w,u,v,stick_angle]=calcSegMOI(lizardnum,'stick', dt, H_tot);

% Outputs the angle of a stick which varies its inertia similarly to the
% lizard, and is subjected to the same angular momentum
[I_tot,z,x,y,w,u,v,magic_angle]=calcSegMOI(lizardnum,'magic_stick', dt, H_tot,
I_rel_com);
```

```
agama_data={filename,'','','','','','','','','','','','';

'm','d','L_act','I','omega','A','H','R_rel_com','V_rel_com','I_rel_com','I_sti
ck','start_idx';

m,d,L_act,I,omega,A,H,R_rel_com,V_rel_com,I_rel_com,I_stick,start_idx};


if sum(max(isnan(agama_data{3,6}(:,:))))~=0
    fprintf('Nan in trial:\n%s\n',filename)
end

% Agama end ------------------------------------------------------------------
% calcSegMOI -----------------------------------------------------------------

function
[I_seg_array,m_seg_array,g_seg_array,d_seg_array,L,rho,L_act,stick_angle]=calc
SegMOI(lizardnum, Segments, dt, H, I_rel_com)
% input:
% SubSystem description {[Seg1 Seg2]} from Seg1 to Seg2 of subsystem
% where:  1=Tail1-Tail2; 2=Tail2-Tail3; 3=Tail3-Tail4;
%         4=Tail4-Hip; 5=Hip-Body; 6=Body-Head
% Segments = {[1 1],[2 2],[3 3],[4 4],[5 5],[6 6]}; % Six-Segemnt Model (Tail-
Head)
% lizardnum=1; %Lizardnumber
% output:
% I_seg_array = Inertia for each subsystem (from tail tip to head)
% m_seg_array = Mass for each subsystem (from tail tip to head)
% g_seg_array = distance to COM measured from posterior end for each subsystem
(from tail tip to head)
% d_seg_array = distance to COM measured from anterior end for each
% subsystem (from tail tip to head)

% for rigid stick calculation
stk=0;
if ischar(Segments)
    if strcmp(Segments,'stick')
        Segments={[1 6]};
        stk=1;
    elseif strcmp(Segments,'magic_stick')
        Segments={[1 6]};
        stk=2;
    else
        fprintf('for stick or magic_stick overload function:\n define Segments
as `stick` or `magic_stick`')
    end
end

%% morphometric data
% Gives height(a), width(b), length(L), total mass(mass_tot) and
% density(rho) of Lizard Markers
% (tail1 tail2 tail3 tail4 hip body head) [m]
% lizardnum=2;
[a, b, L, dc, mass_tot, rho,L_act] = LizardMorphData(lizardnum);
% rho=ones(1,length(L))*1000;

%% calculate MOI of tail segments using ellipsoid solid
% a0 = radius of major base axis
```

```
% a1 = radius of major top axis
% b0 = radius of minor base axis
% b1 = radius of minor top axis
% ------
% I = moment of inertia of segment [kg*m^2]
% m = mass of segment [kg]
% g = center of mass [m] measured from base of frustum (Posterior)
for i=1:length(L);
    a0= a(i)/2;
    a1= a(i+1)/2;
    b0= b(i)/2;
    b1= b(i+1)/2;
    l=L(i);
    [I(i) m(i) g(i)]=MOI_calc(a0,a1,b0,b1,l,rho(i));
end
d=L-g; %COM distance from anterior

%% Approximate Body Inertia, mass and anterior resp. posterior distance to
% segment COM

% Mass Approx:
    % Mass fraction for body segments (incl. head & cut):

    front_av_fraction=0.414587922;
    hind_av_fraction=0.377828418;
    % Estimate mass from total:
    m(6)=mass_tot*front_av_fraction;
    m(5)=mass_tot*hind_av_fraction;

% Inertia Approx:
    % Estimate MOI from alpha*m*length^2+beta*m*width^2 approximation (incl.
    % head and cut)
    front_alpha=0.0474;
    front_beta=0.0729;
    hind_alpha=0.068;
    hind_beta=0.0811;
    % Estimate MOI from optimized values
    %L(5) with cut without?-> how does the intertia react..??
    I(6)=front_alpha*m(6)*L(6)^2+front_beta*m(6)*b(6)^2;
    I(5)=hind_alpha*m(5)*L(5)^2+hind_beta*m(5)*b(5)^2;

% COM to post- (g) and anterior (d) end Approx:
    % COM offset average (normalized to segement length, inc. head)
    front_av_d=0.571945203;%average zeta=Gz/length
    hind_av_d=0.525103941;%average zeta=Gz/length
    % Estimate COM (measured from anterior tip) from length:
    d(6)=L(6)*front_av_d;
    d(5)=L(5)*hind_av_d;
    % Estimate COM (measured from posterior tip) from length incl. Head:
    g=L-d;

    g(5)=g(5)-dc;

%% Sub-system specific calculation

SegNum=length(Segments);
```

```
%for each sub-system:
for i=1:SegNum

    % Distance from origin(first of segments) to center of mass of each
segment:
    Lc_seg{i}=cumsum(L(Segments{i}(1,1):Segments{i}(1,2))); %cumulated sum of
segemnt lengths
    Lc_seg_array(i)=Lc_seg{i}(end); %for total length of segment
    r_seg{i}(1)=g(Segments{i}(1,1));
    for j=(Segments{i}(1,1)+1):Segments{i}(1,2)
        % r is the distance from fist segment to COM of ith segment
        r_seg{i}(j-Segments{i}(1,1)+1)=g(j)+Lc_seg{i}(j-Segments{i}(1,1));
    end

    % SubSystem COM distance from beginning of segment for each segment
    sum_mr_seg{i}=sum(m(Segments{i}(1,1):Segments{i}(1,2)).*r_seg{i});
    sum_m_seg{i}=sum(m(Segments{i}(1,1):Segments{i}(1,2)));
    COM_seg{i}=sum_mr_seg{i}/sum_m_seg{i};

    %distance from segment COM to SubSystem COM
    dcom_seg{i}(Segments{i}(1,1):Segments{i}(1,2))=COM_seg{i}-r_seg{i};    %
Positive for segments anterior to COM

    %Inertia about COM for SubSystems
    Ipa_seg{i} =
m(Segments{i}(1,1):Segments{i}(1,2)).*dcom_seg{i}(Segments{i}(1,1):Segments{i}
(1,2)).^2;
    Icomp_seg{i} = Ipa_seg{i}+I(Segments{i}(1,1):Segments{i}(1,2));

    I_seg{i} = sum(Icomp_seg{i});
    I_seg_array(i) = I_seg{i}(end);
    m_seg{i} = sum(m(Segments{i}(1,1):Segments{i}(1,2)));
    m_seg_array(i) = m_seg{i}(end);
    g_seg{i} = COM_seg{i};
    g_seg_array(i) = g_seg{i}(end);
    d_seg{i} = Lc_seg{i}(end)-g_seg{i};
    d_seg_array(i) = d_seg{i}(end);
end

% calculations for Stick-model with constant Inertia
if stk==1
    if ~exist('I_rel_com','var')&&exist('dt','var')&&exist('H','var')
        stick_angle = zeros(size(H));
        stick_angle(1) = 0;
        I_stick=I_seg_array;

        for i = 2:size(H,1)
            angle_change = H(i)*dt*(1/I_stick);
            if angle_change == NaN
                angle_change = 0;
            end
            stick_angle(i) = stick_angle(i-1)+angle_change;
        end
    else
        fprintf('wrong variables for Stick_calculation:\n
lizardnum,`magic_stick`, dt, H_tot\n')
    end
```

```
end

% calculations for Stick-model with varying inertia
if stk==2
    if exist('dt','var')&&exist('H','var')&&exist('I_rel_com','var')
        magic_angle = zeros(size(H));
        I_tot = zeros(size(H));
        magic_angle(1) = 0;
        for i = 2:size(H,1)
           I_tot(i) = sum(I_rel_com(i,:));
            magic_angle(i) = magic_angle(i-1) + H(i)*dt/I_tot(i);
        end
        stick_angle=magic_angle;
        I_seg_array=I_tot;
    else
        fprintf('wrong variables for Magic_Stick_calculation:\n
lizardnum,`stick`, dt, H_tot,I_rel_com\n')
    end
end

% calcSegMOI end -------------------------------------------------------------
% AnLizardData ---------------------------------------------------------------

function [time,H_tot,I_rel_com, body_angle, H_tot_body, H_tot_tail, R_com,
R_rel_com, R, A, H, omega,V_rel_com,start_idx,H_fraction] =
AnLizardData(filename,pdata,xls_phase_data,I,m,dt,l_com,Segments)
% I, M, and l_com are mx1 vectors of MOI, mass, and length to COM (from
% posterior end) for each segement.
% pdata is Nx2*(m+1) (x-y pairs), where m is number of segments and N is
% number of frames
% dt is time between samples (scalar)
% Expects kinematics in following order:
% [tail1, tail2, tail3, tail4, hipR, hipL, footHR, footHL, body, shoulderR,
shoulderL, footFR, footFL, head]
% WARNING: expects pdata in left-handed coordinate system! (origin at upper
% left of video).  The data are converted to a right-handed system

% Extract Kinematics
rev = repmat([1 -1],length(pdata(:,2)),1);  % Define vector for flipping y-
axis
tail1 = pdata(:, 3:4).*rev;
tail2 = pdata(:, 5:6).*rev;
tail3 = pdata(:, 7:8).*rev;
tail4 = pdata(:, 9:10).*rev;
hipR = pdata(:, 11:12).*rev;
hipL = pdata(:, 13:14).*rev;
% footHR = pdata(:, 15:16).*rev;
% footHL = pdata(:, 17:18).*rev;
body = pdata(:, 19:20).*rev;
shoulderR = pdata(:, 21:22).*rev;
shoulderL = pdata(:, 23:24).*rev;
% footFR = pdata(:, 25:26).*rev;
% footFL = pdata(:, 27:28).*rev;
% head = pdata(:, 29:30).*rev;

%Arrange all Segments of position data we want, converts cm to m
pdata_corrected = [tail1, tail2, tail3, tail4, (hipR+hipL)/2, body,
(shoulderR+shoulderL)/2]/100;
```

```
% Number of Segments
SegNum = length(Segments);

%Arrange Data to SubSystem-Specific model
idx_c=0;
pdata_tmp=[];
for i=1:SegNum
    idx_a=Segments{i}(1,1); % front of segment
    idx_b=Segments{i}(1,2)+1; % end of segment (Segment number +1)
    if idx_c~=idx_a % first Point of next Segment = last Point of previous
Segment?
        pdata_tmp=[pdata_tmp,pdata_corrected(:,2*idx_a-1:2*idx_a)];
    end
    pdata_tmp=[pdata_tmp,pdata_corrected(:,2*idx_b-1:2*idx_b)];
    idx_c=idx_b;
end
pdata_corrected=pdata_tmp;

% extract relevant phases of trial (using trial_phases.xls)
time = pdata(1:length(pdata_corrected(:,1)),2);
time = time-time(1);
% from curl beginn to uncurl end
start_time=roundn(xls_phase_data(7),-4);
end_time=roundn(xls_phase_data(9),-4);
start_idx=1;
end_idx=time(end);

for i=1:length(time)
    if start_time==roundn(time(i,1),-4)
        start_idx=i;
    end
    if end_time==roundn(time(i,1),-4)
        end_idx=i;
    end
end
pdata_corrected=pdata_corrected(start_idx:end_idx,:);
clear start_idx end_idx

%extracting usable data (=not tracked sections) from data sheet
x=sum(abs([pdata_corrected(:,:)])==0.01,2);%editme
start_idx=1;
end_idx=length(x);
si=0;
ei=0;

if min(x)==0
    for i=1:length(x)
        if x(i)==0 && si~=1
            start_idx=i;
            si=1;
        end
        if x(length(x)-(i-1))==0 && ei~=1
            end_idx=length(x)-(i-1);
            ei=1;
        end
    end
```

```
    start_time=roundn(xls_phase_data(4),-4);
    if start_time*500+1<start_idx
        fprintf('tracking data starts after moving_start:\n%s\n',filename)
    end

    pdata_corrected=pdata_corrected(start_idx:end_idx,:);
else
    fprintf('No time where all DataPoints are tracked in this TimtSequence for
file:\n%s\n',filename)
end

if max(x(start_idx:end_idx))~=0
    fprintf('Some DataPoints are not tracked in this TimtSequence for
file:\n%s\n',filename)
end

% Time, starts from zero
time = pdata(start_idx:end_idx,2);
time = time-time(1);

% Define anonymous function for first order centered difference:
cdiff = @(yplus, yminus, h)  (yplus - yminus)/(2*h);

% Extract position vector for each point
k = length(I);       % Num segments
for i = 1:k+1
    % position data for each pair of points (m+1 x n)
    P{i} = pdata_corrected(:,2*i-1:2*i);
end

for i = 1:k
    % vectors from ith point to i+1 point
    u = P{i+1}-P{i};
    % Unit vector from ith point to i+1 point
    U{i} = [u(:,1)./sqrt(sum(u.^2,2)) u(:,2)./sqrt(sum(u.^2,2))];
    % Position of the COM of each link
    R{i} = P{i}+U{i}*l_com(i);
end


% Center of mass location
R_com_gross = zeros(size(R{1}));
for i = 1:k
    R_com_gross = m(i)*R{i}+R_com_gross;
end
R_com = R_com_gross/sum(m);

% position relative to the center of mass
for i = 1:k
    R_rel_com{i} = R{i}-R_com;
    dist_com(:,i) = sqrt(R_rel_com{i}(:,1).^2+R_rel_com{i}(:,2).^2);

    % Inertia of a link relative to the system center of mass
    I_rel_com(:,i) = I(i)+m(i)*dist_com(:,i).^2;
end
```

```
% Calculate velocity relative to the center of mass, total H
n = size(pdata_corrected,1);  % Num samples
for i = 1:k
     % Calculate velocities: angular, from origin, from reference O
     V{i} = zeros(n,2);
     V_rel_com{i} = zeros(n,2);
     omega{i} = zeros(n,1);

    % Get angle of ith segment:
    A{i} = atan2(U{i}(:,2),U{i}(:,1));    % Angle of body segment wrt global
horizontal

    % Convert angle from +- radians to 0-2*pi
    A{i}(A{i}<0) = A{i}(A{i}<0) + 2*pi;

    % Make angle continuous (prevent wrap from 0 to 2pi)
    A{i} = unwrap(A{i});


    % Calculate velocities with centered difference:
    for j = 2:n-1
        % Velocity of ith segment COM:
        V_rel_com{i}(j,:) = cdiff(R_rel_com{i}(j+1,:),R_rel_com{i}(j-1,:),dt);

        % Angular velocity ith segment:
        omega{i}(j,:) = cdiff(A{i}(j+1,:),A{i}(j-1,:),dt);
    end


    % Angular Momentum
    z = zeros(n,1); % Define zero vector for cross product (z-axis data)
    H(:,i) = I(i) * omega{i} + cross([R_rel_com{i} z],m(i)*[V_rel_com{i}
z])*[0 0 1]';
    Hdb{i} = [I(i) * omega{i}   cross([R_rel_com{i} z],m(i)*[V_rel_com{i}
z])*[0 0 1]'];
    Hdb{i} = Hdb{i}(~sum(Hdb{i}==0,2),:);
    H_fraction{i}=Hdb{i}(10:29,1)./sum(Hdb{i}(10:29,:),2);
    H_fraction{i} = H_fraction{i}(~isnan(H_fraction{i}(:,1)),:);
    H_frac_tmp(i)=mean(abs(H_fraction{i}));
end

% H_fraction = H_fraction(~isnan(H_fraction(:,1)),:);
% H_fraction=mean(H_fraction,1);
H_fraction=H_frac_tmp;

%% Prepare outputs:

% Define Last Segment as body angle (normally shoulders to body)
body_angle = A{SegNum};
body_angle = body_angle - body_angle(1);


% Angular momentum
```

```
H_tot = sum(H,2);
H_tot_body = zeros(length(pdata_corrected(:,1)),1);
H_tot_tail = zeros(length(pdata_corrected(:,1)),1);
A_dbl=[];
omega_dbl=[];
for i=1:SegNum
   if Segments{i}(1,1)<=4 || Segments{i}(1,2)<=4
       H_tot_tail = H_tot_tail(:,1)+H(:,i);
   else
       H_tot_body = H_tot_body(:,1)+H(:,i);
   end
   A_dbl = [A_dbl A{i}];
   omega_dbl = [omega_dbl omega{i}];
end
A = A_dbl;
omega=omega_dbl;
end

% AnLizardData end -----------------------------------------------------------
```